REVIEWS OF MODERN PHYSICS, VOLUME 73, APRIL 2001

# Phonons and related crystal properties from density-functional perturbation theory

Stefano Baroni, Stefano de Gironcoli, and Andrea Dal Corso

*SISSA–Scuola Internazionale Superiore di Studi Avanzati and INFM–Istituto Nazionale di Fisica della Materia, I-34014 Trieste, Italy*

Paolo Giannozzi*

*Chemistry Department and Princeton Materials Institute, Princeton University, Princeton, New Jersey 08544*

(Published 6 July 2001)

This article reviews the current status of lattice-dynamical calculations in crystals, using density-functional perturbation theory, with emphasis on the plane-wave pseudopotential method. Several specialized topics are treated, including the implementation for metals, the calculation of the response to macroscopic electric fields and their relevance to long-wavelength vibrations in polar materials, the response to strain deformations, and higher-order responses. The success of this methodology is demonstrated with a number of applications existing in the literature.

## CONTENTS

I. Introduction 516
II. Density-Functional Perturbation Theory 516
A. Lattice dynamics from electronic-structure theory 516
B. Density-functional theory 517
1. The Kohn-Sham equations 517
2. Local-density approximation and beyond 518
C. Linear response 519
1. Monochromatic perturbations 520
2. Homogeneous electric fields 521
3. Relation to the variational principle 523
4. Metals 524
D. Phonons 526
1. Vibrational states in crystalline solids 526
2. Long-wavelength vibrations in polar materials 527
3. Interatomic force constants 528
E. Homogeneous deformations 528
1. Elastic properties 528
2. Piezoelectric properties 529
F. Higher-order responses 530
1. The $2n+1$ theorem 530
2. Nonlinear susceptibilities 531
III. Implementations 532
A. Plane waves and pseudopotentials 532
B. Ultrasoft pseudopotentials 533
C. Localized basis sets, all-electron implementations 535
IV. Other Approaches 536
A. The dielectric approach 536
B. Frozen phonons 537
C. Vibrational properties from molecular dynamics 538
V. Applications 539
A. Phonons in bulk crystals 539
1. Simple semiconductors 539
a. Elemental and III-V semiconductors 539
b. II-VI semiconductors 540
c. Diamond and graphite 541
d. Silicon carbide 541
e. Nitrides 541
f. Other semiconductors 541
g. Second-order Raman spectra in simple semiconductors 542
h. Piezoelectricity in binary semiconductors 542
2. Simple metals and superconductors 542
3. Oxides 543
a. Insulators 544
b. Ferroelectrics 545
c. High-$T_c$ superconductors 545
4. Other materials 546
B. Phonons in semiconductor alloys and superlattices 547
1. GaAs/AlAs superlattices 547
2. GaAs/AlAs alloys 547
3. Si/Ge superlattices and alloys 548
4. AlGaN alloys 548
5. GaP/InP alloys 548
6. Localized vibrations at defects 548
C. Lattice vibrations at surfaces 549
D. Soft phonons and pressure-induced lattice transformations 549
1. Ferroelectrics 549
2. Pressure-induced phase transitions 550
a. Cesium halides 550
b. Cesium hydride 551
c. Silicon dioxide 551
d. Semiconductors 552
e. Solid hydrogen 552
f. Metals 553
3. Other phase transitions 553
E. Thermal properties of crystals and surfaces 553
1. Metals 553
2. Semiconductors and insulators 554
3. Surfaces 554
4. Alloys 554
F. Anharmonic effects 555
G. Isotopic broadening of Raman lines 555
H. Vibrational broadening of electronic core levels 556
VI. Conclusions and Perspectives 556
Acknowledgments 557

*On leave of absence from Scuola Normale Superiore, Pisa, Italy.

 ©2001 The American Physical Society

Appendix A: Plane-Wave Pseudopotential Implementation 557
1. Pseudopotentials 557
2. Matrix elements 557
Appendix B: Force Constants, Ionic Term 558
References 558

## I. INTRODUCTION

The theory of lattice vibrations is one of the best established chapters in modern solid-state physics, and very few of the astonishing successes met by the latter could have been achieved without a strong foundation of the former. A wide variety of physical properties of solids depend on their lattice-dynamical behavior: infrared, Raman, and neutron-diffraction spectra; specific heats, thermal expansion, and heat conduction; phenomena related to the electron-phonon interaction such as the resistivity of metals, superconductivity, and the temperature dependence of optical spectra are just a few of them. As a matter of fact, their understanding in terms of phonons is considered to be one of the most convincing pieces of evidence that our current quantum picture of solids is correct.

The basic theory of lattice vibrations dates back to the thirties, and the treatise of Born and Huang (1954) is still considered today to be the reference textbook in this field. These early formulations were mainly concerned with establishing the general properties of the dynamical matrices—such as, e.g., their symmetry and/or analytical properties—without even considering their connections with the electronic properties that actually determine them. A systematic study of these connections was not performed until the 1970s (De Cicco and Johnson, 1969; Pick, Cohen, and Martin, 1970). The relationship between the electronic and the lattice-dynamical properties of a system is important not only as a matter of principle, but also because (and perhaps mainly because) it is only by exploiting these relations that it is possible to calculate the lattice-dynamical properties of specific systems.

The state of the art of theoretical condensed-matter physics and of computational materials science is such that it is nowadays possible to calculate specific properties of specific (simple) materials using *ab initio* quantum-mechanical techniques whose only input information is the chemical composition of the materials. In the specific case of lattice-dynamical properties, a large number of *ab initio* calculations based on the linear-response theory of lattice vibrations (De Cicco and Johnson, 1969; Pick, Cohen, and Martin, 1970) have been made possible over the past ten years by the achievements of density-functional theory (Hohenberg and Kohn, 1964; Kohn and Sham, 1965) and by the development of density-functional perturbation theory (Zein, 1984; Baroni *et al.*, 1987a), which is a method for applying the former within the general theoretical framework provided by the latter. Thanks to these theoretical and algorithmic advances, it is now possible to obtain accurate phonon dispersions on a fine grid of wave vectors covering the entire Brillouin zone, which compare directly with neutron-diffraction data, and from which several physical properties of the system (such as heat capacities, thermal expansion coefficients, temperature dependence of the band gap, and so on) can be calculated.

The purpose of the present paper is to illustrate in some detail the theoretical framework of density-functional perturbation theory, including several technical details that are useful for its implementation within the plane-wave pseudopotential scheme. We shall also provide a representative, though necessarily incomplete, choice of significant applications to the physics of insulators and metals, including their surfaces, alloys, and microstructures.

## II. DENSITY-FUNCTIONAL PERTURBATION THEORY

### A. Lattice dynamics from electronic-structure theory

The basic approximation which allows one to decouple the vibrational from the electronic degrees of freedom in a solid is the *adiabatic approximation* of Born and Oppenheimer (1927). Within this approximation, the lattice-dynamical properties of a system are determined by the eigenvalues $\mathcal{E}$ and eigenfunctions $\Phi$ of the Schrödinger equation:

$$\left( -\sum_I \frac{\hbar^2}{2M_I} \frac{\partial^2}{\partial \mathbf{R}_I^2} + E(\mathbf{R}) \right) \Phi(\mathbf{R}) = \mathcal{E}\Phi(\mathbf{R}), \tag{1}$$

where $\mathbf{R}_I$ is the coordinate of the $I$th nucleus, $M_I$ its mass, $\mathbf{R} \equiv \{\mathbf{R}_I\}$ the set of all the nuclear coordinates, and $E(\mathbf{R})$ the clamped-ion energy of the system, which is often referred to as the *Born-Oppenheimer energy surface*. In practice, $E(\mathbf{R})$ is the ground-state energy of a system of interacting electrons moving in the field of fixed nuclei, whose Hamiltonian—which acts onto the electronic variables and depends parametrically upon $\mathbf{R}$—reads

$$H_{BO}(\mathbf{R}) = -\frac{\hbar^2}{2m} \sum_i \frac{\partial^2}{\partial \mathbf{r}_i^2} + \frac{e^2}{2} \sum_{i \neq j} \frac{1}{|\mathbf{r}_i - \mathbf{r}_j|} - \sum_{iI} \frac{Z_I e^2}{|\mathbf{r}_i - \mathbf{R}_I|} + E_N(\mathbf{R}), \tag{2}$$

where $Z_I$ is the charge of the $I$th nucleus, $-e$ is the electron charge, and $E_N(\mathbf{R})$ is the electrostatic interaction between different nuclei:

$$E_N(\mathbf{R}) = \frac{e^2}{2} \sum_{I \neq J} \frac{Z_I Z_J}{|\mathbf{R}_I - \mathbf{R}_J|}. \tag{3}$$

The equilibrium geometry of the system is given by the condition that the forces acting on individual nuclei vanish:

$$\mathbf{F}_I \equiv -\frac{\partial E(\mathbf{R})}{\partial \mathbf{R}_I} = 0, \tag{4}$$

whereas the vibrational frequencies $\omega$ are determined by the eigenvalues of the Hessian of the Born-Oppenheimer energy, scaled by the nuclear masses:

$$\det\left|\frac{1}{\sqrt{M_I M_J}}\frac{\partial^2 E(\mathbf{R})}{\partial \mathbf{R}_I \partial \mathbf{R}_J}-\omega^2\right|=0. \tag{5}$$

The calculation of the equilibrium geometry and of the vibrational properties of a system thus amounts to computing the first and second derivatives of its Born-Oppenheimer energy surface. The basic tool for accomplishing this goal is the Hellmann-Feynman theorem (Hellmann, 1937; Feynman, 1939), which states that the first derivative of the eigenvalues of a Hamiltonian, $H_\lambda$, that depends on a parameter $\lambda$ is given by the expectation value of the derivative of the Hamiltonian:

$$\frac{\partial E_\lambda}{\partial \lambda}=\left\langle \Psi_\lambda \left| \frac{\partial H_\lambda}{\partial \lambda} \right| \Psi_\lambda \right\rangle, \tag{6}$$

where $\Psi_\lambda$ is the eigenfunction of $H_\lambda$ corresponding to the $E_\lambda$ eigenvalue: $H_\lambda \Psi_\lambda = E_\lambda \Psi_\lambda$. In the Born-Oppenheimer approximation, nuclear coordinates act as parameters in the electronic Hamiltonian, Eq. (2). The force acting on the $I$th nucleus in the electronic ground state is thus

$$\mathbf{F}_I=-\frac{\partial E(\mathbf{R})}{\partial \mathbf{R}_I}=-\left\langle \Psi(\mathbf{R}) \left| \frac{\partial H_{BO}(\mathbf{R})}{\partial \mathbf{R}_I} \right| \Psi(\mathbf{R}) \right\rangle, \tag{7}$$

where $\Psi(\mathbf{r},\mathbf{R})$ is the electronic ground-state wave function of the Born-Oppenheimer Hamiltonian. This Hamiltonian depends on $\mathbf{R}$ via the electron-ion interaction that couples to the electronic degrees of freedom only through the electron charge density. The Hellmann-Feynman theorem states in this case that

$$\mathbf{F}_I=-\int n_{\mathbf{R}}(\mathbf{r})\frac{\partial V_{\mathbf{R}}(\mathbf{r})}{\partial \mathbf{R}_I}d\mathbf{r}-\frac{\partial E_N(\mathbf{R})}{\partial \mathbf{R}_I}, \tag{8}$$

where $V_{\mathbf{R}}(\mathbf{r})$ is the electron-nucleus interaction,

$$V_{\mathbf{R}}(\mathbf{r})=-\sum_{iI}\frac{Z_I e^2}{|\mathbf{r}_i-\mathbf{R}_I|}, \tag{9}$$

and $n_{\mathbf{R}}(\mathbf{r})$ is the ground-state electron charge density corresponding to the nuclear configuration $\mathbf{R}$. The Hessian of the Born-Oppenheimer energy surface appearing in Eq. (5) is obtained by differentiating the Hellmann-Feynman forces with respect to nuclear coordinates,

$$\frac{\partial^2 E(\mathbf{R})}{\partial \mathbf{R}_I \partial \mathbf{R}_J}\equiv-\frac{\partial \mathbf{F}_I}{\partial \mathbf{R}_J}=\int \frac{\partial n_{\mathbf{R}}(\mathbf{r})}{\partial \mathbf{R}_J}\frac{\partial V_{\mathbf{R}}(\mathbf{r})}{\partial \mathbf{R}_I}d\mathbf{r} + \int n_{\mathbf{R}}(\mathbf{r})\frac{\partial^2 V_{\mathbf{R}}(\mathbf{r})}{\partial \mathbf{R}_I \partial \mathbf{R}_J}d\mathbf{r}+\frac{\partial^2 E_N(\mathbf{R})}{\partial \mathbf{R}_I \partial \mathbf{R}_J}. \tag{10}$$

Equation (10) states that the calculation of the Hessian of the Born-Oppenheimer energy surfaces requires the calculation of the ground-state electron charge density $n_{\mathbf{R}}(\mathbf{r})$ as well as of its *linear response* to a distortion of the nuclear geometry, $\partial n_{\mathbf{R}}(\mathbf{r})/\partial \mathbf{R}_I$. This fundamental result was first stated in the late 1960s by De Cicco and Johnson (1969) and by Pick, Cohen, and Martin (1970). The Hessian matrix is usually called the matrix of the *interatomic force constants*.

### B. Density-functional theory

According to the preceding discussion, the calculation of the derivatives of the Born-Oppenheimer energy surface with respect to the nuclear coordinates requires only a knowledge of the electronic charge-density distribution. This fact is a special case of a much more general property of the systems of interacting electrons, known as the Hohenberg and Kohn (1964) theorem. According to this theorem, no two different potentials acting on the electrons of a given system can give rise to a same ground-state electronic charge density. This property can be used in conjunction with the standard Rayleigh-Ritz variational principle of quantum mechanics to show that a *universal functional*,[1] $F[n(\mathbf{r})]$, of the electron charge density exists such that the functional

$$E[n]=F[n]+\int n(\mathbf{r})V(\mathbf{r})d\mathbf{r} \tag{11}$$

is minimized by the electron charge density of the ground state corresponding to the external potential $V(\mathbf{r})$, under the constraint that the integral of $n(\mathbf{r})$ equals the total number of electrons. Furthermore, the value of the minimum coincides with the ground-state energy. This theorem provides the foundation of what is currently known as *density-functional theory* (DFT; Parr and Yang, 1989; Dreizler and Gross, 1990). It allows an enormous conceptual simplification of the quantum-mechanical problem of searching for the ground-state properties of a system of interacting electrons, for it replaces the traditional description based on wave functions (which depend on $3N$ independent variables, $N$ being the number of electrons) with a much more tractable description in terms of the charge density, which depends on only three variables. Two major problems hamper a straightforward application of this remarkably simple result: (1) the form of the $F$ functional is unknown, and (2) the conditions to be fulfilled for a function $n(\mathbf{r})$ to be considered an acceptable ground-state charge distribution (and hence the domain of the functional $F$) are poorly characterized. The second problem is hardly addressed at all, and one must usually be content to impose the proper normalization of the charge density by the use of a Lagrange multiplier. The first problem can be handled by mapping the system onto an auxiliary system of noninteracting electrons (Kohn and Sham, 1965) and by making appropriate approximations along the lines described in the next subsection.

#### 1. The Kohn-Sham equations

The Hohenberg and Kohn theorem states that all the physical properties of a system of interacting electrons are uniquely determined by its ground-state charge-density distribution. This property holds independently

[1]By *universal* it is meant here that the functional is independent of the external potential acting on the electrons, though it obviously depends on the form of the electron-electron interaction.

of the precise form of the electron-electron interaction. In particular, when the strength of the electron-electron interaction vanishes, $F[n]$ defines the ground-state kinetic energy of a system of noninteracting electrons as a functional of its ground-state charge-density distribution $T_0[n]$. This fact was used by Kohn and Sham (1965) to map the problem of a system of interacting electrons onto an equivalent noninteracting problem. To this end, the unknown functional $F[n]$ is cast in the form

$$F[n]=T_0[n]+\frac{e^2}{2}\int\frac{n(\mathbf{r})n(\mathbf{r}')}{|\mathbf{r}-\mathbf{r}'|}d\mathbf{r}d\mathbf{r}'+E_{xc}[n], \quad (12)$$

where the second term is the classical electrostatic self-interaction of the electron charge-density distribution, and the so-called *exchange-correlation energy* $E_{xc}$ is defined by Eq. (12).[2] Variation of the energy functional with respect to $n(\mathbf{r})$ with the constraint that the number of electrons be kept fixed leads formally to the same equation as would hold for a system of noninteracting electrons subject to an effective potential, also called the *self-consistent field*, (SCF), potential, whose form is

$$V_{SCF}(\mathbf{r})=V(\mathbf{r})+e^2\int\frac{n(\mathbf{r}')}{|\mathbf{r}-\mathbf{r}'|}d\mathbf{r}'+v_{xc}(\mathbf{r}), \quad (13)$$

where

$$v_{xc}(\mathbf{r})\equiv\frac{\delta E_{xc}}{\delta n(\mathbf{r})} \quad (14)$$

is the functional derivative of the exchange-correlation energy, also called the *exchange-correlation potential*.

The power of this trick is that, if one knew the effective potential $V_{SCF}(\mathbf{r})$, the problem for noninteracting electrons could be trivially solved without knowing the form of the noninteracting kinetic-energy functional $T_0$. To this end, one should simply solve the one-electron Schrödinger equation:

$$\left(-\frac{\hbar^2}{2m}\frac{\partial^2}{\partial\mathbf{r}^2}+V_{SCF}(\mathbf{r})\right)\psi_n(\mathbf{r})=\epsilon_n\psi_n(\mathbf{r}). \quad (15)$$

The ground-state charge-density distribution and noninteracting kinetic-energy functional would then be given in terms of the *auxiliary Kohn-Sham orbitals*, $\psi_n(\mathbf{r})$:

$$n(\mathbf{r})=2\sum_{n=1}^{N/2}|\psi_n(\mathbf{r})|^2 \quad (16)$$

$$T_0[n]=-2\frac{\hbar^2}{2m}\sum_{n=1}^{N/2}\int\psi_n^*(\mathbf{r})\frac{\partial^2\psi_n(\mathbf{r})}{\partial\mathbf{r}^2}d\mathbf{r}, \quad (17)$$

where $N$ is the number of electrons, and the system is supposed to be nonmagnetic, so that each of the $N/2$ lowest-lying orbital states accommodates two electrons of opposite spin. In periodic systems the index $n$ running over occupied states can be thought of as a double label, $n\equiv\{v,\mathbf{k}\}$, where $v$ indicates the set of valence bands, and $\mathbf{k}$ is a wave vector belonging to the first Brillouin zone.

The ground-state energy given by Eqs. (11) and (12) can be equivalently expressed in terms of the Kohn-Sham eigenvalues:

$$E[n]=2\sum_{n=1}^{N/2}\epsilon_n-\frac{e^2}{2}\int\frac{n(\mathbf{r})n(\mathbf{r}')}{|\mathbf{r}-\mathbf{r}'|}d\mathbf{r}d\mathbf{r}'+E_{xc}[n]-\int n(\mathbf{r})v_{xc}(\mathbf{r})d\mathbf{r}. \quad (18)$$

Equation (15) has the form of a nonlinear Schrödinger equation whose potential depends on its own eigenfunctions through the electron charge-density distribution. Once an explicit form for the exchange-correlation energy is available, this equation can be solved in a self-consistent way using a variety of methods.

### 2. Local-density approximation and beyond

The Kohn-Sham scheme constitutes a practical way to implement density-functional theory, provided an accurate and reasonably easy-to-use approximation is available for the exchange-correlation energy $E_{xc}[n]$. In their original paper, Kohn and Sham (1965) proposed the assumption that each small volume of the system (so small that the charge density can be thought to be constant therein) contributes the same exchange-correlation energy as an equal volume of a homogeneous electron gas at the same density. With this assumption, the exchange-correlation energy functional and potential read

$$E_{xc}[n]=\int\epsilon_{xc}(n)|_{n=n(\mathbf{r})}n(\mathbf{r})d\mathbf{r}, \quad (19)$$

$$v_{xc}[n](\mathbf{r})=\left(\epsilon_{xc}(n)+n\frac{d\epsilon_{xc}(n)}{dn}\right)_{n=n(\mathbf{r})}, \quad (20)$$

where $\epsilon_{xc}(n)$ is the exchange-correlation energy per particle in a homogeneous electron gas at density $n$. This approximation is known as the *local-density approximation* (LDA). Approximate forms for $\epsilon_{xc}(n)$ have been known for a long time. Numerical results from nearly exact Monte Carlo calculations for the homogeneous electron gas by Ceperley and Alder (1980) have been parametrized by Perdew and Zunger (1981) with a simple analytical form. More accurate parametrizations have been recently proposed by Ortiz and Ballone (1994). All these different forms are very similar in the range of electron densities relevant to condensed-matter applications and yield very similar results.

The LDA is *exact* in the limit of high density or of a slowly varying charge-density distribution (Kohn and

[2]The exchange-correlation energy is the name we give to the part of the energy functional that we do not know how to calculate otherwise. For this reason, it has been named the *stupidity energy* by Feynmann (1972). Whether or not this is a useful concept depends on the magnitude of the energy with respect to the total functional and on the quality of the approximations one can find for it.

Sham, 1965). This approximation has turned out to be much more successful than originally expected (see, for instance, Jones and Gunnarsson, 1989), in spite of its extreme simplicity. For weakly correlated materials, such as semiconductors and simple metals, the LDA accurately describes structural and vibrational properties: the correct structure is usually found to have the lowest energy, while bond lengths, bulk moduli, and phonon frequencies are accurate to within a few percent.

The LDA also has some well-known drawbacks. A large overestimate ($\sim 20\%$) of the crystal cohesive and molecular binding energies is possibly the worst failure of this approximation, together with its inability to properly describe strongly correlated systems, such as transition-metal oxides. Much effort has been put into the search for better functionals than the LDA (see, for instance, Perdew *et al.*, 1999). The use of *gradient corrections* (Becke, 1988; Perdew *et al.*, 1996) to the LDA has become widespread in recent years. Gradient corrections are generally found to improve the account of electron correlations in finite or semi-infinite systems, such as molecules or surfaces; they are less helpful in infinite solids.

In general, DFT is a ground-state theory and Kohn-Sham eigenvalues and eigenvectors do not have a well-defined physical meaning. Nevertheless, for lack of better and equally general methods, Kohn-Sham eigenvalues are often used to estimate excitation energies. The features of the low-lying energy bands in solids obtained in this way are generally considered to be at least qualitatively correct, in spite of the fact that the LDA is known to substantially underestimate the optical gaps in insulators.

### C. Linear response

In Sec. II.A, Eq. (10), we have seen that the electron-density linear response of a system determines the matrix of its interatomic force constants. Let us see now how this response can be obtained within density-functional theory. The procedure described in the following is usually referred to as *density-functional perturbation theory* (DFPT; Zein, 1984; Baroni *et al.*, 1987a; Gonze, 1995b).

In order to simplify the notation and make the argument more general, we assume that the external potential acting on the electrons is a differentiable function of a set of parameters, $\lambda \equiv \{\lambda_i\}$ ($\lambda_i \equiv \mathbf{R}_I$ in the case of lattice dynamics). According to the Hellmann-Feynman theorem, the first and second derivatives of the ground-state energy read

$$\frac{\partial E}{\partial \lambda_i} = \int \frac{\partial V_\lambda(\mathbf{r})}{\partial \lambda_i} n_\lambda(\mathbf{r}) d\mathbf{r}, \tag{21}$$

$$\frac{\partial^2 E}{\partial \lambda_i \partial \lambda_j} = \int \frac{\partial^2 V_\lambda(\mathbf{r})}{\partial \lambda_i \partial \lambda_j} n_\lambda(\mathbf{r}) d\mathbf{r} + \int \frac{\partial n_\lambda(\mathbf{r})}{\partial \lambda_i} \frac{\partial V_\lambda(\mathbf{r})}{\partial \lambda_j} d\mathbf{r}. \tag{22}$$

The electron-density response, $\partial n_\lambda(\mathbf{r})/\partial \lambda_i$, appearing in Eq. (22) can be evaluated by linearizing Eqs. (16), (15), and (13) with respect to wave function, density, and potential variations. Linearization of Eq. (16) leads to

$$\Delta n(\mathbf{r}) = 4\,\mathrm{Re} \sum_{n=1}^{N/2} \psi_n^*(\mathbf{r}) \Delta\psi_n(\mathbf{r}), \tag{23}$$

where the finite-difference operator $\Delta^\lambda$ is defined as

$$\Delta^\lambda F = \sum_i \frac{\partial F_\lambda}{\partial \lambda_i} \Delta\lambda_i. \tag{24}$$

The superscript $\lambda$ has been omitted in Eq. (23), as well as in any subsequent formulas where such an omission does not give rise to ambiguities. Since the external potential (both unperturbed and perturbed) is real, each Kohn-Sham eigenfunction and its complex conjugate are degenerate. As a consequence, the imaginary part of the sum appearing in Eq. (23) vanishes, so that the prescription to keep only the real part can be dropped.

The variation of the Kohn-Sham orbitals, $\Delta\psi_n(\mathbf{r})$, is obtained by standard first-order perturbation theory (Messiah, 1962):

$$(H_{SCF} - \epsilon_n)|\Delta\psi_n\rangle = -(\Delta V_{SCF} - \Delta\epsilon_n)|\psi_n\rangle, \tag{25}$$

where

$$H_{SCF} = -\frac{\hbar^2}{2m}\frac{\partial^2}{\partial \mathbf{r}^2} + V_{SCF}(\mathbf{r}) \tag{26}$$

is the unperturbed Kohn-Sham Hamiltonian,

$$\Delta V_{SCF}(\mathbf{r}) = \Delta V(\mathbf{r}) + e^2 \int \frac{\Delta n(\mathbf{r}')}{|\mathbf{r}-\mathbf{r}'|} d\mathbf{r}' + \left.\frac{dv_{xc}(n)}{dn}\right|_{n=n(\mathbf{r})} \Delta n(\mathbf{r}) \tag{27}$$

is the first-order correction to the self-consistent potential, and $\Delta\epsilon_n = \langle\psi_n|\Delta V_{SCF}|\psi_n\rangle$ is the first-order variation of the Kohn-Sham eigenvalue $\epsilon_n$.

In the atomic physics literature, an equation analogous to Eq. (25) is known as the Sternheimer equation, after the work in which it was first used to calculate atomic polarizabilities (Sternheimer, 1954). A self-consistent version of the Sternheimer equation was introduced by Mahan (1980) to calculate atomic polarizabilities within density-functional theory in the LDA. Similar methods are known in the quantum chemistry literature under the generic name of *analytic evaluation of second-order energy derivatives* (Gerratt and Mills, 1968; Amos, 1987). In the specific context of the Hartree-Fock approximation, the resulting algorithm is called the *coupled Hartree-Fock method* (Gerratt and Mills, 1968).

Equations (23)–(27) form a set of self-consistent equations for the perturbed system completely analogous to the Kohn-Sham equations in the unperturbed case—Eqs. (13), (15), and (16)—with the Kohn-Sham eigenvalue equation, Eq. (15), being replaced by the solution of a linear system, Eq. (25). In the present case, the self-consistency requirement manifests itself in the dependence of the right-hand side upon the solution of the linear system. As $\Delta V_{SCF}(\mathbf{r})$ is a linear functional of

$\Delta n(\mathbf{r})$, which in turn depends linearly on the $\Delta\psi$'s, the whole self-consistent calculation can be cast in terms of a generalized linear problem. Note, however, that the right-hand side of Eq. (25) for $\Delta\psi_n$ depends through $\Delta n$ on the solution of all the similar equations holding for the $\Delta\psi_m$ $(m\neq n)$. Hence all the $N$ equations, Eq. (25), are linearly coupled to each other, and the set of all the $\Delta\psi$'s is the solution of a linear problem whose dimension is $(NM/2\times NM/2)$, $M$ being the size of the basis set used to describe the $\psi$'s. The explicit form of this big linear equation can be worked out directly from Eqs. (23)–(27), or it can equivalently be derived from a variational principle, as explained in Sec. II.C.3. Whether this large linear system is better solved directly by iterative methods or by the self-consistent solution of the smaller linear systems given by Eq. (25) is a matter of computational strategy.

The first-order correction to a given eigenfunction of the Schrödinger equation, given by Eq. (25), is often expressed in terms of a sum over the spectrum of the unperturbed Hamiltonian,

$$\Delta\psi_n(\mathbf{r})=\sum_{m\neq n}\psi_m(\mathbf{r})\frac{\langle\psi_m|\Delta V_{SCF}|\psi_n\rangle}{\epsilon_n-\epsilon_m} \tag{28}$$

running over all the states of the system, occupied and empty, with the exception of the state being considered, for which the energy denominator would vanish. Using Eq. (28), the electron charge-density response, Eq. (23), can be cast into the form

$$\Delta n(\mathbf{r})=4\sum_{n=1}^{N/2}\sum_{m\neq n}\psi_n^*(\mathbf{r})\psi_m(\mathbf{r})\frac{\langle\psi_m|\Delta V_{SCF}|\psi_n\rangle}{\epsilon_n-\epsilon_m}. \tag{29}$$

Equation (29) shows that the contributions to the electron-density response coming from products of occupied states cancel each other, so that the $m$ index can be thought of as attaching to conduction states only. This is equivalent to saying that the electron-density distribution does not respond to a perturbation, which acts only on the occupied-state manifold (or, more generally, to the component of any perturbation which couples occupied states among each other).

The explicit evaluation of $\Delta\psi_n(\mathbf{r})$ from Eq. (28) would require a knowledge of the full spectrum of the Kohn-Sham Hamiltonian and extensive summations over conduction bands. In Eq. (25), instead, only knowledge of the occupied states of the system is needed to construct the right-hand side of the equation, and efficient iterative algorithms—such as the conjugate gradient (Press *et al.*, 1989; Štich *et al.*, 1989; Payne *et al.*, 1992) or minimal residual (Press *et al.* 1989; Saad and Schultz, 1986) methods—can be used for solution of the linear system. In this way the computational cost of determining of the density response to a single perturbation is of the same order as that needed to calculate the unperturbed ground-state density.

The left-hand side of Eq. (25) is singular because the linear operator appearing therein has a null eigenvalue. However, we saw above that the response of the system to an external perturbation depends only on the component of the perturbation that couples the occupied-state manifold with the empty-state one. The projection onto the empty-state manifold of the first-order correction to occupied orbitals can be obtained from Eq. (25) by replacing its right-hand side with $-P_c\Delta V_{SCF}|\psi_n\rangle$, where $P_c$ is the projector onto the empty-state manifold, and by adding to the linear operator on its left-hand side $H_{SCF}-\epsilon_n$, a multiple of the projector onto the occupied-state manifold, $P_v$, so as to make it nonsingular:

$$(H_{SCF}+\alpha P_v-\epsilon_n)|\Delta\psi_n\rangle=-P_c\Delta V_{SCF}|\psi_n\rangle. \tag{30}$$

In practice, if the linear system is solved by the conjugate-gradient or any other iterative method and the trial solution is chosen orthogonal to the occupied-state manifold, orthogonality is maintained during iteration without regard for the extra $P_v$ term on the left-hand side of Eq. (30).

The above discussion applies to insulators in which the gap is finite. In metals a finite density of states (DOS) occurs at the Fermi energy, and a change in the orbital occupation number may occur upon the application of an infinitesimal perturbation. The modifications of DFPT needed to treat the linear response of metals have been discussed by de Gironcoli (1995) and will be presented in some detail in Sec. II.C.4.

### 1. Monochromatic perturbations

One of the greatest advantages of DFPT—as compared to other nonperturbative methods for calculating the vibrational properties of crystalline solids (such as the frozen-phonon or molecular-dynamics spectral analysis methods)—is that within DFPT the responses to perturbations of different wavelengths are decoupled. This feature allows one to calculate phonon frequencies at arbitrary wave vectors $\mathbf{q}$ avoiding the use of supercells and with a workload that is essentially independent of the phonon wavelength. To see this in some detail, we first rewrite Eq. (30) by explicitly indicating the wave vector $\mathbf{k}$ and band index $v$ of the unperturbed wave function $\psi_v^{\mathbf{k}}$, and by projecting both sides of the equation over the manifold of states of wave vector $\mathbf{k}+\mathbf{q}$. Translational invariance requires that the projector onto the $\mathbf{k}+\mathbf{q}$ manifold, $P^{\mathbf{k}+\mathbf{q}}$, commute with $H_{SCF}$ and with the projectors onto the occupied- and empty-state manifolds, $P_v$ and $P_c$. By indicating with $P^{\mathbf{k}+\mathbf{q}}P_v=P_v^{\mathbf{k}+\mathbf{q}}$ and $P^{\mathbf{k}+\mathbf{q}}P_c=P_c^{\mathbf{k}+\mathbf{q}}$ the projectors onto the occupied and empty states of wave vector $\mathbf{k}+\mathbf{q}$, one can rewrite Eq. (30) as

$$(H_{SCF}+\alpha P_v^{\mathbf{k}+\mathbf{q}}-\epsilon_v^{\mathbf{k}})|\Delta\psi_v^{\mathbf{k}+\mathbf{q}}\rangle=-P_c^{\mathbf{k}+\mathbf{q}}\Delta V_{SCF}|\psi_v^{\mathbf{k}}\rangle, \tag{31}$$

where $|\Delta\psi_v^{\mathbf{k}+\mathbf{q}}\rangle=P^{\mathbf{k}+\mathbf{q}}|\Delta\psi_v^{\mathbf{k}}\rangle$. When one decomposes the perturbing potential $\Delta V_{SCF}$ into Fourier components,

$$\Delta V_{SCF}(\mathbf{r})=\sum_{\mathbf{q}}\Delta v_{SCF}^{\mathbf{q}}(\mathbf{r})e^{i\mathbf{q}\cdot\mathbf{r}}, \tag{32}$$

where $\Delta v^{\mathbf{q}}_{SCF}(\mathbf{r})$ is a lattice-periodic function, Eq. (31) can be cast into the form

$$\left( H^{\mathbf{k}+\mathbf{q}}_{SCF} + \alpha \sum_{v'} |u^{\mathbf{k}+\mathbf{q}}_{v'}\rangle\langle u^{\mathbf{k}+\mathbf{q}}_{v'}| - \epsilon^{\mathbf{k}}_{v} \right) |\Delta u^{\mathbf{k}+\mathbf{q}}_{v}\rangle = -\left[ 1 - \sum_{v'} |u^{\mathbf{k}+\mathbf{q}}_{v'}\rangle\langle u^{\mathbf{k}+\mathbf{q}}_{v'}| \right] \Delta v^{\mathbf{q}}_{SCF} |u^{\mathbf{k}}_{v}\rangle, \tag{33}$$

where $v'$ runs over the occupied states at $\mathbf{k}+\mathbf{q}$, $u^{\mathbf{k}}_{v}$ and $\Delta u^{\mathbf{k}+\mathbf{q}}_{v}$ are the periodic parts of the unperturbed wave function and of the $\mathbf{k}+\mathbf{q}$ Fourier component of its first-order correction, respectively, and the coordinate-representation kernel of the operator $H^{\mathbf{k}+\mathbf{q}}_{SCF}$, $h^{\mathbf{k}+\mathbf{q}}_{SCF}(\mathbf{r},\mathbf{r}') = \langle \mathbf{r}| H^{\mathbf{k}+\mathbf{q}}_{SCF} |\mathbf{r}'\rangle$, is defined in terms of the kernel of the self-consistent field Hamiltonian, $h^{(0)}_{SCF}(\mathbf{r},\mathbf{r}') = \langle \mathbf{r}| H_{SCF} |\mathbf{r}'\rangle$, by the relation

$$h^{\mathbf{k}+\mathbf{q}}_{SCF}(\mathbf{r},\mathbf{r}') = e^{-i(\mathbf{k}+\mathbf{q})\cdot\mathbf{r}} h^{0}_{SCF}(\mathbf{r},\mathbf{r}') e^{i(\mathbf{k}+\mathbf{q})\cdot\mathbf{r}'}. \tag{34}$$

Equation (33) shows that the time-consuming step of the self-consistent process, Eq. (30), can be carried out working on lattice-periodic functions only, and the corresponding numerical workload is therefore independent of the wavelength of the perturbation.

Let us now see how the other two steps of the self-consistent process, Eqs. (23) and (27), can be carried out in a similar way by treating each Fourier component of the perturbing potential and of the charge-density response independently. The Fourier components of any real function (such as $\Delta n$ and $\Delta v$) with wave vectors $\mathbf{q}$ and $-\mathbf{q}$ are complex conjugates of each other: $\Delta n^{-\mathbf{q}}(\mathbf{r}) = [\Delta n^{\mathbf{q}}(\mathbf{r})]^*$, and similarly for the potential. Because of time-reversal symmetry, a similar result applies to wave functions: $\Delta u^{\mathbf{k}+\mathbf{q}}_{v}(\mathbf{r}) = [\Delta u^{-\mathbf{k}-\mathbf{q}}_{v}(\mathbf{r})]^*$. Taking into account these relations, the Fourier component of the charge-density response at wave vector $\mathbf{q}$ is obtained from Eq. (23):

$$\Delta n^{\mathbf{q}}_{v}(\mathbf{r}) = 4 \sum_{\mathbf{k}v} u^{\mathbf{k}*}_{v}(\mathbf{r}) \Delta u^{\mathbf{k}+\mathbf{q}}_{v}(\mathbf{r}). \tag{35}$$

Equation (27) is a *linear* relation between the self-consistent variation of the potential and the variation of the electron charge-density distribution. The Fourier component of the self-consistent potential response reads

$$\Delta v^{\mathbf{q}}_{SCF}(\mathbf{r}) = \Delta v^{\mathbf{q}}(\mathbf{r}) + e^2 \int \frac{\Delta n^{\mathbf{q}}(\mathbf{r}')}{|\mathbf{r}-\mathbf{r}'|} e^{-i\mathbf{q}\cdot(\mathbf{r}-\mathbf{r}')} d\mathbf{r}' + \left. \frac{dv_{xc}(n)}{dn} \right|_{n=n(\mathbf{r})} \Delta n^{\mathbf{q}}(\mathbf{r}). \tag{36}$$

The sampling of the Brillouin zone needed for the evaluation of Eq. (35) is analogous to that needed for the calculation of the unperturbed electron charge density, Eq. (16), and it requires in most cases an equal number of discrete $\mathbf{k}$ points. An exception to this rule occurs when calculating the response of insulators to macroscopic electric fields—as discussed in Sec. II.C.2—and for the calculation of phonons in metals in the presence of Kohn anomalies—as discussed in Sec. II.C.4.

In conclusion, Eqs. (33), (35), and (36) form a set of self-consistent relations for the charge-density and wave-function linear response to a perturbation of a wave vector $\mathbf{q}$, which can be solved in terms of lattice-periodic functions only, and which is decoupled from all other sets of similar equations holding for other Fourier components of the same perturbation. Thus perturbations of different periodicity can be treated independently of each other with a numerical workload that is, for each perturbation, of the same order as that needed for the unperturbed system.

### 2. Homogeneous electric fields

The electron-density response to a homogeneous (*macroscopic*) electric field requires a special treatment. In fact, several electrostatic properties of an infinite solid are, strictly speaking, ill defined in the long-wavelength limit because the electrostatic potential describing a homogeneous electric field $\mathbf{E}$, $[V_{\mathbf{E}}(\mathbf{r}) = e\mathbf{E}\cdot\mathbf{r}]$, is both unbounded from below and incompatible with Born-von-Kármán periodic boundary conditions. In the linear regime, however, these pathologies can be efficiently treated in an elementary way. As in the harmonic approximation, the lattice-dynamical properties of polar insulators depend for long wavelengths on the linear response to a homogeneous electric field (see Sec. II.D.2), so we shall limit our analysis here to the linear regime and postpone the discussion of nonlinear electrostatic effects until Sec. II.F.

From a mathematical point of view, the main difficulty in treating macroscopic electric fields stems from the fact that the position operator $\mathbf{r}$ is ill defined in a periodic system as are its matrix elements between wave functions satisfying Born-von-Kármán boundary conditions. The wave-function response to a given perturbation, Eq. (28), however, depends only on the *off-diagonal* matrix elements of the perturbing potential between eigen-functions of the unperturbed Hamiltonian. Such matrix elements are indeed well defined even for a macroscopic electric field, as can be seen by rewriting them in terms of the commutator between $\mathbf{r}$ and the unperturbed Hamiltonian, which is a lattice-periodic operator:

$$\langle \psi_m | \mathbf{r} | \psi_n \rangle = \frac{\langle \psi_m | [H_{SCF}, \mathbf{r}] | \psi_n \rangle}{\epsilon_m - \epsilon_n}, \quad \forall m \neq n. \tag{37}$$

If the self-consistent potential acting on the electrons is local, the above commutator is simply proportional to the momentum operator:

$$[H_{SCF}, \mathbf{r}] = -\frac{\hbar^2}{m} \frac{\partial}{\partial \mathbf{r}}. \tag{38}$$

Otherwise, the commutator will contain an explicit contribution from the nonlocal part of the potential (Baroni and Resta, 1986b; Baroni *et al.*, 1987a; Hybertsen and Louie, 1987).

When calculating the response of a crystal to an applied electric field $\mathbf{E}_0$, one must consider that the screened field acting on the electrons is

$$\mathbf{E}=\mathbf{E}_0-4\pi\mathbf{P}, \tag{39}$$

where $\mathbf{P}$ is the electronic polarization linearly induced by the screened (i.e., self-consistent) field $\mathbf{E}$:

$$\mathbf{P}=-\frac{e}{V}\int_V \mathbf{r}\Delta^{\mathbf{E}}n(\mathbf{r})d\mathbf{r}. \tag{40}$$

In addition to the macroscopic screening expressed by Eq. (39), the density response to an external macroscopic electric field $\mathbf{E}_0$ also involves microscopic Fourier components,

$$\Delta^{\mathbf{E}}n(\mathbf{r})=4\sum_{n=1}^{N/2}\psi_n^*(\mathbf{r})\Delta^{\mathbf{E}}\psi_n(\mathbf{r}), \tag{41}$$

responsible for the so-called *local fields*, which must be taken into account in the self-consistent procedure.

Equation (40) is, of course, well defined for any finite system. The electric polarization of a macroscopic piece of matter, however, is ill defined in that it depends on the details of the charge distribution at the surface of the sample. Nevertheless, the polarization linearly induced by a given perturbation is well defined, and Eq. (40) can in fact be recast into a boundary-insensitive form (Littlewood, 1980). To see this, we use Eq. (23) and we obtain from Eq. (40)

$$\begin{aligned}\mathsf{P}_\alpha&=-\frac{4e}{V}\sum_{n=1}^{N/2}\langle\psi_n|r_\alpha|\Delta^{\mathbf{E}}\psi_n\rangle\\&=-\frac{4e}{V}\sum_{n=1}^{N/2}\sum_{m=N/2+1}^{\infty}\frac{\langle\psi_n|[H_{SCF},r_\alpha]||\psi_m\rangle}{(\epsilon_n-\epsilon_m)}\\&\quad\times\langle\psi_m|\Delta^{\mathbf{E}}\psi_n\rangle,\end{aligned} \tag{42}$$

where the subscript $\alpha$ indicates Cartesian components. Let us introduce the wave function $\overline{\psi}_n^\alpha(\mathbf{r})$ defined as

$$\overline{\psi}_n^\alpha(\mathbf{r})=\sum_{m\neq n}\psi_m(\mathbf{r})\frac{\langle\psi_m|[H_{SCF},r_\alpha]|\psi_n\rangle}{(\epsilon_m-\epsilon_n)}. \tag{43}$$

Here $\overline{\psi}$ satisfies an equation of the same kind as Eq. (30) with the perturbing potential on its right-hand side replaced by $[H_{SCF},r_\alpha]$:

$$(H_{SCF}-\epsilon_n)|\overline{\psi}_n^\alpha\rangle=P_c[H_{SCF},r_\alpha]|\psi_n\rangle. \tag{44}$$

The induced polarization, Eq. (42), can be recast in the form

$$\mathsf{P}_\alpha=-\frac{4e}{V}\sum_{n=1}^{N/2}\langle\overline{\psi}_n^\alpha|\Delta^{\mathbf{E}}\psi_n\rangle, \tag{45}$$

where the anti-Hermitian character of the commutator has been used.

The first-order correction to a crystal wave function due to a perturbing homogeneous electric field $\mathbf{E}$ is given by the response to the full, i.e., macroscopic *and* microscopic, perturbation

$$(H_{SCF}-\epsilon_n)|\Delta^{\mathbf{E}}\psi_n\rangle=-e\sum_\alpha\mathsf{E}_\alpha|\overline{\psi}_n^\alpha\rangle-P_c\Delta V^{lf}|\psi_n\rangle, \tag{46}$$

where

$$\Delta V^{lf}(\mathbf{r})=e^2\int\frac{\Delta^{\mathbf{E}}n(\mathbf{r}')}{|\mathbf{r}-\mathbf{r}'|}d\mathbf{r}'+\left.\frac{dv_{xc}(n)}{dn}\right|_{n=n(\mathbf{r})}\Delta^{\mathbf{E}}n(\mathbf{r}). \tag{47}$$

The terms of the sum appearing in Eq. (45) implicitly behave as the inverse of the difference between a conduction and a valence energy eigenvalue to the third power, $\sim(\epsilon_c-\epsilon_v)^{-3}$. One of the energy denominators results from the standard first-order perturbation calculation of the perturbed wave function $\Delta^{\mathbf{E}}\psi_n$, Eq. (28). A second energy denominator comes from the term $\overline{\psi}$ on the right-hand side of Eq. (46), which requires by itself the solution of a linear equation analogous to that of first-order perturbation theory, Eq. (44). The third energy denominator comes from $\overline{\psi}$, which appears explicitly in brackets in Eq. (45). This dependence of the terms of the sum upon the direct gaps at different $\mathbf{k}$ points of the Brillouin zone may require a rather fine sampling of the Brillouin zone when the fundamental gap is small. In these cases, the number of $\mathbf{k}$ points needed to compute the dielectric constant is substantially larger than that needed by a standard unperturbed calculation (Baroni and Resta, 1986a, 1986b; de Gironcoli *et al.*, 1989).

The self-consistent cycle defined by Eqs. (39)–(47) can be performed starting from a given external macroscopic electric field $\mathbf{E}_0$ and updating at each iteration, via Eqs. (45), (39), (41), and (47), the macroscopic and microscopic parts of the electronic density response and the perturbing potential, one then solve Eq. (46) for $\Delta^{\mathbf{E}}\psi$ and repeats. However, for computational purposes, it is simpler and more convenient to keep the value of the screened electric field $\mathbf{E}$ fixed and let only the microscopic components of the potential vary while iterating Eqs. (46), (41), and (47). The macroscopic polarization is then calculated only at the end, when self-consistency is achieved, using Eq. (45). Physically, this is equivalent to calculating the polarization response to a given screened electric field $\mathbf{E}$ instead of to the bare electric field $\mathbf{E}_0$.

The electronic contribution to the dielectric tensor, $\epsilon_\infty^{\alpha\beta}$, for the general (low-symmetry) case, can be derived from simple electrostatics. Using Eq. (39) and the definition of $\epsilon_\infty^{\alpha\beta}$, one has

$$\mathsf{E}_{0\alpha}=(\mathsf{E}_\alpha+4\pi\mathsf{P}_\alpha)=\sum_\beta\epsilon_\infty^{\alpha\beta}\mathsf{E}_\beta. \tag{48}$$

Using Eq. (45) to calculate the polarization induced in the $\alpha$ direction when a field is applied in the $\beta$ direction, one finally obtains

$$\epsilon_\infty^{\alpha\beta}=\delta_{\alpha\beta}-\frac{16\pi e}{V\mathsf{E}_\beta}\sum_{n=1}^{N/2}\langle\overline{\psi}_n^\alpha|\Delta^{\mathsf{E}_\beta}\psi_n\rangle. \tag{49}$$

### 3. Relation to the variational principle

The Kohn-Sham equations are the Euler equations which solve the Hohenberg-Kohn variational principle. The equations of DFPT introduced in Sec. II.C can be seen as a set of equations that solve *approximately* the variational principle when the external potential is perturbed. Alternatively, these equations can be thought of as exactly minimizing an approximate energy functional (Gonze *et al.*, 1992; Gonze, 1995a, 1997). To see this point in some detail, let us consider the energy functional as depending explicitly on the set of Kohn-Sham orbitals $\psi \equiv \{\psi_n\}$ (assumed to be real) and parametrically on the external potential $V(\mathbf{r})$:

$$E[\psi;V] = -2\frac{\hbar^2}{2m}\sum_{n=1}^{N/2}\int \psi_n(\mathbf{r})\frac{\partial^2\psi_n(\mathbf{r})}{\partial\mathbf{r}^2}d\mathbf{r} + \int V(\mathbf{r})n(\mathbf{r})d\mathbf{r} + \frac{e^2}{2}\int\frac{n(\mathbf{r})n(\mathbf{r}')}{|\mathbf{r}-\mathbf{r}'|}d\mathbf{r}d\mathbf{r}' + E_{xc}[n]. \tag{50}$$

The functional derivative of the above functional with respect to $\psi_n$ is

$$\frac{\delta E}{\delta\psi_n(\mathbf{r})} = 2H_{SCF}\psi_n(\mathbf{r}). \tag{51}$$

The Euler equation thus reads

$$H_{SCF}|\psi_n\rangle = \sum_{m=1}^{N/2}\Lambda_{nm}|\psi_m\rangle, \tag{52}$$

where the $\Lambda$'s are a set of Lagrange multipliers introduced so as to enforce the orthonormality of the $\psi$'s. Equation (52) is invariant with respect to a unitary transformation within the manifold of the $\psi$'s, so that the usual Kohn-Sham equation, Eq. (15), is recovered in a representation that diagonalizes the $\Lambda$ matrix.

Let us now indicate by $\psi^{(0)}$ the solutions of the Kohn-Sham equations corresponding to a particular choice of the external potential $V^{(0)}(\mathbf{r})$ (the *unperturbed* potential), and let us indicate by $\Delta V$ and $\Delta\psi$ the differences between the actual potential and orbitals and their unperturbed values. The energy functional, Eq. (50), can be equally seen as depending on $\Delta\psi$ and $\Delta V$: $E \equiv E[\{\psi^{(0)}+\Delta\psi\};V^{(0)}+\Delta V]$. We now consider the *approximate* functional $E^{(2)}$, which is obtained from $E$ by truncating its Taylor expansion in terms of $\Delta\psi$ and $\Delta V$ to second order:

$$E^{(2)}[\{\Delta\psi\};\Delta V] = E[\{\psi^{(0)}\};V^{(0)}] + \int\frac{\delta E}{\delta V(\mathbf{r})}\Delta V(\mathbf{r})d\mathbf{r} + \sum_{n=1}^{N/2}\int\frac{\delta E}{\delta\psi_n(\mathbf{r})}\Delta\psi_n(\mathbf{r})d\mathbf{r} + \sum_{n=1}^{N/2}\int\frac{\delta^2 E}{\delta\psi_n(\mathbf{r})\,\delta V(\mathbf{r}')} \times\Delta\psi_n(\mathbf{r})\Delta V(\mathbf{r}')d\mathbf{r}d\mathbf{r}' + \frac{1}{2}\sum_{n,m=1}^{N/2}\int\frac{\delta^2 E}{\delta\psi_n(\mathbf{r})\,\delta\psi_m(\mathbf{r}')} \times\Delta\psi_n(\mathbf{r})\Delta\psi_m(\mathbf{r}')d\mathbf{r}d\mathbf{r}', \tag{53}$$

where we have omitted the second derivative with respect to $V$ because $E$ is linear in $V$. Besides Eq. (51), the required functional derivatives are

$$\left.\frac{\delta E}{\delta V(\mathbf{r})}\right|_{\psi=\psi^{(0)}} = n^{(0)}(\mathbf{r}) \tag{54}$$

$$\left.\frac{\delta^2 E}{\delta\psi_n(\mathbf{r})\,\delta V(\mathbf{r}')}\right|_{\psi=\psi^{(0)}} = 2\psi_n^{(0)}(\mathbf{r})\,\delta(\mathbf{r}-\mathbf{r}') \tag{55}$$

$$\left.\frac{\delta^2 E}{\delta\psi_n(\mathbf{r})\,\delta\psi_m(\mathbf{r}')}\right|_{\psi=\psi^{(0)}} = 2h_{SCF}^{(0)}(\mathbf{r},\mathbf{r}')\,\delta_{mn} + 4K(\mathbf{r},\mathbf{r}')\psi_n^{(0)}(\mathbf{r})\psi_m^{(0)}(\mathbf{r}'), \tag{56}$$

where

$$K(\mathbf{r},\mathbf{r}') = \frac{e^2}{|\mathbf{r}-\mathbf{r}'|} + \frac{\delta^2 E_{xc}}{\delta n(\mathbf{r})\,\delta n(\mathbf{r}')}, \tag{57}$$

and $h_{SCF}^{(0)}(\mathbf{r},\mathbf{r}')$ is the kernel of the unperturbed Kohn-Sham Hamiltonian. The energy functional, Eq. (53), must be minimized under the constraint that the resulting solutions lead to an orthonormal set of occupied states:

$$\langle\psi_n^{(0)}+\Delta\psi_n|\psi_m^{(0)}+\Delta\psi_m\rangle = \delta_{nm}. \tag{58}$$

This leads to the Euler equations

$$H_{SCF}^{(0)}|\Delta\psi_n\rangle - \sum_{m=1}^{N/2}\Lambda_{nm}|\Delta\psi_m\rangle = -\Delta V_{SCF}|\psi_n^{(0)}\rangle + \sum_{m=1}^{N/2}(\Lambda_{nm}-\epsilon_n\delta_{nm})|\psi_m^{(0)}\rangle, \tag{59}$$

where the $\Lambda$'s are a set of Lagrange multipliers introduced so as to enforce the constraint in Eq. (58), and

$$\Delta V_{SCF}(\mathbf{r}) = \Delta V(\mathbf{r}) + 2\sum_{n=1}^{N/2}\int K(\mathbf{r},\mathbf{r}')\psi_n^{(0)}(\mathbf{r}')\Delta\psi_n(\mathbf{r}')d\mathbf{r}' \tag{60}$$

is the first-order variation of the self-consistent potential. We now project both sides of Eq. (59) onto $\psi_k^{(0)}$. Taking into account that by Eq. (58) $\langle\Delta\psi_n|\psi_k^{(0)}\rangle = \mathcal{O}(\Delta^2)$, to linear order in $\Delta$ one obtains

$$\Lambda_{mn} - \epsilon_n\delta_{nm} = \langle\psi_m^{(0)}|\Delta V_{SCF}|\psi_n^{(0)}\rangle. \tag{61}$$

To linear order in $\Delta$, Eq. (59) can thus be cast in the form

$$(H^{(0)}_{SCF}-\epsilon_n)|\Delta\psi_n\rangle = -\Delta V_{SCF}|\psi^{(0)}_n\rangle + \sum_{m=1}^{N/2} |\psi^{(0)}_m\rangle\langle\psi^{(0)}_m|\Delta V_{SCF}|\psi^{(0)}_n\rangle = -P_c\Delta V_{SCF}|\psi^{(0)}_n\rangle, \quad (62)$$

which is essentially the same as Eq. (30). The set of perturbed orbitals $\{\Delta\psi\}$ is the solution of $N$ coupled linear systems whose dimension is the size of the basis set $M$ [Eq. (62) or Eq. (30), where the coupling comes from the dependence of the self-consistent potential on all the orbitals]. Alternatively, it can be seen as a huge linear system of dimension $M\times N/2$, which is obtained by inserting the expression for $\Delta V_{SCF}$, Eq. (60), into Eqs. (62) or (30). The latter is naturally derived from the minimization of the functional $E^{(2)}$, Eq. (53), which is quadratic.

This variational approach shows that the error on the functional to be minimized, Eq. (53), is proportional to the *square* of the error on the minimization variables $\Delta\psi$. This fact can be exploited in a calculation of the second-order mixed derivatives, Eq. (22). It can be shown that a variational expression can be constructed for mixed derivatives as well (Gonze *et al.*, 1992; Gonze, 1997).

#### 4. Metals

Density-functional perturbation theory, as presented above, is directly applicable to metals, provided the (electronic) temperature vanishes, so that a clear-cut separation between occupied and empty states is possible. In this case, however, the number of $k$ points needed to correctly represent the effect of the Fermi surface would be very large. Practical implementations of DFPT to metallic systems have been discussed by Quong and Klein (1992) and by de Gironcoli (1995), in the pseudopotential formalism, and by Savrasov (1992), in the linearized muffin-tin orbital framework. In the following, we shall closely follow the formulation of de Gironcoli (1995), which is based on the smearing technique for dealing with Fermi-surface effects.

In the smearing approach, each Kohn-Sham energy level is broadened by a smearing function,

$$\delta_\sigma(\epsilon) = \frac{1}{\sigma}\tilde{\delta}(\epsilon/\sigma), \quad (63)$$

where $\tilde{\delta}(x)$ is any function that integrates to 1—so that $\delta_\sigma(\epsilon)$ tends to the Dirac $\delta$ function in the limit of vanishing smearing width $\sigma$. Many kinds of smearing functions $\tilde{\delta}(x)$ can be used: Fermi-Dirac broadening,[3] Lorentzian, Gaussian (Fu and Ho, 1983), Gaussian combined with polynomials (Methfessel and Paxton, 1989), or cold smearing (Marzari *et al.*, 1999) functions, to recall just a few of those used in the literature. While the choice of a given smearing function is to some extent a matter of personal taste and computational convenience, the specific choice of Fermi-Dirac broadening allows one to account explicitly for the effects of a finite temperature ($T=\sigma/k_B$) when needed. The (local) density of states resulting from the broadened energy levels will be the original density of states, convoluted with the smearing function:

$$n(\mathbf{r},\epsilon) = \sum_n \frac{1}{\sigma}\tilde{\delta}\left(\frac{\epsilon-\epsilon_n}{\sigma}\right)|\psi_n(\mathbf{r})|^2, \quad (64)$$

where the sum refers both to the discrete **k**-vector index and to band and spin indices for all bands. From this basic quantity the electron density follows:

$$n(\mathbf{r}) = \int_{-\infty}^{\epsilon_F} n(\mathbf{r},\epsilon)\,d\epsilon = \sum_n \tilde{\theta}\left(\frac{\epsilon_F-\epsilon_n}{\sigma}\right)|\psi_n(\mathbf{r})|^2, \quad (65)$$

where $\tilde{\theta}(x)=\int_{-\infty}^{x}\tilde{\delta}(y)\,dy$ is a smooth approximation to the step function, and the Fermi energy is determined by the normalization to the total number of electrons,

$$N = \int_{-\infty}^{\epsilon_F} n(\epsilon)\,d\epsilon = \sum_n \tilde{\theta}\left(\frac{\epsilon_F-\epsilon_n}{\sigma}\right). \quad (66)$$

The advantage of this procedure is that after convolution the (modified) local density of states can be computed accurately on a discrete grid of points in the Brillouin zone, provided that the average separation between neighboring eigenvalues is small with respect to the broadening width $\sigma$.

Given the definition of the local density of states, Eq. (64), the consistent way to define the auxiliary Kohn-Sham kinetic-energy functional—or its analog in the finite-temperature theory (Mermin, 1965)—is through the Legendre transform of the single-particle energy integral:

$$T_s[n] = \int_{-\infty}^{\epsilon_F}\epsilon n(\epsilon)\,d\epsilon - \int V_{SCF}(\mathbf{r})n(\mathbf{r})\,d\mathbf{r} = \sum_n\left[-\frac{\hbar^2}{2m}\tilde{\theta}\left(\frac{\epsilon_F-\epsilon_n}{\sigma}\right)\int\psi^*_n(\mathbf{r})\frac{\partial^2\psi_n(\mathbf{r})}{\partial\mathbf{r}^2}\,d\mathbf{r} + \sigma\tilde{\theta}_1\left(\frac{\epsilon_F-\epsilon_n}{\sigma}\right)\right], \quad (67)$$

where $\tilde{\theta}_1(x)=\int_{-\infty}^{x}y\tilde{\delta}(y)\,dy$. Note that when a finite electronic temperature is considered the Kohn-Sham auxiliary functional $T_s[n]$ contains both the kinetic energy and the entropy contribution to the electronic free energy of the independent-particle system. These two contributions appear separately in the last expression for $T_s[n]$ in Eq. (67), where it can be verified that for Fermi-Dirac broadening $\tilde{\theta}_1(x)=f\log(f)+(1-f)\log(1-f)$, with $f=\tilde{\theta}(x)$ as required. With the definitions above, for any kind of smearing function, the usual Kohn-Sham equations follow from the minimization of the total energy. The price to be paid for the computational simplicity of the smearing approach is that the computed total energy depends on the chosen broaden-

[3] In this case the broadening function is the derivative of the Fermi-Dirac distribution function: $\tilde{\delta}(x)=1/2[1+\cosh(x)]^{-1}$.

ing width, and results for finite broadening widths must be corrected for, unless the shape of the smearing function is such that this dependence is reduced to within acceptable values. Various discussions of this issue can be found in the literature (Methfessel and Paxton, 1989; De Vita, 1992; de Gironcoli, 1995; Marzari *et al.*, 1999).

Forces and other first-order energy derivatives can be computed in the usual way from Eqs. (8) and (21) which require only a knowledge of the unperturbed electronic density. Similarly second-order derivatives are computed from Eq. (22) where the first order variation of the density is also needed. Direct variation of Eq. (65) provides the required expression for $\Delta n(\mathbf{r})$:

$$\Delta n(\mathbf{r}) = \sum_n \tilde{\theta}_{F,n}[\psi_n^*(\mathbf{r})\Delta\psi_n(\mathbf{r}) + \text{c.c.}] + \sum_n |\psi_n(\mathbf{r})|^2 \tilde{\delta}_{F,n}(\Delta\epsilon_F - \Delta\epsilon_n), \tag{68}$$

where we have defined $\tilde{\theta}_{n,m} = \tilde{\theta}[(\epsilon_n - \epsilon_m)/\sigma]$ and $\tilde{\delta}_{n,m} = (1/\sigma)\tilde{\delta}[(\epsilon_n - \epsilon_m)/\sigma]$. The last term in Eq. (68) accounts for possible changes in occupation numbers induced by shifts in the single-particle energies ($\Delta\epsilon_n = \langle\psi_n|\Delta V_{SCF}|\psi_n\rangle$) as well as in the Fermi energy of the system. Whether or not this term is present depends on the thermodynamic ensemble used: it is absent if the chemical potential is kept fixed, whereas it might be present if the number of electrons is fixed. Even in this last case the Fermi energy is unaffected by the perturbation to linear order, unless the perturbation is lattice periodic (monochromatic with $\mathbf{q}=0$). Let us neglect this term for the time being and come back to it at the end of the section.

Substituting in Eq. (68) the definition for $\Delta\psi_n(\mathbf{r})$ from standard perturbation theory, Eq. (28), and exploiting the symmetry between the two contributions in square brackets, one obtains the following well-known expression for the first-order variation of the electronic density in a metal:

$$\Delta n(\mathbf{r}) = \sum_{n,m} \frac{\tilde{\theta}_{F,n} - \tilde{\theta}_{F,m}}{\epsilon_n - \epsilon_m} \psi_n^*(\mathbf{r})\psi_m(\mathbf{r})\langle\psi_m|\Delta V_{SCF}|\psi_n\rangle, \tag{69}$$

where the term in $\Delta\epsilon_n$ in Eq. (68) has become the $n=m$ term in the above sum and the incremental ratio $(\tilde{\theta}_{F,n} - \tilde{\theta}_{F,m})/(\epsilon_n - \epsilon_m)$ must be substituted for its limit, $-\tilde{\delta}_{F,n}$, whenever $\epsilon_m \to \epsilon_n$. This limit is always finite for any finite broadening linewidth or temperature, and this expression is therefore numerically stable even in the presence of vanishingly small virtual excitation energies.

In order to avoid a double sum over occupied and unoccupied states, we use the relation $\tilde{\theta}(x) + \tilde{\theta}(-x) = 1$ and the symmetry between $i$ and $j$ to get

$$\Delta n(\mathbf{r}) = 2\sum_{n,m} \frac{\tilde{\theta}_{F,n} - \tilde{\theta}_{F,m}}{\epsilon_n - \epsilon_m} \tilde{\theta}_{m,n} \psi_n^*(\mathbf{r})\psi_m(\mathbf{r}) \times \langle\psi_m|\Delta V_{SCF}|\psi_n\rangle, \tag{70}$$

where the sum over the first index can be limited to states that have non-negligible occupation. This expression can be further simplified, avoiding the explicit sum over the second index, by rewriting it as

$$\Delta n(\mathbf{r}) = 2\sum_n \psi_n^*(\mathbf{r})\Delta\psi_n(\mathbf{r}), \tag{71}$$

where the $\Delta\psi_n$'s satisfy the equation

$$[H_{SCF} + Q - \epsilon_n]\Delta\psi_n = -[\tilde{\theta}_{F,n} - P_n]\Delta V_{SCF}|\psi_n\rangle, \tag{72}$$

with

$$Q = \sum_k \alpha_k |\psi_k\rangle\langle\psi_k|, \quad P_n = \sum_m \beta_{n,m}|\psi_m\rangle\langle\psi_m|,$$

and

$$\beta_{n,m} = \tilde{\theta}_{F,n}\tilde{\theta}_{n,m} + \tilde{\theta}_{F,m}\tilde{\theta}_{m,n} + \alpha_m \frac{\tilde{\theta}_{F,n} - \tilde{\theta}_{F,m}}{\epsilon_n - \epsilon_m}\tilde{\theta}_{m,n}. \tag{73}$$

In the above equations, the $\alpha_k$'s are chosen in such a way that the $Q$ operator makes the linear system, Eq. (72), nonsingular for all nonvanishing $\Delta\psi_n$. A possible simple choice is

$$\alpha_k = \max(\epsilon_F + \Delta - \epsilon_k, 0), \tag{74}$$

with $\Delta \approx 3-4\sigma$. Another, even simpler, choice is to set $\alpha_k$ equal to the occupied bandwidth plus, say, $3\sigma$ for all partially occupied states, and equal to zero when the state is totally unoccupied. It can be easily verified that, since $\alpha_k$ vanishes when $\psi_k$ is unoccupied, $\beta_{n,m}$ also vanishes when any of its indices refers to an unoccupied state. Therefore the $Q$ and $P$ operators involve only the small number of partially filled bands, and the first-order variation of the wave functions and of the charge density can be computed avoiding any explicit reference to unoccupied states, much in the same way as for insulating materials. In fact, if the above scheme is applied to an insulator using a smearing width much smaller than its fundamental band gap, all the metallic equations, Eqs. (71)–(73), reduce numerically to their insulating analogs, Eqs. (23) and (30).

The expression for the charge density linearly induced by a given perturbation, Eqs. (69) and (70), involves an energy denominator that vanishes for metals. In one dimension, this vanishing denominator gives rise to a divergence in the screening of perturbations whose wave vector is twice the Fermi momentum, or $2k_F$. This divergence is smeared in two dimensions and suppressed in three dimensions by volume effects. However, if the topology of the Fermi surface is such that two finite portions of it are parallel and connected by a wave vector, which for convenience we shall name $2k_F$ (*nesting*), the screening to perturbations of wave vector $2k_F$ will diverge even in three dimension. This is the physical mechanism giving rise to Kohn anomalies in the vibrational spectra of certain metals. The sampling of the Brillouin zone necessary to evaluate the sum over (partially) occupied states in Eqs. (69) and (70) is in ordinary

cases similar to that needed to calculate the unperturbed charge-density distribution. Near a Kohn anomaly, however, a fine sampling of the Fermi surface is necessary, and the number of needed points in the Brillouin zone is correspondingly larger.

Periodic ($\mathbf{q}=0$) perturbations may induce a shift of the Fermi energy. In this case Eq. (71) must be modified:

$$\Delta n(\mathbf{r})=2\sum_n \psi_n^*(\mathbf{r})\Delta\psi_n(\mathbf{r})+n(\mathbf{r},\epsilon_F)\Delta\epsilon_F, \tag{75}$$

all other technical details remaining unchanged. In order to find out the appropriate value of the Fermi energy shift, let us examine the perturbation in the $\mathbf{q}\to 0$ limit. Let us consider the Fourier transform of the self-consistent perturbing potential $\Delta V_{SCF}(\mathbf{q})=1/V\int \Delta V_{SCF}(\mathbf{r})e^{-i\mathbf{q}\cdot\mathbf{r}}d\mathbf{r}$. Its macroscopic ($\mathbf{q}\approx 0$) component reads

$$\Delta V_{SCF}(\mathbf{q})=\Delta V(\mathbf{q})+\frac{4\pi e^2}{q^2}\Delta n(\mathbf{q})+\frac{dv_{xc}}{dn}\Delta n(\mathbf{q}), \tag{76}$$

where the last term is the exchange-correlation contribution, $\Delta V(\mathbf{q})=-(4\pi e^2/q^2)\Delta n_{ext}(\mathbf{q})$ is the macroscopic electrostatic component of the external perturbing potential, and $\Delta n_{ext}(\mathbf{q})$ is finite in the $\mathbf{q}\to 0$ limit. On the other hand, the macroscopic component of the density response is

$$\Delta n(\mathbf{q})=-n(\epsilon_F)\Delta V_{SCF}(\mathbf{q})+\Delta n^{lf}(\mathbf{q}), \tag{77}$$

where $\Delta n^{lf}$ is the density response to the nonmacroscopic (local fields) components of the self-consistent potential. As $\Delta n^{lf}$ and the DOS at the Fermi energy, $n(\epsilon_F)$, are both finite, $\Delta V_{SCF}$ and $\Delta n$ must not diverge when $\mathbf{q}\to 0$, otherwise Eqs. (76) and (77) could not be satisfied at the same time. This implies, from Eq. (76), macroscopic charge neutrality for the perturbed system, that is, $\Delta n_{ext}(\mathbf{q})=\Delta n(\mathbf{q})+\mathcal{O}(q^2)$ for $\mathbf{q}\approx 0$, a condition that in turn implies in Eq. (77)

$$\Delta V_{SCF}(\mathbf{q})=-\frac{\Delta n_{ext}(\mathbf{q})-\Delta n^{lf}(\mathbf{q})}{n(\epsilon_F)}+\mathcal{O}(q^2). \tag{78}$$

The lattice-periodic ($\mathbf{q}=0$) result can be obtained by taking the $\mathbf{q}\to 0$ limit of the above equations. In this case, however, it is customary to set arbitrarily to zero the macroscopic electrostatic component of the self-consistent potential. The charge neutrality condition is thus enforced by a compensating shift in the Fermi energy, equal and opposite to the above result:

$$\Delta\epsilon_F=\frac{\Delta n_{ext}(\mathbf{q}=0)+\int n(\mathbf{r},\epsilon_F)\Delta V_{SCF}(\mathbf{r})d\mathbf{r}}{n(\epsilon_F)}. \tag{79}$$

### D. Phonons

#### 1. Vibrational states in crystalline solids

In crystalline solids, the nuclear positions appearing in the definition of the interatomic force constants Eq. (5), are labeled by an index $I$, which indicates the unit cell $l$ to which a given atom belongs and the positions of the atom within that unit cell $I\equiv\{l,s\}$. The position of the $I$th atom is thus

$$\mathbf{R}_I\equiv\mathbf{R}_l+\boldsymbol{\tau}_s+\mathbf{u}_s(l), \tag{80}$$

where $\mathbf{R}_l$ is the position of the $l$th unit cell in the Bravais lattice, $\boldsymbol{\tau}_s$ is the equilibrium position of the atom in the unit cell, and $\mathbf{u}_s(l)$ indicates the deviation from equilibrium of the nuclear position. Because of translational invariance, the matrix of the interatomic force constants, Eq. (10), depends on $l$ and $m$ only through the difference $\mathbf{R}\equiv\mathbf{R}_l-\mathbf{R}_m$:

$$C_{st}^{\alpha\beta}(l,m)\equiv\frac{\partial^2 E}{\partial u_s^\alpha(l)\partial u_t^\beta(m)}=C_{st}^{\alpha\beta}(\mathbf{R}_l-\mathbf{R}_m), \tag{81}$$

where the Greek superscripts indicate Cartesian components. The Fourier transform of $C_{st}^{\alpha\beta}(\mathbf{R})$ with respect to $\mathbf{R}$, $\tilde{C}_{st}^{\alpha\beta}(\mathbf{q})$, can be seen as the second derivative of the Born-Oppenheimer energy surface with respect to the amplitude of a lattice distortion of definite wave vector:

$$\tilde{C}_{st}^{\alpha\beta}(\mathbf{q})\equiv\sum_{\mathbf{R}} e^{-i\mathbf{q}\cdot\mathbf{R}}C_{st}^{\alpha\beta}(\mathbf{R})=\frac{1}{N_c}\frac{\partial^2 E}{\partial u_s^{*\alpha}(\mathbf{q})\partial u_t^\beta(\mathbf{q})}, \tag{82}$$

where $N_c$ is the number of unit cells in the crystal, and the vector $\mathbf{u}_s(\mathbf{q})$ is defined by the distortion pattern

$$\mathbf{R}_I[\mathbf{u}_s(\mathbf{q})]=\mathbf{R}_l+\boldsymbol{\tau}_s+\mathbf{u}_s(\mathbf{q})e^{i\mathbf{q}\cdot\mathbf{R}_l}. \tag{83}$$

Phonon frequencies $\omega(\mathbf{q})$ are solutions of the secular equation

$$\det\left|\frac{1}{\sqrt{M_sM_t}}\tilde{C}_{st}^{\alpha\beta}(\mathbf{q})-\omega^2(\mathbf{q})\right|=0. \tag{84}$$

Translational invariance can be alternatively stated in this context by saying that a lattice distortion of wave vector $\mathbf{q}$ does not induce a force response in the crystal at wave vector $\mathbf{q}'\neq\mathbf{q}$, in agreement with the analysis carried out in Sec. II.C.1. Because of this property, interatomic force constants are most easily calculated in reciprocal space and, when they are needed in direct space, can be readily obtained by Fourier transform (see Sec. II.D.3).

The reciprocal-space expression for the matrix of interatomic force constants Eq. (10), is the sum of an electronic and an ionic contribution:

$$\tilde{C}_{st}^{\alpha\beta}(\mathbf{q})={}^{el}\tilde{C}_{st}^{\alpha\beta}(\mathbf{q})+{}^{ion}\tilde{C}_{st}^{\alpha\beta}(\mathbf{q}), \tag{85}$$

where

$${}^{el}\tilde{C}_{st}^{\alpha\beta}(\mathbf{q})=\frac{1}{N_c}\left[\int\left(\frac{\partial n(\mathbf{r})}{\partial u_s^\alpha(\mathbf{q})}\right)^*\frac{\partial V_{ion}(\mathbf{r})}{\partial u_t^\beta(\mathbf{q})}d\mathbf{r}+\int n(\mathbf{r})\frac{\partial^2 V_{ion}(\mathbf{r})}{\partial u_s^{*\alpha}(\mathbf{q})\partial u_t^\beta(\mathbf{q})}d\mathbf{r}\right], \tag{86}$$

and

$$V_{ion}(\mathbf{r})=\sum_{ls} v_s[\mathbf{r}-\mathbf{R}_l-\boldsymbol{\tau}_s-\mathbf{u}_s(l)], \tag{87}$$

$v_s$ being the ionic (pseudo-) potential corresponding to the $s$th atomic species. All the derivatives must be calculated for $\mathbf{u}_s(\mathbf{q})=0$. The ionic contribution comes from the ion-ion interaction energy [the last term of Eq. (10)] and does not depend on the electronic structure. The explicit expression of ${}^{ion}\tilde{C}_{st}^{\alpha\beta}(\mathbf{q})$ for periodic systems is given in the appendix.

Using Eqs. (83) and (87), the derivatives of the potential appearing in Eq. (86) read

$$\frac{\partial V_{ion}(\mathbf{r})}{\partial u_s^{\alpha}(\mathbf{q})}=-\sum_l \frac{\partial v_s(\mathbf{r}-\mathbf{R}_l-\boldsymbol{\tau}_s)}{\partial \mathbf{r}} e^{i\mathbf{q}\cdot\mathbf{R}_l}, \tag{88}$$

while the corresponding derivative of the electron charge-density distribution is given by Eqs. (33) and (35).

### 2. Long-wavelength vibrations in polar materials

In polar semiconductors and insulators, the long-range character of the Coulomb forces gives rise to macroscopic electric fields for longitudinal optic (LO) phonons in the long-wavelength limit. At any finite wavelength, polar semiconductors are dealt with in the same way as nonpolar ones. In the long-wavelength limit, however, phonons are coupled to macroscopic electric fields, which must be treated with some care because the corresponding electronic potential, $V_{\mathbf{E}}(\mathbf{r})=e\mathbf{E}\cdot\mathbf{r}$, is not lattice periodic (see Sec. II.C.2). A physically transparent picture of the coupling between zone-center phonons and macroscopic electric fields is provided by Huang's phenomenological model, (Born and Huang, 1954) which we discuss briefly in the case of a cubic (or tetrahedral) lattice with two atoms per unit cell. The most general quadratic expression of the energy as a function of the phonon optic coordinates $\mathbf{u}$ and the *electrical degrees of freedom* (i.e., the field itself, $\mathbf{E}$) is

$$E(\mathbf{u},\mathbf{E})=\frac{1}{2}M\omega_0^2u^2-\frac{\Omega}{8\pi}\epsilon_{\infty}\mathsf{E}^2-eZ^{\star}\mathbf{u}\cdot\mathbf{E}, \tag{89}$$

where $M$ is the nuclear reduced mass, $\Omega$ is the volume of the unit cell, $\epsilon_{\infty}$ the electronic dielectric constant of the crystal (i.e., the static dielectric constant with clamped nuclei, $\mathbf{u}=0$), and the coupling $Z^{\star}$, between $\mathbf{u}$ and $\mathbf{E}$, is known as the *Born effective charge* of the ions [see, for example, Böttger (1983), Sec. 1.5]. The variables that are conjugate to $\mathbf{u}$ and $\mathbf{E}$ are the force $\mathbf{F}$ acting on the ions and the electrical induction $\mathbf{D}$:

$$\mathbf{F}\equiv-\frac{\partial E}{\partial \mathbf{u}}=-M\omega_0^2\mathbf{u}+eZ^{\star}\mathbf{E}, \tag{90}$$

$$\mathbf{D}\equiv-\frac{4\pi}{\Omega}\frac{\partial E}{\partial \mathbf{E}}=\frac{4\pi}{\Omega}eZ^{\star}\mathbf{u}+\epsilon_{\infty}\mathbf{E}. \tag{91}$$

In the absence of free external charges, the Maxwell equations give

$$\mathrm{rot}\,\mathbf{E}\sim i\mathbf{q}\times\mathbf{E}=0, \tag{92}$$

$$\mathrm{div}\,\mathbf{D}\sim i\mathbf{q}\cdot\mathbf{D}=0. \tag{93}$$

For transverse modes ($\mathbf{E}\perp\mathbf{q}$), Eq. (92) gives $\mathbf{E}_T=0$, and Eq. (90) $\mathbf{F}_T=-M\omega_0^2\mathbf{u}$: the transverse frequency is therefore $\omega_T=\omega_0$. For longitudinal modes ($\mathbf{E}\parallel\mathbf{q}$), Eq. (93) gives $\mathbf{D}_L=0$ and Eq. (91) gives $\mathbf{E}_L=-(4\pi eZ^{\star}/\Omega\epsilon_{\infty})\mathbf{u}$; Eq. (90) gives $\mathbf{F}_L=-(M\omega_0^2+4\pi e^2Z^{\star 2}/\Omega\epsilon_{\infty})\mathbf{u}$. The longitudinal frequency is therefore $\omega_L=\sqrt{\omega_0^2+4\pi e^2Z^{\star 2}/\Omega\epsilon_{\infty}M}$. These results, which are *exact* in the case of cubic and tetrahedral systems, can be easily generalized to crystals of arbitrary symmetry (Böttger, 1983).

The first-principles calculation of $\epsilon_{\infty}$ and $Z^{\star}$ proceeds from Eqs. (90) and (91). Let us start, for instance, from Eq. (91) which—expressed in terms of the macroscopic electric polarization of the medium and generalized to the case of many atoms per cell—reads

$$\mathbf{P}=\frac{1}{\Omega}\sum_s eZ^{\star}{}_s\mathbf{u}_s+\frac{\epsilon_{\infty}-1}{4\pi}\mathbf{E}. \tag{94}$$

In the general, low-symmetry case, Eq. (94) must be read as a tensor equation stating that the Born effective-charge tensor of the $s$th ion is the partial derivative of the macroscopic polarization with respect to a periodic displacement of all the ions of the $s$ species at zero macroscopic electric field:

$$eZ^{\star}{}_s^{\alpha\beta}=\Omega\left.\frac{\partial \mathsf{P}_{\alpha}}{\partial u_s^{\beta}(\mathbf{q}=0)}\right|_{\mathbf{E}=0}, \tag{95}$$

while the electronic dielectric-constant tensor is the derivative of the polarization with respect to the macroscopic electric field at clamped nuclei:

$$\epsilon_{\infty}^{\alpha\beta}=\delta_{\alpha\beta}+4\pi\left.\frac{\partial \mathsf{P}_{\alpha}}{\partial \mathsf{E}_{\beta}}\right|_{\mathbf{u}_s(\mathbf{q}=0)=0}. \tag{96}$$

In the long-wavelength limit, the matrix of the force constants can be split into the sum of an analytic and a nonanalytic contribution (Born and Huang, 1954; Cochran and Cowley, 1962):

$$\tilde{C}_{st}^{\alpha\beta}={}^{an}\tilde{C}_{st}^{\alpha\beta}+{}^{na}\tilde{C}_{st}^{\alpha\beta}, \tag{97}$$

where the analytic part, ${}^{an}\tilde{C}$, is the matrix obtained from the response to a zone-center phonon, calculated at zero macroscopic electric field. The nonanalytic part has the general form (Cochran and Cowley, 1962)

$$\begin{aligned}{}^{na}\tilde{C}_{st}^{\alpha\beta}&=\frac{4\pi}{\Omega}e^2\frac{\Sigma_{\gamma}Z^{\star}{}_s^{\gamma\alpha}q_{\gamma}\Sigma_{\nu}Z^{\star}{}_t^{\nu\beta}q_{\nu}}{\Sigma_{\gamma,\nu}q_{\gamma}\epsilon_{\infty}^{\gamma\nu}q_{\nu}}\\&=\frac{4\pi}{\Omega}e^2\frac{(\mathbf{q}\cdot\mathbf{Z}^{\star}_s)_{\alpha}(\mathbf{q}\cdot\mathbf{Z}^{\star}_t)_{\beta}}{\mathbf{q}\cdot\boldsymbol{\epsilon}^{\infty}\cdot\mathbf{q}}.\end{aligned} \tag{98}$$

Equation (98) shows that all the information necessary to deal with the nonanalytic part of the dynamical matrix is contained in the macroscopic dielectric constant of the system and in the Born effective charges $Z^{\star}$, whereas the analytic contribution can be calculated by just ignoring any macroscopic polarization associated with the phonon. All these quantities can be easily obtained within DFPT (Giannozzi *et al.*, 1991).

It is worth mentioning that effective charges can be calculated using an approach to the electrostatics of quantum dielectrics based on topological concepts, the *Berry's phase* approach to macroscopic polarization (King-Smith and Vanderbilt, 1993; Resta, 1994). When used at the same level of accuracy, the linear-response and Berry's phase approaches yield the same results within numerical uncertainties.

#### 3. Interatomic force constants

The considerations developed so far in the present section allow, in principle, calculation of the vibrational frequencies at any (finite or infinite) phonon wavelength. Phonon frequencies are usually rather smooth functions of the wave vector, so that suitable interpolation techniques can be used when complete dispersions are needed. Simple concepts from (discrete) Fourier analysis show that the smoother the phonon dispersions, (i.e., the smoother the matrix elements of $\tilde{C}$ as functions of $\mathbf{q}$), the shorter is the range of real-space interatomic force constants:

$$C_{st}^{\alpha\beta}(\mathbf{R}) = \frac{1}{N_c} \sum_{\mathbf{q}} e^{i\mathbf{q}\cdot\mathbf{R}} \tilde{C}_{st}^{\alpha\beta}(\mathbf{q}), \tag{99}$$

i.e., the smaller the number of their nonvanishing values (to any given accuracy). Real-space interatomic force constants can thus be readily obtained by Fourier analyzing a set of force-constant matrices calculated and tabulated over a uniform grid of points in reciprocal space. The most efficient way of calculating all these Fourier transforms numerically is the *fast Fourier transform* (FFT) technique (see, for examples, Press *et al.*, 1989). Once real-space interatomic force constants have been thus obtained, dynamical matrices in reciprocal-space (and, hence, vibrational) frequencies can be obtained at any wave vector (not necessarily contained in the original grid) by FFT. The shorter the range of real-space force constants, the coarser will be the reciprocal-space grid needed for such Fourier interpolation. In practice, the size of the reciprocal-space grid will be assessed *a posteriori* by verifying that it yields vanishing real-space constants (to within a given accuracy) beyond some cutoff radius. A simple rule of thumb is to include in the FFT grid enough points in the Brillouin zone so as to reach neighbor interactions extending up to 2–3 bond lengths, and to check the accuracy of the interpolation against the full calculation on some points *not* included in the grid.

The above considerations apply to metals, away from Kohn anomalies, and to nonpolar insulators. The presence of Kohn anomalies in metals is associated with long-range interatomic force constants propagating along the direction of the wave vector of the anomaly. Catching the details of the anomaly with a regular grid of wave vectors in the Brillouin zone would be very impractical. In these cases, once the position of the anomaly has been located, it is much simpler to refine the grid locally just around the anomaly.

In polar materials, by contrast, real-space interatomic force constants are long ranged in all directions, as a consequence of the long-range dipole-dipole interaction between ionic effective charges. For this reason, Fourier interpolation would be inefficient in this case. The dipole-dipole interaction is precisely the physical origin of the nonanalytic behavior of the reciprocal-space dynamical matrices in the long-wavelength limit, whose form is, however, known exactly in terms of the ionic effective charges [Eq. (98)]. Equation (98) expresses the long-wavelength limit of the reciprocal-space force constants of *any* system whose atoms carry a charge equal to $Z^\star_s$. If the force constants of a system of point charges $Z^\star_s$ is subtracted from those calculated for the physical system under consideration, the resulting difference will be analytic in the long-wavelength limit and its Fourier transform short ranged. For polar materials, Fourier interpolation is thus efficiently applicable to the analytic contribution to the reciprocal-space force constants, whereas the full nonanalytic behavior can be easily restored by adding the force constants of a suitable point-charge model (Giannozzi *et al.* 1991). A description of the technical details necessary to implement Fourier interpolation of reciprocal-space force constants in the general case of materials with anisotropic effective charges can be found in Gonze and Lee (1997).

### E. Homogeneous deformations

#### 1. Elastic properties

Elastic constants can be viewed as force constants associated with homogeneous strains, i.e., with macroscopic distortions of the crystal. In any finite system, there is no conceptual difference between a strain and a microscopic distortion, and linear-response techniques are straightforwardly applicable in both cases. In an infinite system, on the contrary, one cannot directly apply linear-response techniques, because a homogeneous strain changes the boundary conditions of the Hamiltonian. The use of perturbation theory requires instead the existence of a common basis set for the perturbed and unperturbed systems. It has been suggested that, in order to use perturbation theory for homogeneous deformations, one can introduce an intermediate fictitious Hamiltonian that is related to the unperturbed one by a unitary transformation and that obeys the same boundary conditions as the strained Hamiltonian (Baroni *et al.*, 1987b).

Let us consider for simplicity a system under an isotropic strain (dilatation) of amplitude $\alpha$, $\{\mathbf{R}\} \rightarrow \{\alpha\mathbf{R}\}$, whose corresponding elastic constant is the bulk modulus. The Kohn-Sham Hamiltonian $H^\alpha$ for the strained crystal is given by

$$H_{SCF}^{\alpha} = -\frac{\hbar^2}{2m}\frac{\partial^2}{\partial \mathbf{r}^2} + V_{ion}^{\alpha}(\mathbf{r}) + e^2 \int \frac{n^{\alpha}(\mathbf{r}')}{|\mathbf{r}-\mathbf{r}'|} d\mathbf{r}' + v_{xc}[n^{\alpha}(\mathbf{r})], \tag{100}$$

where the electron-ion potential $V_{ion}^{\alpha}$ is

$$V^{\alpha}_{ion}(\mathbf{r}) = \sum_{ls} v_s(\mathbf{r} - \alpha\mathbf{R}_l - \alpha\boldsymbol{\tau}_s). \tag{101}$$

The intermediate (fictitious) strained Hamiltonian $\tilde{H}^{\alpha}$ is obtained from the unperturbed one, $H$, through a scale transformation:

$$\tilde{H}^{\alpha}(\mathbf{r}, \partial/\partial\mathbf{r}) = H_{SCF}(\mathbf{r}/\alpha, \alpha\partial/\partial\mathbf{r}). \tag{102}$$

$\tilde{H}^{\alpha}$ obeys the same boundary conditions as the physical strained Hamiltonian $H^{\alpha}$, and hence perturbation theory can be used to calculate the relative energy difference. At the same time $\tilde{H}^{\alpha}$ and $H$ differ by a unitary transformation and their spectra are trivially related:

$$\begin{aligned} &\tilde{\epsilon}^{\alpha}_n = \epsilon_n, \\ &\tilde{\psi}^{\alpha}_n(\mathbf{r}) = \alpha^{-3/2}\psi_n(\mathbf{r}/\alpha), \\ &\tilde{n}^{\alpha}(\mathbf{r}) = \alpha^{-3} n(\mathbf{r}/\alpha). \end{aligned} \tag{103}$$

The energy change due to a strain can thus be computed in two steps: first one calculates the energy difference between the unperturbed crystal and the fictitious strained one described by $\tilde{H}^{\alpha}$; one then computes the energy difference between the latter and the physical strained system using perturbation theory. The first step is trivial. The second step is less so, because $\tilde{H}^{\alpha}$ is not a proper Kohn-Sham Hamiltonian: the Hartree and exchange-correlation terms in $\tilde{H}^{\alpha}$ are not the Hartree and exchange-correlation potentials generated by $\tilde{n}^{\alpha}$. One can write $\tilde{H}^{\alpha}$ as a genuine Kohn-Sham Hamiltonian, provided that the definition of the external potential is changed:

$$\begin{aligned} \tilde{H}^{\alpha} = &-\frac{\hbar^2\alpha^2}{2m}\frac{\partial^2}{\partial\mathbf{r}^2} + \tilde{V}^{\alpha}_{ext}(\mathbf{r}) + e^2\int\frac{\tilde{n}^{\alpha}(\mathbf{r}')}{|\mathbf{r}-\mathbf{r}'|}d\mathbf{r}' \\ &+ v_{xc}[\tilde{n}^{\alpha}(\mathbf{r})], \end{aligned} \tag{104}$$

where

$$\begin{aligned} \tilde{V}^{\alpha}_{ext}(\mathbf{r}) = &\sum_{ls} v_s(\mathbf{r}/\alpha - \mathbf{R}_l - \boldsymbol{\tau}_s) + e^2\left(1 - \frac{1}{\alpha}\right) \\ &\times \int\frac{n(\mathbf{r}')}{|\mathbf{r}/\alpha - \mathbf{r}'|}d\mathbf{r}' + v_{xc}[\alpha^{-3}n(\mathbf{r}/\alpha)] \\ &+ v_{xc}[n(\mathbf{r}/\alpha)]. \end{aligned} \tag{105}$$

The energy difference between the fictitious and the real strained systems, $E^{\alpha} - \tilde{E}^{\alpha}$, can now be calculated by perturbation. The details are given in Baroni *et al.* (1987b). This method can be straightforwardly extended to generic elastic constants. The algebra involved is, however, quite heavy.

It must be remarked that only bare elastic constants are calculated in this way. In Eq. (101) the coordinates of different atoms within a same unit cell are assumed to undergo the same homogeneous scale transformation as the positions of different unit cells. This is not true in general, as atoms rearrange themselves within each unit cell so as to minimize the total energy as a function of the applied strain. To see how the elastic constants are affected by the internal relaxation of the atomic positions, let us write the more general second-order expression of the crystal energy per unit cell as a second-order polynomial of the macroscopic (strain) and microscopic (phonon) modes:

$$\begin{aligned} E = &\frac{\Omega}{2}\sum_{\alpha\beta,\gamma\delta}\lambda^0_{\alpha\beta,\gamma\delta}e_{\alpha\beta}e_{\gamma\delta} + \frac{1}{2}\sum_{s\alpha,t\beta}C^{\alpha\beta}_{st}u^{\alpha}_s u^{\beta}_t \\ &+ \Omega\sum_{s\alpha\gamma\delta}\zeta_{s\alpha\gamma\delta}u^{\alpha}_s e_{\gamma\delta}, \end{aligned} \tag{106}$$

where $\Omega$ is the unit-cell volume, $\lambda^0$ is the (bare) elastic constant matrix, $e$ is the strain tensor, $C$ is the zone-center reciprocal-space matrix of force constants, $u$ are atomic displacements in the unit cell, and $\zeta$ is the coupling between macroscopic strain and atomic displacements (the matrix of the so-called *internal-strain parameters*). Crystal symmetry determines the number of independent nonvanishing terms in $\lambda^0$, $C$, and $\zeta$. If we allow the atoms to relax for a given strain state, minimization of the energy with respect to the $u$'s yields

$$E = \frac{\Omega}{2}\sum_{\alpha\beta,\gamma\delta}\lambda_{\alpha\beta,\gamma\delta}e_{\alpha\beta}e_{\gamma\delta}, \tag{107}$$

where

$$\lambda_{\alpha\beta,\gamma\delta} = \lambda^0_{\alpha\beta,\gamma\delta} - \Omega\sum_{s\mu,t\nu}\zeta_{s\mu\alpha\beta}(C^{-1})^{\mu\nu}_{st}\zeta_{t\nu\gamma\delta}. \tag{108}$$

Both the force constants and the coupling between macroscopic strain and atomic displacements can be readily calculated within DFPT.

### 2. Piezoelectric properties

The piezoelectric constants form a third-order tensor $\gamma_{\alpha,\gamma\delta}$, defined as the derivative of the macroscopic electric polarization with respect to a homogeneous strain, at vanishing macroscopic field. This quantity—which has been demonstrated to be independent of surface effects (Martin, 1972), i.e., independent of surface termination—could in principle be evaluated as the electric-polarization response to a given applied strain. Alternatively, and somewhat more conveniently, it can also be calculated as the stress linearly induced by an electric field at zero strain. The latter definition was used by de Gironcoli *et al.* (1989) to calculate the piezoelectric tensor in III-V semiconductor compounds. The two definitions are equivalent and can be deduced by expanding the energy of the system to second order in the macroscopic perturbations (strain $e_{\alpha\beta}$ and electric field $\mathsf{E}_{\alpha}$):

$$\begin{aligned} E = &\frac{\Omega}{2}\sum_{\alpha\beta,\gamma\delta}\lambda_{\alpha\beta,\gamma\delta}e_{\alpha\beta}e_{\gamma\delta} - \Omega\sum_{\alpha,\gamma\delta}\gamma_{\alpha,\gamma\delta}\mathsf{E}_{\alpha}e_{\gamma\delta} \\ &- \frac{\Omega}{8\pi}\sum_{\alpha,\beta}\epsilon^{\alpha\beta}_0\mathsf{E}_{\alpha}\mathsf{E}_{\beta}. \end{aligned} \tag{109}$$

The link with the microscopic description is provided by expanding the crystal energy to second order in the external (strain and electric field) and internal (phonon) degrees of freedom:

$$E=\frac{\Omega}{2}\sum_{\alpha\beta,\gamma\delta}\lambda^{0}_{\alpha\beta,\gamma\delta}e_{\alpha\beta}e_{\gamma\delta}-\Omega\sum_{\alpha,\gamma\delta}\gamma_{\alpha,\gamma\delta}\mathsf{E}_{\alpha}e_{\gamma\delta}$$
$$-\frac{\Omega}{8\pi}\sum_{\alpha,\beta}\epsilon^{\alpha\beta}_{\infty}\mathsf{E}_{\alpha}\mathsf{E}_{\beta}+\frac{1}{2}\sum_{s\alpha,t\beta}C^{\alpha\beta}_{st}u^{\alpha}_{s}u^{\beta}_{t}$$
$$+\sum_{s\alpha\gamma\delta}\zeta_{s\alpha\gamma\delta}u^{\alpha}_{s}e_{\gamma\delta}-\Omega e\sum_{s\alpha\beta}Z^{\star\alpha\beta}_{s}u^{\alpha}_{s}\mathsf{E}_{\beta}, \qquad (110)$$

where $\lambda^0$, $\gamma^0$, and $\epsilon_\infty$ are the purely electronic (i.e., clamped-ion) contributions to the elastic, piezoelectric, and dielectric constants respectively, and the coupling between atomic displacements and macroscopic variables (electric field and strain) are expressed by the effective charges $Z^\star$ and internal strain parameters $\zeta$. Once the macroscopic variables, $\mathsf{E}$ and $e$ are fixed, the equilibrium values of the internal degrees of freedom are given by the condition that the derivatives of Eq. (110) with respect to the atomic displacements vanish. When these equilibrium atomic positions as functions of the macroscopic electric field and strain are inserted in Eq. (110), the resulting expression defines the total piezoelectric constants as

$$\gamma_{\alpha,\gamma\delta}=\gamma^{0}_{\alpha,\gamma\delta}+\sum_{s\mu,t\nu}Z^{\star\mu\alpha}_{s}(C^{-1})^{\mu\nu}_{st}\zeta_{t\nu\gamma\delta}. \qquad (111)$$

The two resulting contributions to the piezoelectric constants are often of opposite sign and close in absolute value, so that a well-converged calculation is needed in order to extract a reliable value for their sum (de Gironcoli *et al.*, 1989).

The problem of a proper definition of piezoelectric properties in a crystal displaying a spontaneous macroscopic polarization has been raised recently by Sághi-Szabó *et al.* (1998) and further discussed by Vanderbilt (2000).

### F. Higher-order responses

#### 1. The $2n+1$ theorem

In Sec. II.C we saw that the knowledge of the first-order derivatives of the wave functions is enough to calculate the second-order derivatives of the total energy. This is a special case of a very general theorem, known as the $2n+1$ theorem, which states that knowledge of the derivatives of the wave functions up to order $n$ allows one to calculate the derivatives of the energy up to order $2n+1$. This theorem, well known in quantum mechanics for many years, is a consequence of the variational principle and it is also valid in density-functional theory. In this context, its usefulness derives from the fact that the third-order derivatives of the total energy can be obtained from the first-order derivatives of the wave functions. This opens the possibility of studying phenomena that depend upon third-order anharmonic terms in the energy expansion—such as phonon linewidths, Raman-scattering cross sections, or nonlinear optical responses—with a computational effort of the same order as for harmonic properties (because the time-consuming step is the calculation of the first-order derivatives of the wave functions).

Several proofs of the $2n+1$ theorem can be found in the literature. In a DFT framework this theorem was first proved by Gonze and Vigneron (1989). Explicit expressions of the energy derivatives up to fourth order have been worked out by Gonze (1995b). The scope of this theorem is much more general, as it concerns properties of the extrema of any functional depending upon some parameters (Epstein, 1974). Let $E[\boldsymbol{\psi},\lambda]$ be a generic functional of $\boldsymbol{\psi}$ which, for $\lambda=0$, has an extremum at $\boldsymbol{\psi}^{(0)}$: $\delta E[\boldsymbol{\psi}^{(0)},0]/\delta\boldsymbol{\psi}=0$. The position of the extremum will depend on the value of the parameter $\lambda$: $\boldsymbol{\psi}(\lambda)=\boldsymbol{\psi}^{(0)}+\Delta\boldsymbol{\psi}(\lambda)$. The value of the functional at the extremum will be

$$E_{\min}(\lambda)=E[\boldsymbol{\psi}^{(0)}+\Delta\boldsymbol{\psi}(\lambda),\lambda], \qquad (112)$$

where $\Delta\boldsymbol{\psi}(\lambda)$ is determined, for any given value of $\lambda$, by the extremum condition

$$\frac{\partial E[\boldsymbol{\psi}^{(0)}+\Delta\boldsymbol{\psi},\lambda]}{\partial\Delta\boldsymbol{\psi}}=0. \qquad (113)$$

When $\lambda$ is small, both $\Delta\boldsymbol{\psi}(\lambda)$ and $E_{\min}(\lambda)$ will be well approximated by their Taylor expansion in powers of $\lambda$:

$$\Delta\boldsymbol{\psi}(\lambda)=\sum_{l=1}^{\infty}\frac{1}{l!}\frac{d^{l}\boldsymbol{\psi}}{d\lambda^{l}}\lambda^{l}\equiv\sum_{l=1}^{\infty}\Delta\boldsymbol{\psi}^{(l)}\lambda^{l}, \qquad (114)$$

$$E_{\min}(\lambda)=\sum_{l=0}^{\infty}\frac{1}{l!}\frac{d^{l}E_{\min}}{d\lambda^{l}}\lambda^{l}\equiv\sum_{l=0}^{\infty}E^{(l)}\lambda^{l}. \qquad (115)$$

The $2n+1$ theorem states that a knowledge of $\Delta\boldsymbol{\psi}^{(l)}$ up to order $n$ is enough to determine $E^{(l)}$ up to order $2n+1$. To demonstrate this, it is convenient to first expand $E[\boldsymbol{\psi}^{(0)}+\Delta\boldsymbol{\psi},\lambda]$ into a Taylor series treating $\Delta\boldsymbol{\psi}$ and $\lambda$ as independent variables:

$$E[\boldsymbol{\psi}^{(0)}+\Delta\boldsymbol{\psi},\lambda]=\sum_{p=0}^{\infty}\sum_{k=0}^{\infty}\frac{1}{k!p!}\frac{\delta^{k+p}E[\boldsymbol{\psi}^{(0)},0]}{\delta\boldsymbol{\psi}^{k}\delta\lambda^{p}}(\Delta\boldsymbol{\psi})^{k}\lambda^{p}, \qquad (116)$$

where we use the notation

$$\frac{\delta^{k}E}{\delta\boldsymbol{\psi}^{k}}(\Delta\boldsymbol{\psi})^{k}=\left(\sum_{i}\Delta\psi_{i}\frac{\partial}{\partial\psi_{i}}\right)^{k}E. \qquad (117)$$

Variation of Eq. (116) with respect to $\Delta\boldsymbol{\psi}$ leads to the extremum condition

$$\mathbf{f}=\frac{\partial E[\boldsymbol{\psi}^{(0)}+\Delta\boldsymbol{\psi},\lambda]}{\partial\Delta\boldsymbol{\psi}}$$
$$=\sum_{p=0}^{\infty}\sum_{k=1}^{\infty}\frac{1}{(k-1)!p!}\frac{\delta^{k+p}E[\boldsymbol{\psi}^{(0)},0]}{\delta\boldsymbol{\psi}^{k}\delta\lambda^{p}}(\Delta\boldsymbol{\psi})^{k-1}\lambda^{p}$$
$$=0. \qquad (118)$$

Introducing Eq. (114) into Eq. (118) allows one to formally expand $\mathbf{f}$ as a power series of $\lambda$ only. The resulting

expression for $\mathbf{f}$ must vanish identically order by order in $\lambda$. By equating the coefficients of $\lambda^n$ in the Taylor expansion to zero, Eq. (118) yields an infinite number of equations $\mathbf{f}^{(n)}=0$, which determine $\Delta\boldsymbol{\psi}^{(n)}$.

Introducing Eq. (114) into Eq. (116) allows one to formally expand $E$ as a power series of $\lambda$ only and therefore to calculate the explicit form of $E^{(l)}$. Since a term quadratic in $\Delta\boldsymbol{\psi}^{(l)}\lambda^l$ is of order $\lambda^{2l}$, $E^{(2n+1)}$ could depend only linearly upon $\Delta\boldsymbol{\psi}^{(l)}\lambda^l$, if $l>n$. Showing that for $l>n$ the coefficient of $\Delta\boldsymbol{\psi}^{(l)}\lambda^l$ in $E^{(2n+1)}$ is $\mathbf{f}^{(2n+1-l)}$ we prove the $2n+1$ theorem, since this force is zero by the minimum condition. We start by extracting $\Delta\boldsymbol{\psi}^{(l)}\lambda^l$ from the product $(\Delta\boldsymbol{\psi})^k$ appearing in Eq. (116), using the relationship

$$\begin{aligned}(\Delta\boldsymbol{\psi})^k&=(\Delta\boldsymbol{\psi}-\Delta\boldsymbol{\psi}^{(l)}\lambda^l+\Delta\boldsymbol{\psi}^{(l)}\lambda^l)^k\\&=k\Delta\boldsymbol{\psi}^{(l)}\lambda^l(\Delta\boldsymbol{\psi})^{k-1}+(\Delta\boldsymbol{\psi}-\Delta\boldsymbol{\psi}^{(l)}\lambda^l)^k\\&\quad+\mathcal{O}(\lambda^{2n+1}),\end{aligned}\tag{119}$$

valid for $l>n$. The only term that is linear in $\Delta\boldsymbol{\psi}^{(l)}\lambda^l$ is the first term on the right-hand side of Eq. (119). Inserting this term in Eq. (116) and recalling the definition of $\mathbf{f}$, Eq. (118), we can write $E^{(2n+1)}$ as

$$\begin{aligned}E^{(2n+1)}&=\Delta\boldsymbol{\psi}^{(2n+1)}\lambda^{2n+1}\mathbf{f}^{(0)}+\cdots+\Delta\boldsymbol{\psi}^{(l)}\lambda^l\mathbf{f}^{(2n+1-l)}\\&\quad+\cdots+\Delta\boldsymbol{\psi}^{(n+1)}\lambda^{(n+1)}\mathbf{f}^{(n)}\\&\quad+P^{(2n+1)}(\boldsymbol{\psi}^{(1)},\ldots,\boldsymbol{\psi}^{(n)}),\end{aligned}\tag{120}$$

where $P^{(2n+1)}$ is a polynomial of degree $2n+1$. From the condition $\mathbf{f}^{(i)}=0$ for every $i$, we get

$$E^{(2n+1)}=P^{(2n+1)}(\boldsymbol{\psi}^{(1)},\ldots,\boldsymbol{\psi}^{(n)}),\tag{121}$$

which proves the $2n+1$ theorem.

In order to apply this theorem to density-functional theory, we can take as $\boldsymbol{\psi}$ a vector whose elements are the coefficients of all the occupied wave functions $\{\psi_i\}$ on a given basis and $\lambda$ as a parameter measuring the magnitude of the perturbation. The orthogonality constraint can be dealt with as shown for instance by Mauri *et al.* (1993), writing the total energy functional of density-functional theory for nonorthonormalized orbitals. The demonstration presented here, applied to this functional, provides high-order derivatives of the DFT energy. Note that the $\boldsymbol{\psi}$ are arbitrary linear combinations of the occupied eigenstates of the Hamiltonian, which are only required to minimize the total energy functional. For instance, in a crystalline solid, $\boldsymbol{\psi}$ could represent Wannier functions if they are used instead of Bloch functions to describe the electronic states. As an alternative to the path followed here, the $2n+1$ theorem can also be demonstrated for constrained functionals, with Lagrange multipliers used to impose the orthogonality of the orbitals (Gonze, 1995a).

### 2. Nonlinear susceptibilities

Within density-functional theory, the third-order derivatives of the energy, Eq. (11), are, (Gonze and Vigneron, 1989)

$$\begin{aligned}E^{(3)}&=2\sum_{n=1}^{N/2}\langle\Delta\psi_n|\Delta V_{SCF}-\Delta\epsilon_n|\Delta\psi_n\rangle\\&\quad+2\sum_{n=1}^{N/2}\left(\left\langle\Delta\psi_n\left|\frac{\partial^2 V}{\partial\lambda^2}\right|\psi_n\right\rangle+\text{c.c.}\right)\\&\quad+2\sum_{n=1}^{N/2}\left\langle\psi_n\left|\frac{\partial^3 V}{\partial\lambda^3}\right|\psi_n\right\rangle+\frac{1}{6}\int K^{(3)}(\mathbf{r}_1,\mathbf{r}_2,\mathbf{r}_3)\\&\quad\times\Delta n(\mathbf{r}_1)\Delta n(\mathbf{r}_2)\Delta n(\mathbf{r}_3)d\mathbf{r}_1 d\mathbf{r}_2 d\mathbf{r}_3,\end{aligned}\tag{122}$$

where $K^{(3)}$ is the third-order functional derivative of the exchange and correlation energy with respect to the density. In this section, we have dropped the indication of the order in $\lambda$ from $\Delta\psi_n$, which is always a first-order term.

The solution of Eq. (30) yields a projection onto the conduction manifold of the first-order change of the wave functions. Therefore we need to recast Eq. (122) in a form that does not depend on the projection of $|\Delta\psi_i\rangle$ on the valence manifold. This expression for $E^{(3)}$ exists, since the total energy functional is invariant with respect to a unitary transformation within the manifold of the occupied orbitals. The required transformation has been carried out by Debernardi and Baroni (1994) and by Dal Corso and Mauri (1994). After some algebra one obtains

$$\begin{aligned}E^{(3)}&=2\sum_{n=1}^{N/2}\langle\Delta\psi_n|P_c\Delta V_{SCF}P_c|\Delta\psi_n\rangle\\&\quad-2\sum_{n,m=1}^{N/2}\langle\Delta\psi_n|P_c|\Delta\psi_m\rangle\langle\psi_m|\Delta V_{SCF}|\psi_n\rangle\\&\quad+2\sum_{n=1}^{N/2}\left(\left\langle\Delta\psi_n\left|P_c\frac{\partial^2 V}{\partial\lambda^2}\right|\psi_n\right\rangle+\text{c.c.}\right)\\&\quad+2\sum_{n=1}^{N/2}\left\langle\psi_n\left|\frac{\partial^3 V}{\partial\lambda^3}\right|\psi_n\right\rangle+\frac{1}{6}\int K^{(3)}(\mathbf{r}_1,\mathbf{r}_2,\mathbf{r}_3)\\&\quad\times\Delta n(\mathbf{r}_1)\Delta n(\mathbf{r}_2)\Delta n(\mathbf{r}_3)d\mathbf{r}_1 d\mathbf{r}_2 d\mathbf{r}_3.\end{aligned}\tag{123}$$

When the perturbation $\lambda$ is an atomic displacement, as in Sec. II.D, $E^{(3)}$ gives the first anharmonic corrections to the energy. These corrections are responsible, for instance, for the decay of the phonon modes into vibrations of lower frequency. The linewidth of the phonon lines in Raman scattering, after subtraction of isotopic and inhomogeneous broadening, is proportional to $E^{(3)}$ if higher-order processes are neglected. Theoretical and experimental values are compared in Sec. V.F. Equation (123) can be generalized to metals by the techniques introduced in Sec. II.C.4. The first application has recently been presented by Lazzeri (1999).

When the perturbation $\lambda$ is an electric field, as in Sec. II.C.2, $E^{(3)}$ is proportional to the nonlinear optical susceptibilities of a material at low frequency. Unfortunately, in this case, Eq. (123) cannot be directly used to compute $E^{(3)}$. In fact, it contains a term $\langle\psi_m|\Delta^{\mathbf{E}}V_{SCF}|\psi_n\rangle$ that becomes ill defined when $n=m$ [Eq. (37) cannot be applied: the energy denominator

vanishes]. The same problem also arises when Eq. (123) is generalized to mixed third-order derivatives of the energy and one perturbation is an electric field. These derivatives allow one to account, theoretically, for the intensities of nonresonant Raman lines (Baroni and Resta, 1986a) or for nonlinear infrared absorption.

A solution to this problem was proposed by Dal Corso and Mauri (1994) switching to a Wannier representation for the electronic orbitals, and applying the $2n+1$ theorem to a total energy functional that was originally proposed by Nunes and Vanderbilt (1994). This functional, for a periodic insulating solid in a finite electric field exploits the properties of localized orbitals. It is written as

$$E[\{w_{0,m}\},\mathsf{E}_0]=\sum_l \sum_{m,n=1}^{N} \langle w_{0,m}|H+e\mathsf{E}_0 x|w_{l,n}\rangle \times(2\delta_{0m,ln}-\langle w_{l,n}|w_{0,m}\rangle), \tag{124}$$

where $H$ is the unperturbed Hamiltonian of the solid, $\mathsf{E}_0$ is the electric field, $x$ is the position operator, and $\{w_{l,m}\}$ are functions—in general nonorthonormal—localized around the unit cell identified by the Bravais lattice vector $R_l$. The function $w_{l,m}$ is obtained by translating the function centered at the origin by a vector $R_l$: $w_{l,m}(x)=w_{0,m}(x-R_l)$. In practical applications, $w_{0,m}$ is constrained to vanish outside a localization region of radius $R_c$ centered at the origin. For simplicity in Eq. (124), we have limited ourselves to one-dimensional systems of noninteracting electrons. The electron-electron interaction—when dealt with within any self-consistent-field scheme—does not yield any additional problems. We stress here that the expectation value of $x$ is well defined for any finite cutoff radius $R_c$. Furthermore, we note that even if no orthogonality constraints are imposed on the $w_{l,m}$'s, at the minimum they become approximately orthonormal, as shown by Mauri *et al.* (1993).

In analogy with Eq. (123), one can show that the nonlinear optical susceptibility $\chi^{(2)}$ is given by

$$\chi^{(2)}=-3E^{(3)}/\mathsf{E}_0^3 =-\frac{3}{\mathsf{E}_0^2}\left(\sum_{m=1}^{N} e\langle w_{0,m}^{(1)}|P_c x P_c|w_{0,m}^{(1)}\rangle - \sum_{m,n=1}^{N}\sum_l e\langle w_{0,m}|x|w_{l,n}\rangle\langle w_{l,n}^{(1)}|P_c|w_{0,m}^{(1)}\rangle\right), \tag{125}$$

where the $w^{(1)}$'s are solutions of a linear system similar to Eq. (46), which can be obtained from the condition $\delta E^{(2)}/\delta w^{(1)}=0$:

$$-P_c e\mathsf{E}_0 x|w_{0,m}\rangle=HP_c|w_{0,m}^{(1)}\rangle - \sum_{n=1}^{N}\sum_l P_c|w_{l,n}^{(1)}\rangle\langle w_{l,n}|H|w_{0,m}\rangle, \tag{126}$$

where $P_c=1-\Sigma_{n=1}^{N}\Sigma_l|w_{l,n}\rangle\langle w_{l,n}|$ is the projector on the conduction bands in the Wannier representation.

Equation (125) is difficult to implement since it requires an electronic structure code that calculates localized Wannier functions. However, Eq. (125) can be rewritten in terms of Bloch functions. We recall that Wannier functions are defined in terms of Bloch functions $\psi_n^k(x)$ as

$$w_{0,n}(x)=\frac{\Omega}{2\pi}\int_{BZ} dk\,\psi_n^k(x), \tag{127}$$

where the integral is done over the first Brillouin zone, $\Omega$ is the dimension of the unit cell, the Bloch functions are normalized on the unit cell, and $\psi_n^{k+G}(x)=\psi_n^k(x)$; here $G$ is a reciprocal-lattice vector. Inserting this definition in Eq. (125) and using the relationship

$$x\psi_n^k(x)=-(i\partial/\partial k)\,\psi_n^k(x)+e^{ikx}(i\partial/\partial k)\,u_n^k(x),$$

where $u_n^k(x)=e^{-ikx}\psi_n^k(x)$ are the periodic parts of the Bloch wave functions, one finally obtains

$$\chi^{(2)}=3i\frac{e\Omega}{2\pi\mathsf{E}_0^2}\sum_{m,n=1}^{N}\int_{BZ} dk \times\left\langle u_m^k\left|\frac{\partial}{\partial k}(|u_n^k\rangle\langle\tilde{u}_n^{k(1)}|)\right|\tilde{u}_m^{k(1)}\right\rangle, \tag{128}$$

where $\tilde{u}_n^{k(1)}=P_c u_n^{k(1)}$.

The formalism, as introduced in this paper, allows one to access nonlinear phenomena in a frequency range where one can assume that the electrons are in the ground state. The generalization to finite frequencies, starting from time-dependent DFT, has been explored by Dal Corso *et al.* (1996).

## III. IMPLEMENTATIONS

### A. Plane waves and pseudopotentials

The first—and still today by far the most numerous—implementations of DFPT were based on the plane-wave pseudopotential method (Pickett, 1989). Plane waves have many attractive features: they are simple to use, orthonormal by construction, and unbiased by atomic positions. Unlike calculations based on localized (atomiclike) basis sets, those made with plane waves can be simply checked for convergence by increasing the size of the basis set, as given by the kinetic-energy cutoff. The FFT algorithm allows one to quickly go back and forth from reciprocal to real space. An especially important advantage of plane waves is the absence of Pulay (1969) terms in the calculation of energy derivatives. As a consequence the Hellmann-Feynman expressions for forces and for force constants are valid without any correction when a plane-waves basis set is used.

Plane waves are used in conjunction with pseudopotentials. A pseudopotential is a fictitious electron-ion interaction potential, acting on valence electrons only, that mimics the interaction with the inner electrons—which are supposed to be frozen in the core—as well as the

effective repulsion exerted by the latter on the former due to their mutual orthogonality. Modern *norm-conserving* pseudopotentials (Hamann, Schlüter, and Chiang, 1979) are determined uniquely from the properties of the isolated atom, while the requirement of norm conservation ensures an optimal *transferability*. By the latter expression one indicates the ability of the pseudopotentials to provide results whose quality is to a large extent independent of the local chemical environment of the individual atoms. Norm-conserving pseudopotentials are angular momentum dependent, (i.e., they are *nonlocal* operators) and special care must be taken to ensure that the atomic valence (pseudo-) wave functions associated with them are sufficiently smooth in the atomic (pseudo)core that they can be efficiently dealt with using a plane-wave basis set. Experience has shown that the use of pseudopotentials is practically equivalent to the frozen-core approximation within an all-electron approach. The pseudopotential approximation implicitly assumes that the energy functional is linear with respect to the partition of the total charge into core and valence contributions. In some atoms (such as, alkali atoms) the loss of accuracy due to neglect of nonlinearity in the exchange-correlation energy functional can be intolerably high. For such cases the *nonlinear core correction* of Louie *et al.* (1982) turns out to be very useful.

From a computational point of view, it is very convenient to recast the angular-momentum-dependent part of a pseudopotential into a sum over a few projectors (Kleinman and Bylander, 1982). This is called the *separable form* of a pseudopotential. The use of plane waves and of separable pseudopotentials, together with the FFT and iterative diagonalization or minimization techniques, allows a fast and efficient solution of the Kohn-Sham equations for systems containing up to hundreds of atoms in the unit cell. The technical aspects of the implementation of the Kohn-Sham equations in a plane-wave-pseudopotential (PW-PP) framework have been extensively described in the literature (see, for example, Pickett, 1989; Payne *et al.*, 1992; Giannozzi, 1995).

The implementation of DFPT in a PW-PP framework is a straightforward extension of the implementation of the Kohn-Sham equations. The only modifications to the theory expounded in Sec. II are related to the nonlocal character of pseudopotentials. In DFT calculations this is accounted for by modifying the electron-ion interaction term in the energy functional, Eq. (11), as follows:

$$E[n]=F[n]+2\sum_{n=1}^{N/2}\int \psi_n^*(\mathbf{r})V(\mathbf{r},\mathbf{r}')\psi_n(\mathbf{r}')d\mathbf{r}d\mathbf{r}', \tag{129}$$

where $V(\mathbf{r},\mathbf{r}')$ is a sum of atomic nonlocal pseudopotentials. The results of Sec. II.D must be generalized accordingly. Equations (21) and (22) become

$$\frac{\partial E}{\partial \lambda_i}=2\sum_{n=1}^{N/2}\left\langle \psi_n\left|\frac{\partial V_\lambda}{\partial \lambda_i}\right|\psi_n\right\rangle \tag{130}$$

and

$$\frac{\partial^2 E}{\partial \lambda_i \partial \lambda_j}=2\sum_{n=1}^{N/2}\left(\left\langle \psi_n\left|\frac{\partial^2 V_\lambda}{\partial \lambda_i \partial \lambda_j}\right|\psi_n\right\rangle + \left\langle \frac{\partial \psi_n}{\partial \lambda_i}\left|\frac{\partial V_\lambda}{\partial \lambda_j}\right|\psi_n\right\rangle + \text{c.c.}\right). \tag{131}$$

Equation (86) for the electronic contribution to the force constants is modified as

$${}^{el}\tilde{C}_{st}^{\alpha\beta}(\mathbf{q})=\frac{2}{N_c}\sum_{n=1}^{N/2}\left(\left\langle \frac{\partial \psi_n}{\partial u_s^\alpha(\mathbf{q})}\left|\frac{\partial V_{ion}}{\partial u_t^\beta(\mathbf{q})}\right|\psi_n\right\rangle + \text{c.c.} + \left\langle \psi_n\left|\frac{\partial^2 V_{ion}}{\partial u_s^{*\alpha}(\mathbf{q})\partial u_t^\beta(\mathbf{q})}\right|\psi_n\right\rangle\right). \tag{132}$$

The procedure outlined above can easily be extended to the case of pseudopotentials with nonlinear core corrections (Dal Corso, Baroni *et al.*, 1993). In this case, the exchange-correlation functional $E_{xc}[n]$ must be replaced in Eq. (12) by $E_{xc}[n+n_c]$, where $n(\mathbf{r})$ is the atomic valence charge density, and $n_c(\mathbf{r})$ is the core charge, or a suitable smooth approximation to it (Louie *et al.*, 1982). The exchange-correlation potential $v_{xc}(\mathbf{r})$ of Eq. (13) is replaced by $v_{xc}[n+n_c](\mathbf{r})$. Energy derivatives will contain additional terms. The following contribution must be added to first derivatives, Eq. (21):

$$\frac{\partial E^{cc}}{\partial \lambda_i}=\int v_{xc}[n+n_c](\mathbf{r})\frac{\partial n_c(\mathbf{r})}{\partial \lambda_i}d\mathbf{r}. \tag{133}$$

Let us specialize to the case of monochromatic atomic perturbations. The following term must be added to the screened potential used to calculate the linear response, Eq. (36):

$$\frac{\partial V_{cc}(\mathbf{r})}{\partial u_s^\alpha(\mathbf{q})}=\int \left.\frac{dv_{xc}(n)}{dn}\right|_{n=n(\mathbf{r})+n_c(\mathbf{r})}\frac{\partial n_c(\mathbf{r})}{\partial u_s^\alpha(\mathbf{q})}d\mathbf{r}, \tag{134}$$

where the core charge $n_c(\mathbf{r})$ is written as a sum of ionic terms, as in Eq. (87). The force constants, Eq. (86), will contain additional terms:

$${}^{cc}\tilde{C}_{st}^{\alpha\beta}(\mathbf{q})=\frac{1}{N_c}\left[\int v_{xc}[n+n_c](\mathbf{r})\frac{\partial^2 n_c(\mathbf{r})}{\partial u_s^{*\alpha}(\mathbf{q})\partial u_t^\beta(\mathbf{q})}d\mathbf{r} + \int \left(\frac{\partial n(\mathbf{r})}{\partial u_s^\alpha(\mathbf{q})}+\frac{\partial n_c(\mathbf{r})}{\partial u_s^\alpha(\mathbf{q})}\right)^*\frac{\partial V_{cc}(\mathbf{r})}{\partial u_t^\beta(\mathbf{q})}d\mathbf{r}\right]. \tag{135}$$

The matrix elements of the relevant quantities between plane waves are in the Appendix.

### B. Ultrasoft pseudopotentials

In typical bulk semiconductors (e.g., Si, Ge, GaAs, AlAs) at equilibrium volume 100–150 plane waves per atom are sufficient for most applications. However, many atoms—transition metals, first-row elements like F, O, and to a lesser extent N and C—require hard pseudopotentials to ensure transferability, and their treatment demands impractically large plane-wave basis sets. One can try to exploit the many degrees of freedom that are present in pseudopotential generation to obtain

softer pseudopotentials. Several recipes have been proposed to get optimally smooth pseudopotentials (for example, by acting on the form of pseudo wave functions in the core region). Simple and effective recipes have been described by Vanderbilt (1985), Rappe *et al.* (1990), and Troullier and Martins (1991).

A more radical approach to the challenge posed by hard pseudopotentials was proposed by Vanderbilt (1990), who introduced *ultrasoft pseudopotentials*. In this scheme, the orbitals are allowed to be as soft as possible in the core regions so that their plane wave expansion converges rapidly; this comes at the price of giving up both the norm conservation and the standard orthonormality constraint of atomic orbitals. Orthonormality is recovered by introducing a generalized overlap operator which depends on the ionic positions. The full electron density is obtained by adding to the square modulus of the orbitals an augmentation charge localized in the core regions. Despite its technical complexity, this approach has proved to be extremely successful in treating large-scale electronic structure problems.

In the ultrasoft scheme, the atomic pseudopotential is separated into a local $V_{loc}$ and a nonlocal $V_{NL}$ part. The nonlocal potential is written in the separable form, as a sum of projectors. The ionic potential is written as a sum over all the atoms $I$ of projectors:

$$V_{NL}(\mathbf{r},\mathbf{r}')=\sum_I \sum_{ij} D_{ij}^{(0)I}\beta_i^I(\mathbf{r}-\mathbf{R}_I)\beta_j^{*I}(\mathbf{r}'-\mathbf{R}_I), \tag{136}$$

where the functions $\beta_i^I(\mathbf{r})$ and the coefficients $D_{ij}^{(0)I}$ are computed in an atomic calculation, as described by Vanderbilt (1990) and Laasonen *et al.* (1993).

The charge density is computed by augmenting the square modulus of the orbitals with a term that recovers the full valence charge density:

$$\begin{aligned} n(\mathbf{r}) &= 2\sum_{n=1}^{N/2} |\psi_n(\mathbf{r})|^2 + 2\sum_{n=1}^{N/2}\sum_I \sum_{ij} Q_{ij}^I(\mathbf{r}-\mathbf{R}_I)\langle\psi_n|\beta_i^I\rangle \\ &\quad\times\langle\beta_j^I|\psi_n\rangle \\ &= 2\sum_{n=1}^{N/2}\langle\psi_n|\Lambda(\mathbf{r})|\psi_n\rangle. \end{aligned} \tag{137}$$

Consistent with this definition, the orbitals are postulated to obey generalized orthogonality constraints $\langle\psi_n|S|\psi_m\rangle=\delta_{nm}$, with an overlap operator $S$ given by

$$S(\mathbf{r},\mathbf{r}')=\delta(\mathbf{r}-\mathbf{r}')+\sum_I \sum_{ij} q_{ij}^I\beta_i^I(\mathbf{r}-\mathbf{R}_I)\beta_j^{*I}(\mathbf{r}'-\mathbf{R}_I), \tag{138}$$

where $q_{ij}^I=\int Q_{ij}^I(\mathbf{r})d\mathbf{r}$. The $S$ operator depends on the atomic positions, as do the constraints obeyed by the orbitals.

The orbitals are determined by minimizing the total energy within the above constraints. This yields a generalized Kohn-Sham equation,

$$H_{SCF}|\psi_n\rangle=\epsilon_n S|\psi_n\rangle, \tag{139}$$

where $H_{SCF}$ is the Kohn-Sham Hamiltonian,

$$H_{SCF}=-\frac{\hbar^2}{2m}\frac{\partial^2}{\partial\mathbf{r}^2}+V_{KS}. \tag{140}$$

Here $V_{KS}$ is the Kohn-Sham potential, $V_{KS}=\tilde{V}_{NL}+V_{loc}+V_{Hxc}$, while $V_{Hxc}$ is the Hartree and exchange-correlation potential, and $\tilde{V}_{NL}$ is the nonlocal part, Eq. (136), in which the atomic coefficients $D_{ij}^{(0)I}$ are replaced by screened coefficients $D_{ij}^I$ (Laasonen *et al.*, 1993).

$$D_{ij}^I=D_{ij}^{(0)I}+\int Q_{ij}^I(\mathbf{r})V_{eff}(\mathbf{r})d\mathbf{r}, \tag{141}$$

where $V_{eff}=V_{loc}+V_{Hxc}$. The forces acting on the atoms are obtained as in Sec. II.C, differentiating the total energy with respect to the atomic displacements and using the Hellmann-Feynman theorem. In the ultrasoft pseudopotential case, however, the orthogonality constraints change as the atoms move, thus giving rise to additional terms in the forces. Differentiating the generalized orthogonality constraints with respect to atomic displacements $u_s^\alpha$ for the $s$th atom, we obtain the following relationship:

$$\left\langle\frac{\partial\psi_n}{\partial u_s^\alpha}\middle|S\middle|\psi_m\right\rangle+\left\langle\psi_n\middle|S\middle|\frac{\partial\psi_m}{\partial u_s^\alpha}\right\rangle=-\left\langle\psi_n\middle|\frac{\partial S}{\partial u_s^\alpha}\middle|\psi_m\right\rangle, \tag{142}$$

which, used in the expression of the forces, gives

$$F_s^\alpha=-2\sum_{n=1}^{N/2}\left\langle\psi_n\middle|\frac{\partial V_{KS}}{\partial u_s^\alpha}-\epsilon_n\frac{\partial S}{\partial u_s^\alpha}\middle|\psi_n\right\rangle, \tag{143}$$

where the partial derivative of $V_{KS}$ is

$$\begin{aligned} \frac{\partial V_{KS}(\mathbf{r}_1,\mathbf{r}_2)}{\partial u_s^\alpha} &= \frac{\partial V_{NL}(\mathbf{r}_1,\mathbf{r}_2)}{\partial u_s^\alpha} \\ &\quad+\int\frac{\partial V_{loc}(\mathbf{r}_3)}{\partial u_s^\alpha}\Lambda(\mathbf{r}_3;\mathbf{r}_1,\mathbf{r}_2)d\mathbf{r}_3 \\ &\quad+\int V_{eff}(\mathbf{r}_3)\frac{\partial\Lambda(\mathbf{r}_3;\mathbf{r}_1,\mathbf{r}_2)}{\partial u_s^\alpha}d\mathbf{r}_3, \end{aligned} \tag{144}$$

with no derivative of the Hartree and exchange-correlation potential.

In order to compute the interatomic force constant and hence the dynamical matrix, we need the mixed second derivatives of the total energy with respect to the displacements $u_s^\alpha$ and $u_t^\beta$ of the atoms at sites $s$ and $t$. These expressions have been derived by Dal Corso *et al.* (1997). Here we report only the final results. [A full derivation is given by Dal Corso (2001).] Taking the derivative of the Hellmann-Feynman forces, one finds that the electronic contribution to $C_{st}^{\alpha\beta}$ contains four terms. The first, $C_{st}^{(1)\alpha\beta}$, corresponds to the expectation value of the second derivative of the electron-ion potential, and the additional second derivative of the overlap matrix:

$$C_{st}^{(1)\alpha\beta}=2\sum_{n=1}^{N/2}\left\langle\psi_n\middle|\left[\frac{\partial^2(\tilde{V}_{NL}+V_{loc})}{\partial u_s^\alpha\partial u_t^\beta}-\epsilon_n\frac{\partial^2 S}{\partial u_s^\alpha\partial u_t^\beta}\right]\middle|\psi_n\right\rangle, \tag{145}$$

where the second derivative of $\tilde{V}_{NL}$ is performed at fixed charge density as before. The second term, $C_{st}^{(2)\alpha\beta}$, is

$$C_{st}^{(2)\alpha\beta}=2\sum_{n=1}^{N/2}\left[\left\langle\frac{\partial\psi_n}{\partial u_s^\alpha}\middle|P_c^+\middle|\phi_{t,n}^\beta\right\rangle+\text{H.c.}\right], \tag{146}$$

where $P_c^+=1-\Sigma_{m=1}^N S|\psi_m\rangle\langle\psi_m|$ is the projector on the conduction-band subspace, H.c. indicates the Hermitian conjugate with respect to the $s\alpha,t\beta$ indices, and $\phi$ is defined as

$$|\phi_{t,n}^\beta\rangle=\left[\frac{\partial(\tilde{V}_{NL}+V_{loc})}{\partial u_t^\beta}-\epsilon_n\frac{\partial S}{\partial u_t^\beta}\right]|\psi_n\rangle, \tag{147}$$

and again the derivative of $\tilde{V}_{NL}$ is performed at fixed density. In the norm-conserving pseudopotential scheme, the electronic contribution to $C_{st}^{\alpha\beta}$ is simply given by the sum of $C_{st}^{(1)\alpha\beta}$ and $C_{st}^{(2)\alpha\beta}$ calculated for $S=1$ and $\Lambda(\mathbf{r})=|\mathbf{r}\rangle\langle\mathbf{r}|$. In the ultrasoft pseudopotential scheme one must consider two additional contributions to $C_{st}^{\alpha\beta}$ which have no counterparts in the norm-conserving scheme. $C_{st}^{(3)\alpha\beta}$ is the interaction between the change in the augmentation charge $\Delta^{t\beta}n(\mathbf{r})$ due to the atomic displacement $u_t^\beta$ [see Eq. (152) below] and the change in $V_{Hxc}$ due to the displacement $u_s^\alpha$ [see Eq. (27)]:

$$C_{st}^{(3)\alpha\beta}=\frac{1}{2}\int\left[\frac{\partial V_{Hxc}(\mathbf{r})}{\partial u_s^\alpha}\Delta^{t\beta}n(\mathbf{r})d\mathbf{r}+\text{H.c.}\right]. \tag{148}$$

Finally, $C_{st}^{(4)\alpha\beta}$ is analogous to $C_{st}^{(2)\alpha\beta}$ but with the projector on the conduction-states subspace replaced by that on the valence-state subspace. Since the perturbation formalism provides explicitly only $P_c|\partial\psi_i/\partial u_s^\alpha\rangle$, the valence-state component must be derived from the constraints imposed by the orthogonality condition, Eq. (142). One finally obtains

$$C_{st}^{(4)\alpha\beta}=-2\sum_{n,m=1}^{N/2}\left\langle\psi_n\middle|\frac{\partial S}{\partial u_s^\alpha}\middle|\psi_m\right\rangle\langle\psi_m|\phi_{t,n}^\beta\rangle+\text{H.c.} \tag{149}$$

We note that in the norm-conserving scheme, the left-hand side of Eq. (142) vanishes since $S=1$, and Eq. (142) allows one to show that the contribution to $C_{st}^{\alpha\beta}$ from the valence-states component of $|\partial\psi_i/\partial u_s^\alpha\rangle$ is zero. In the ultrasoft case, Eq. (142) is used to evaluate such a component in terms of the unperturbed orbitals, as given in Eq. (149).

The key ingredient for evaluating the dynamical matrix is $P_c|\partial\psi_n/\partial u_s^\alpha\rangle$, which can be determined, within first-order perturbation theory, by solving the linear system

$$(H_{SCF}-\epsilon_n S)P_c\left|\frac{\partial\psi_n}{\partial u_s^\alpha}\right\rangle=-P_c^+\left[\frac{dV_{KS}}{du_s^\alpha}-\epsilon_n\frac{\partial S}{\partial u_s^\alpha}\right]|\psi_n\rangle, \tag{150}$$

where

$$\left[\frac{dV_{KS}}{du_s^\alpha}-\epsilon_n\frac{\partial S}{\partial u_s^\alpha}\right]|\psi_n\rangle=|\phi_{s,n}^\alpha\rangle+\int\frac{\partial V_{Hxc}(\mathbf{r})}{\partial u_s^\alpha}\Lambda(\mathbf{r})|\psi_n\rangle d\mathbf{r}. \tag{151}$$

Equation (150) is the generalization to the ultrasoft case of the self-consistent linear system given in Eq. (25). The perturbing term depends on the variation of the charge density $\partial n(\mathbf{r})/\partial u_s^\alpha$ through $\partial V_{Hxc}(\mathbf{r})/\partial u_s^\alpha$, while $\partial n(\mathbf{r})/\partial u_s^\alpha$ is a functional of $P_c|\partial\psi_n/\partial u_s^\alpha\rangle$:

$$\frac{\partial n(\mathbf{r})}{\partial u_s^\alpha}=4\sum_{n=1}^{N/2}\left\langle\frac{\partial\psi_n}{\partial u_s^\alpha}\middle|P_c^+\Lambda(\mathbf{r})\middle|\psi_n\right\rangle+\Delta^{s\alpha}n(\mathbf{r}). \tag{152}$$

The term $\Delta^{s\alpha}n(\mathbf{r})$, peculiar to the ultrasoft scheme, has two contributions: $\Delta^{s\alpha}n(\mathbf{r})=\delta^{s\alpha}n(\mathbf{r})+\delta^{s\alpha}n_{ortho}(\mathbf{r})$. The former term,

$$\delta^{s\alpha}n(\mathbf{r})=2\sum_{n=1}^{N/2}\left\langle\psi_n\middle|\frac{\partial\Lambda(\mathbf{r})}{\partial u_s^\alpha}\middle|\psi_n\right\rangle, \tag{153}$$

accounts for the displacement of the augmentation charge at fixed orbitals, whereas the latter,

$$\delta^{s\alpha}n_{ortho}(\mathbf{r})=-2\sum_{n,m=1}^{N/2}\left\langle\psi_n\middle|\frac{\partial S}{\partial u_s^\alpha}\middle|\psi_m\right\rangle\times\langle\psi_m|\Lambda(\mathbf{r})|\psi_n\rangle, \tag{154}$$

appears because of the orthogonality constraints, similar to the $C_{st}^{(4)\alpha\beta}$ term in the interatomic force constants.

The above formalism can be generalized to metallic systems along the same lines as described in Sec. II.C.4. The presence of the fractional occupation numbers modifies the definition of the valence-states subspace, and the terms $\delta^{s\alpha}n_{ortho}(\mathbf{r})$ and $C_{st}^{(4)\alpha\beta}$ must be modified accordingly. For instance, $\delta^{s\alpha}n_{ortho}(\mathbf{r})$ becomes

$$\delta^{s\alpha}n_{ortho}(\mathbf{r})=-2\sum_{n,m=1}^{N/2}[\tilde{\theta}_{F,n}\tilde{\theta}_{n,m}+\tilde{\theta}_{F,m}\tilde{\theta}_{m,n}]\times\left\langle\psi_n\middle|\frac{\partial S}{\partial u_s^\alpha}\middle|\psi_m\right\rangle\langle\psi_m|\Lambda(\mathbf{r})|\psi_n\rangle. \tag{155}$$

### C. Localized basis sets, all-electron implementations

All-electron implementations of DFPT based on localized basis sets exist for both the linearized muffin-tin orbitals (LMTO) method (Savrasov, 1992; Savrasov, 1996) and the linearized augmented plane-waves (LAPW) method (Yu and Krakauer, 1994). LMTO and LAPW are among the most popular all-electron methods in DFT calculations. Their extension to DFPT calculations is especially useful for systems containing transition metals (e.g., high-temperature superconductors and most ferroelectrics) for which the PW-PP approach is not very practical. An earlier implementation using a mixed basis set (localized atomiclike states plus plane

waves) in a pseudopotential formalism (Zein, 1992) and a more recent one (Heid and Bohnen, 1999) are also known.

Localized basis sets and mixed-basis implementations are more complex than plane-wave implementations. Part of the additional complexity arises from Pulay terms in derivatives. The origin of such terms is easily understood. The first derivative of the energy functional [see Eq. (53)] contains the Hellmann-Feynman term, as in Eq. (21), plus a term $\tilde{F}$, coming from implicit dependence through the wave function,

$$\frac{\partial E}{\partial \lambda} = \int n(\mathbf{r}) \frac{\partial V(\mathbf{r})}{\partial \lambda} d\mathbf{r} + \tilde{F}, \tag{156}$$

where

$$\tilde{F} = 2 \sum_{n=1}^{N/2} \int \frac{\partial \psi_n^*(\mathbf{r})}{\partial \lambda} (H_{SCF} - \epsilon_n) \psi_n(\mathbf{r}) d\mathbf{r} + \text{c.c.} \tag{157}$$

vanishes if the wave functions are exact Kohn-Sham orbitals. This is not always true if the wave functions are *approximate* Kohn-Sham orbitals. Let us expand the wave functions into a basis set $\phi_n$, taken to be orthonormal for simplicity:

$$\psi_n(\mathbf{r}) = \sum_j c_j^{(n)} \phi_j(\mathbf{r}). \tag{158}$$

The solution of the Kohn-Sham equations reduces to the solution of a secular equation

$$\sum_k (H_{jk} - \epsilon_n) c_k^{(n)} = 0, \tag{159}$$

where

$$H_{jk} = \int \phi_j^*(\mathbf{r}) H_{SCF} \phi_k(\mathbf{r}) d\mathbf{r}. \tag{160}$$

By inserting the expansion of the Kohn-Sham orbitals into Eq. (157) one finds

$$\tilde{F} = 2 \sum_{n=1}^{N/2} \sum_{jk} \left( c_j^{*(n)} c_k^{(n)} \int \frac{\partial \phi_j^*(\mathbf{r})}{\partial \lambda} (H_{SCF} - \epsilon_n) \phi_k(\mathbf{r}) d\mathbf{r} + \frac{\partial c_j^{*(n)}}{\partial \lambda} (H_{jk} - \epsilon_n) c_k^{(n)} \right) + \text{c.c.} \tag{161}$$

The second term vanishes exactly [see Eq. (159)]. The first term does not vanish if the basis set is not complete and if the basis set depends explicitly on $\lambda$. In realistic calculations using atomic-centered basis sets, the Pulay contribution cannot be neglected. Accurate and reliable calculations of forces and of the force constants require a very careful account of the Pulay terms, which are absent if a plane-wave basis set is used.

LMTO-based linear-response techniques have been used to calculate phonon spectra and electron-phonon couplings in several elemental metals (Savrasov *et al.*, 1994; Savrasov and Savrasov, 1996) and more recently in doped $BaBiO_3$ (Meregalli and Savrasov, 1998) and $CaCuO_2$ (Savrasov and Andersen, 1996). The method has recently been extended to the calculation of spin fluctuations (Savrasov, 1998).

LAPW-based linear-response techniques were first used in the study of the lattice dynamics of CuCl (Wang *et al.*, 1994) and later applied to several materials: SiC (Wang *et al.*, 1996a); ferroelectrics $KNbO_3$ (Yu and Krakauer, 1995; Waghmare *et al.*, 1998; Wang *et al.*, 1996b) and $SrTiO_3$ (LaSota *et al.*, 1998); and the high-$T_c$ superconductor $La_2CuO_4$ (Wang *et al.*, 1999).

The mixed-basis approach has been tested by calculating the phonon dispersions for simple metals containing localized $4d$ electrons: Ag and Y (Heid and Bohnen, 1999) and Ru (Heid, Pintschovius, *et al.*, 2000); it has also been applied to sapphire ($\alpha - Al_2O_3$; Heid, Strauch, and Bohnen, 2000).

## IV. OTHER APPROACHES

### A. The dielectric approach

Historically, the microscopic theory of lattice dynamics was first formulated in terms of *dielectric matrices* (Pick, Cohen, and Martin, 1970). The basic ingredient is the inverse dielectric matrix $\epsilon^{-1}(\mathbf{r},\mathbf{r}')$, relating, in the linear regime, the external perturbation $\Delta V$ to the total electrostatic potential experienced by an external test charge:

$$\Delta V_{test}(\mathbf{r}) = \int \epsilon^{-1}(\mathbf{r},\mathbf{r}') \Delta V(\mathbf{r}') d\mathbf{r}'. \tag{162}$$

As an alternative, the theory can be formulated in terms of the electron polarizability $\chi(\mathbf{r},\mathbf{r}')$, which gives the charge-density linear response to the external perturbation:

$$\Delta n(\mathbf{r}) = \int \chi(\mathbf{r},\mathbf{r}') \Delta V(\mathbf{r}') d\mathbf{r}'. \tag{163}$$

These two response functions are simply related as

$$\epsilon^{-1}(\mathbf{r},\mathbf{r}') = \delta(\mathbf{r}-\mathbf{r}') - \int \frac{e^2}{|\mathbf{r}-\mathbf{r}_1|} \chi(\mathbf{r}_1,\mathbf{r}) d\mathbf{r}_1. \tag{164}$$

Within density-functional theory, one can also define the independent-electron polarizability, $\chi_0(\mathbf{r},\mathbf{r}')$, as the charge-density response to variation of the total Kohn-Sham potential:

$$\Delta n(\mathbf{r}) = \int \chi_0(\mathbf{r},\mathbf{r}') \Delta V_{SCF}(\mathbf{r}') d\mathbf{r}'. \tag{165}$$

The expression for $\chi_0(\mathbf{r},\mathbf{r}')$ in terms of Kohn-Sham orbitals has the well-known form

$$\chi_0(\mathbf{r},\mathbf{r}') = \sum_{n,m} \frac{f_n - f_m}{\epsilon_n - \epsilon_m} \psi_n^*(\mathbf{r}) \psi_m(\mathbf{r}) \psi_m^*(\mathbf{r}') \psi_n(\mathbf{r}'), \tag{166}$$

where $f_n$ is the occupancy of the state $f_n = \tilde{\theta}[(\varepsilon_F - \varepsilon_n)/\sigma]$ in the notation of Sec. II.C.4, and the sums over $n$ and $m$ extend to both occupied and empty states. As shown in Sec. II.C.4, only terms involving virtual

transitions from occupied or partially occupied states to empty or partially empty states contribute.

Combining Eqs. (163) and (165) and recalling the relationship between the bare and the Kohn-Sham self-consistent perturbing potential, Eqs. (60) and (57),

$$\Delta V_{SCF}(\mathbf{r}) = \Delta V(\mathbf{r}) + \int K(\mathbf{r},\mathbf{r}')\Delta n(\mathbf{r}')d\mathbf{r}', \tag{167}$$

one gets an integral equation for $\chi$:

$$\chi(\mathbf{r},\mathbf{r}') = \chi_0(\mathbf{r},\mathbf{r}') + \int \chi_0(\mathbf{r},\mathbf{r}_1)K(\mathbf{r}_1,\mathbf{r}_2)\chi(\mathbf{r}_2,\mathbf{r}')d\mathbf{r}_1 d\mathbf{r}_2, \tag{168}$$

or equivalently

$$\chi^{-1}(\mathbf{r},\mathbf{r}') = \chi_0^{-1}(\mathbf{r},\mathbf{r}') - K(\mathbf{r},\mathbf{r}'). \tag{169}$$

This equation, projected onto a plane-wave basis set, becomes a matrix equation, one for each $\mathbf{q}$ point in the Brillouin zone, that can be solved by matrix inversion.

The original dielectric matrix approach has the major drawback that the perturbation must be described by a local potential, and thus it cannot be applied to the lattice dynamics problem if modern nonlocal pseudopotentials are employed to describe the electron-ion interaction. In fact, in this case, not only the unperturbed external potential, but also the perturbation itself is described by a nonlocal operator, and Eq. (163) is not appropriate. For these reasons the calculation of dielectric matrices has been of limited utility for the study of vibrational properties—see for some early examples the empirical pseudopotential calculations of Bertoni *et al.* (1972), Resta and Baldereschi (1981), and Resta (1983). Dielectric matrices have been successfully employed in the study of the macroscopic dielectric properties of simple materials (Baroni and Resta, 1986b) and, more generally, these are an essential ingredient in calculations based on the GW approximation, a theory of electronic structure based on many-body perturbation theory (Hedin, 1999). In these latter cases, in fact, even if the unperturbed external potential is described by nonlocal pseudopotentials, the perturbation of interest is only local, and Eqs. (163) and the following ones still apply.

A modification of the dielectric matrix approach that removes its limitation to local pseudopotentials has been devised by Quong and Klein (1992). The response to the bare potential is stored in a bare response $\Delta n_b(\mathbf{r})$,

$$\Delta n_b(\mathbf{r}) = \int \chi_0(\mathbf{r},\mathbf{r}')\Delta V(\mathbf{r}')d\mathbf{r}' = \sum_{n,m} \frac{f_n - f_m}{\epsilon_n - \epsilon_m} \psi_n^*(\mathbf{r})\psi_m(\mathbf{r})\langle \psi_m|\Delta V|\psi_n\rangle, \tag{170}$$

which need be calculated only once for all nonlocal potentials as well. Then Eq. (165) is applied together with Eq. (167) to yield $\Delta n(\mathbf{r})$,

$$\Delta n(\mathbf{r}) = \Delta n_b(\mathbf{r}) + \int \chi_0(\mathbf{r},\mathbf{r}_1)K(\mathbf{r}_1,\mathbf{r}_2)\Delta n(\mathbf{r}_2)d\mathbf{r}_1 d\mathbf{r}_2. \tag{171}$$

This equation is solved for $\Delta n(\mathbf{r})$ by inverting the kernel of the above integral equation (a matrix in a plane-wave basis):

$$\left(\delta(\mathbf{r}-\mathbf{r}') - \int \chi_0(\mathbf{r},\mathbf{r}_1)K(\mathbf{r}_1,\mathbf{r}')d\mathbf{r}_1\right). \tag{172}$$

The second-order change in the energy can then be calculated as usual.

This approach has been used for the calculations of force constants in Au (Quong, 1994); of electron-phonon coupling (Liu and Quong, 1996) and of thermal expansion in metals (Quong and Liu, 1997); and of the structural stability and electron-phonon coupling in Li (Liu *et al.*, 1999).

This modified dielectric matrix approach is conceptually rather similar to the original DFPT. The main difference is the replacement of the self-consistency cycle needed in DFPT with the construction and inversion of kernel in Eq. (172). This operation is rather time consuming, since it requires the inversion of large matrices and an expensive sum over unoccupied bands, but need be done only once for any given point in the Brillouin zone where the vibrations are computed (as opposed to the self-consistency in DFPT, which must be performed for each phonon mode).

For small systems the overall computational workload of the two approaches is similar, but the size of the systems that can be treated by the dielectric approach is limited by the growing dimension of the kernel operator, Eq. (172).

### B. Frozen phonons

The frequencies of selected phonon modes can be calculated from energy differences—or from the forces acting on atoms—produced by finite, periodic, displacements of a few atoms in an otherwise perfect crystal at equilibrium. The first such so-called *frozen-phonon* LDA calculations were already being performed in the early 1980s (see, for instance, Yin and Cohen, 1982). A frozen-phonon calculation for lattice vibrations at a generic $\mathbf{q}$ vector requires a supercell having $\mathbf{q}$ as a reciprocal-lattice vector and whose linear dimensions must be therefore at least of the order of $2\pi/|\mathbf{q}|$. In practice, the size of the supercell that one can afford to deal with has traditionally limited the application of this technique to zone-center or selected zone-boundary phonon modes in relatively simple materials. However, zone-center phonons are also the best characterized because they may be Raman or infrared active, so that they do not require neutron spectroscopy to be detected. Moreover, the frozen-phonon and linear-response techniques may be combined to study anharmonic effects that would otherwise be difficult to calculate directly from perturbation theory (Baroni and Resta, 1986a; Debernardi, 1999).

Phonon dispersions along high-symmetry lines in simple materials are determined by the so-called *interplanar force constants* (i.e., by the forces acting on planes perpendicular to the phonon wave vector when

another such plane is rigidly moved from equilibrium). Lattice vibrations along some high-symmetry lines in cubic semiconductors have been calculated in this way using reasonably sized supercells (Kunc and Martin, 1983). More recently several authors (Wei, and Chou, 1992, 1994; Frank *et al.*, 1995; Ackland *et al.*, 1997; Parlinski *et al.*, 2000) have started to calculate phonon dispersions from the interatomic force constants determined in real space using the frozen-phonon approach.

The main advantage of the frozen-phonon approach is that it does not require any specialized computer code, as DFPT does. This technique can in fact be straightforwardly implemented using any standard total energy and force code, and only moderate care is needed in the evaluation of numerical derivatives. The principal limitation is the unfavorable scaling of the computational workload with the range of the interatomic force constants, $\mathcal{R}_{IFC}$. In fact, the calculation of interatomic force constants within the frozen-phonon approach requires the use of supercells whose linear dimensions must be larger than $\mathcal{R}_{IFC}$, thus containing a number of atoms $N_{at}^{SC} \sim \mathcal{R}_{IFC}^3$. As the computer workload of standard DFT calculations scales as the cube of the number of atoms in the unit cell, the cost of a complete interatomic-force-constant calculation will scale as $3N_{at} \times \mathcal{R}_{IFC}^9$, where $N_{at}$ is the number of (inequivalent) atoms in the elementary unit cell (the factor of 3 accounts for the three generally independent phonon polarizations). The calculation of interatomic force constants using DFPT requires instead the evaluation of the dynamical matrices on a regular grid of wave vectors in the Brillouin zone, whose spacing must be chosen of the order of the inverse of the range of the interatomic force constants: $\Delta q \sim 2\pi/\mathcal{R}_{IFC}$ (see Sec. II.D.3). The number of $\mathbf{q}$ points in such a grid is of the order of $\mathcal{R}_{IFC}^3$. As the computational cost for the calculation of each column of the dynamical matrix is of the order of $N_{at}^3$—and the number of such columns is $3N_{at}$—the total cost for the calculation of the interatomic force constants (and, hence, of complete phonon dispersions) using DFPT is of the order of $\mathcal{R}_{IFC}^3 \times 3N_{at}^4$.

Another problem closely related to these considerations is that of the calculation of phonon dispersions in polar materials. In Secs. II.D.2 and II.D.3 we saw that the long-range character of the dipole-dipole interactions in polar insulators determines the nonanalytic behavior of the dynamical matrices as functions of the wave vector in the long-wavelength limit. The real-space counterpart of this property is that interatomic force constants are long ranged as they decay with the inverse cube of the distance. Interpolation of the dynamical matrices in reciprocal space as well as calculation of the long-range tails of the interatomic force constants in real space is made difficult by this problem. Within DFPT, the standard remedy is to treat separately the nonanalytic part of the dynamical matrix, using information on the ionic effective charges and crystal dielectric constant, as explained in Secs. II.D.2 and II.D.3. Frozen-phonon supercell calculations, in contrast, do not directly provide such information,[4] which must instead be extracted from the limiting behavior of interplanar force constants (Kern *et al.*, 1999), supplied by a separate calculation using the Berry's phase approach (King-Smith and Vanderbilt, 1993; Resta, 1994),[5] borrowed from DFPT calculations (Parlinski *et al.*, 1998), or fitted to the experiment (Parlinski *et al.*, 2000).

### C. Vibrational properties from molecular dynamics

All the methods described so far are static, zero-temperature, methods. In the last 15 years the combined use of molecular dynamics and density-functional theory (Car and Parrinello, 1985) has become a very powerful tool for the *ab initio* study of condensed-matter systems at finite temperature. In molecular-dynamics simulations, atomic trajectories are generated from the classical equations. Equilibrium properties are then estimated as time averages over the trajectories, which also contain information on the dynamics of the system, i.e., on phonon modes. In fact, the vibrational density of states—which exhibits peaks at the phonon frequencies—can in principle be computed by Fourier transforming the atomic velocity autocorrelation function (Rahman, 1964). *Ab initio* molecular-dynamics simulations are usually performed using supercells which contain a small number of atoms (from a few tens to a few hundreds) and periodic boundary conditions. Because of this, only phonons that are zone-center phonons of the supercell are accessible to the simulation.

Straightforward estimates of phonon frequencies from molecular-dynamics simulations suffer from three types of problems. First, at low temperature all the systems are strongly harmonic and, hence, poorly ergodic. The time necessary to reach equilibrium may thus be impractically long. In these cases, bringing the system to thermal equilibrium may require technical tricks such as coupling to Nosé-Hoover thermostats (Martyna *et al.*, 1992).

The second problem is that the simulation time necessary to attain a frequency resolution, $\Delta\omega$, cannot be shorter than $\tau \gtrsim 2\pi/\Delta\omega$. In practice, this time may be too long for first-principles molecular-dynamics simulations. This problem can be overcome by using more sophisticated spectral estimating methods, such as the multiple signal classification (MUSIC) algorithm (Lawrence Marple, 1987), to extract information on phonon modes from relatively short molecular-dynamics runs. MUSIC exploits the harmonic character of phonon modes and has proven to be very accurate and useful in simple situations. In more complicated cases, where the frequencies are too many and too close with respect to the inverse length of the run, MUSIC suffers from instabilities

[4]This is a fact occasionally overlooked in the literature. See, for example, Parlinski *et al.* (1997) and the comment by Detraux *et al.* (1998).

[5]Note that the Berry's phase approach cannot be used to calculate the dielectric constant.

that may prevent the full determination of the spectrum. An improved self-consistent MUSIC algorithm has been developed (Kohanoff *et al.*, 1992; Kohanoff, 1994) to cope with instabilities and to extract information on eigenvectors as well. In this algorithm, a first estimate of the frequencies is followed by a determination of the eigenvectors through a least-squares fit of the trajectory, including orthogonality constraints. Then the trajectory is projected onto each of the normal modes. At this point each projected trajectory contains one main frequency component. This component is reestimated using MUSIC, and the scheme is iterated until self-consistency in the frequencies is achieved.

Finally, when molecular-dynamics simulations are used to predict the temperature dependence of individual vibrational modes and the thermal behavior of properties that depend on them, the results may depend on the size of the simulation (super)cell. In fact, even though in the harmonic approximation a mode commensurate with the simulation cell is strictly decoupled from those that are not, this is not the case at high temperature when anharmonic effects are important. As a consequence, neglect of modes that are not commensurate with the simulation cell may affect the evaluation of frequencies of commensurate modes which, in the harmonic approximation, would be directly accessible to the simulation.

Molecular-dynamics simulations are complementary to lattice-dynamical calculations in the sense that the latter are better suited to low temperatures, whereas the former are subject to ergodicity problems. Lattice dynamics are by definition limited to the (quasi)harmonic regime, while molecular dynamics naturally account for all the anharmonic effects occurring at high temperature, provided the size of the simulation cell is large enough to allow a proper description of the relevant phonon-phonon interactions.

## V. APPLICATIONS

### A. Phonons in bulk crystals

Phonon dispersions in crystals have long been calculated using model force constants in which some form of interatomic potential is assumed and the parameters of the model are adjusted so as to reproduce some known experimental results. Although this approach works reasonably well in some cases, in others it has serious drawbacks that call for more predictive methods. The typical experimental data used to fix the parameters in the model are the phonon frequencies themselves. Model force constants can be seen as a compact way to encode the available experimental input, with very limited predictive power when applied to other properties. In many cases only a few selected frequencies (usually of infrared and Raman-active modes) are known, and the results of model calculations in the rest of the Brillouin zone are questionable. Even when the entire dispersion spectrum is known (usually by neutron-diffraction measurements), knowledge of phonon frequencies alone is not sufficient to determine the force constants completely: knowledge of the phonon displacement patterns would be needed as well. The latter experimental information is seldom available and, in the few cases in which the pattern has been measured, comparison with the results of even the best models is sometimes very poor.

Using DFPT one can compute the interatomic force constants from first principles and, as they are usually accurate, both good frequencies and good displacement patterns are obtained, without need of experimental inputs.

Most, if not all, calculations described in the following sections are done at the level of the local-density approximation, which usually provides very good results. The performance of the generalized gradient approximation (GGA) in the manner proposed by Perdew *et al.* (1996) has been tested by Favot and Dal Corso (1999). It was found that the GGA systematically lowered the frequencies of phonon branches with positive Grüneisen parameters. This effect was correlated with the GGA's expansion of the lattice constant, since GGA phonon frequencies computed at the experimental lattice constants are higher than the corresponding LDA phonon frequencies. A similar trend was found for magnetic Fe and Ni (Dal Corso and de Gironcoli, 2000). In this case GGA equilibrium geometries are much superior to those determined by the LDA, and phonon dispersions are correspondingly closer to the experimental results (Dal Corso and de Gironcoli, 2000). In diamond, Al, and Cu, the LDA and GGA equilibrium geometries and phonon dispersions have similar accuracy with respect to the experimental data. Si is an exception, since the LDA phonon dispersions are already in very good agreement with experiment and the GGA slightly worsens the comparison (Favot and Dal Corso, 1999).

In most applications phonon dispersions are computed at the theoretical equilibrium geometry (lattice parameters and internal coordinates). This choice is mandatory when the experimental geometry is poorly known, but it is also, in our opinion, the most consistent one when comparing with experimental data at low temperature. Inclusion of thermal expansion may become necessary in some cases when comparing with room-temperature and higher-temperature data. See Sec. V.E for the treatment of thermal effects.

#### 1. Simple semiconductors

##### *a. Elemental and III-V semiconductors*

The phonon spectra and effective charges of the group-IV semiconductors Si and Ge (diamond structure) and of the zinc-blende structure III-V semiconductors GaAs, GaSb, AlAs, and AlSb were calculated by Giannozzi *et al.* (1991). The calculated phonon dispersions and densities of states for the latter four compounds are shown in Fig. 1, together with experimental data. Zone-center phonons, effective charges, and dielectric constants of nine III-V zinc-blende semiconductors were computed, along with their piezoelectric constants, by de Gironcoli *et al.* (1989). The phonon

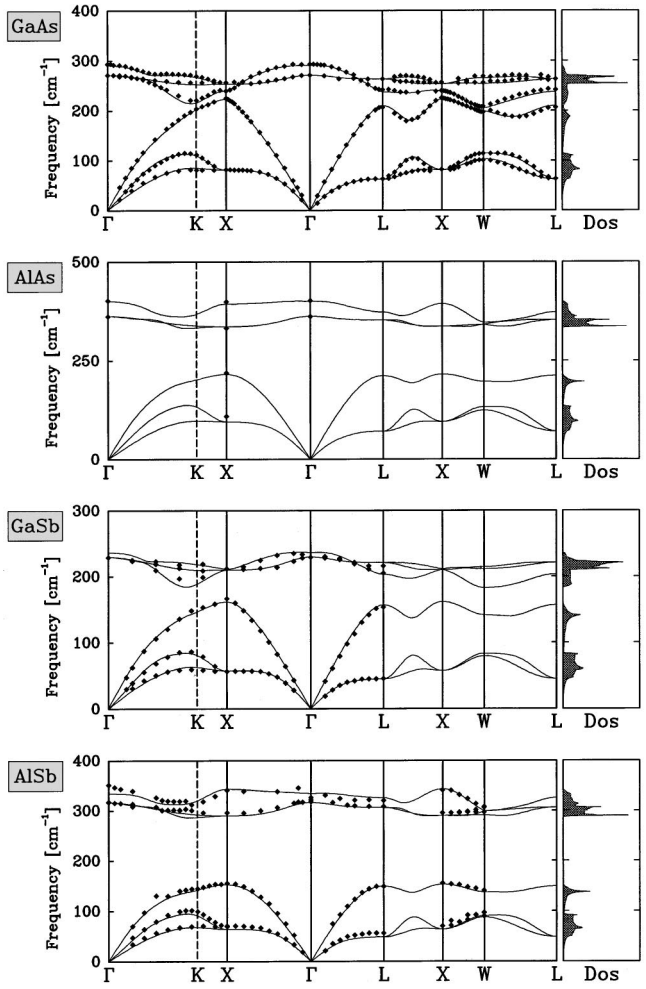


FIG. 1. Calculated phonon dispersions and densities of states for binary semiconductors GaAs, AlAs, GaSb, and AlSb: ◆, experimental data. From Giannozzi *et al.*, 1991.

dispersions of Si were calculated as well by Savrasov (1996) as a test of the LMTO implementation of DFPT. Dispersions for InP appear in a paper devoted to the (110) surface phonons of InP (Fritsch, Pavone, and Schröder, 1995); dispersions for both GaP and InP were published in a study of phonons in $GaInP_2$ alloys (Ozoliņš and Zunger, 1998). For all these materials, phonon spectra and effective charges are in very good agreement with experiments, where available. For AlAs—for which experimental data are very scarce—these calculations provide the only reliable prediction of the entire phonon dispersion curve. For Si, the calculated phonon displacement patterns compare favorably to those extracted from inelastic neutron-scattering experiments (Kulda *et al.*, 1994).

In all these materials the interatomic force constants turn out to be quite long ranged along the (110) direction. This feature had already been observed in early calculations (Herman, 1959; Kane, 1985; Fleszar and Resta, 1986) and is related to the peculiar topology of diamond and zinc-blende lattices, with bond chains propagating along the (110) directions.

The force constants of GaAs and of AlAs are especially interesting in view of their use in complex GaAlAs systems such as superlattices, disordered superlattices, and alloys. While the phonon dispersions in GaAs are experimentally well characterized, bulk samples of AlAs of good quality are not available, and little experimental information on its vibrational modes has been collected. For several years it has been assumed that the force constants of GaAs and those of AlAs are very similar and that one can obtain the dynamical properties of AlAs using the force constants of GaAs and the masses of AlAs (the *mass approximation*; Meskini and Kunc, 1978). The DFPT calculations provided convincing evidence that the mass approximation holds to a very good extent between GaAs and AlAs (Giannozzi *et al.*, 1991). This transferability of force constants makes it possible to calculate rather easily and accurately the vibrational spectra of complex GaAlAs systems (Baroni, Giannozzi, and Molinari, 1990; Molinari *et al.*, 1992; Baroni, de Gironcoli, and Giannozzi, 1990; Rossi *et al.*, 1993). Somewhat surprisingly, the mass approximation does not seem to be valid when the interatomic force constants for a well-known and widely used model, the bond-charge model (BCM), are employed. A six-parameter bond-charge model for GaAs that gives dispersions comparing favorably with experiments and *ab initio* calculations, yields, when used in the mass approximation, AlAs dispersions quite different from first-principles results. This clearly shows that information on the vibrational frequencies alone is not sufficient to fully determine the force constants, even when complete phonon dispersions are experimentally available. In order to obtain more realistic dispersions for AlAs in the mass approximation, one has to fit the bond-charge model for GaAs to both frequencies and at least a few selected eigenvectors (Colombo and Giannozzi, 1995).

### b. II-VI semiconductors

The II-VI zinc-blende semiconductors ZnSe, ZnTe, CdSe, and CdTe present some additional difficulties in a plane-wave-pseudopotential (PP-PW) framework with respect to their III-V or group-IV counterparts. The cation *d* states are close in energy to the *s* valence states so that the *d* electrons should be included among the valence electrons. Phonon calculations performed several years ago, when the inclusion of localized *d* states in the pseudopotential was difficult, showed that the effects of cation *d* electrons could also be accounted for by including the *d* states in the core and by using the nonlinear core-correction approximation. The results showed an accuracy comparable to that previously achieved for elemental and III-V semiconductors (Dal Corso, Baroni *et al.*, 1993). Similar calculations have been more recently performed for hexagonal (wurtzite structure) CdS (Debernardi *et al.*, 1997; Zhang *et al.*, 1996) and CdSe (Widulle, Kramp *et al.*, 1999) and compared with the results of inelastic neutron scattering experiments.

*c. Diamond and graphite*

The phonon dispersions of diamond, together with the internal-strain parameter, thermal-expansion coefficient in the quasiharmonic approximation, and the mode Grüneisen parameter dispersion curves, were calculated by Pavone *et al.* (1993). A unique feature that they found in diamond was the presence of an *overbending* of the uppermost phonon branch, whose frequencies have a minimum at the Brillouin zone center (instead of a maximum as in the other elemental semiconductors Si and Ge). This feature has important consequences for second-order Raman spectra (see Sec. V.A.1.g).

High-pressure spectra, up to 1000 GPa, for diamond are reported in Xie, Chen, *et al.* (1999). Under pressure, the phonon frequencies of the $X_4$ and $L_3'$ modes gradually go higher than those of $X_1$ and $L_2'$, respectively. The overbending of the uppermost phonon branch decreases with the increase of pressure.

Phonon dispersion along the $A$-$\Gamma$-$K$-$M$ line of graphite was calculated by Pavone *et al.* (1996). The curve exhibits an overbending similar to that of diamond for in-plane dispersion. The dispersion between graphitic planes is very flat. The peculiar behavior of low-frequency branches along the $\Gamma$-$K$ line can be related to the long range of interatomic force constants along the zigzag chains in the graphitic planes.

*d. Silicon carbide*

Silicon carbide (SiC) may crystallize in a large variety of tetrahedrally coordinated polymorphs. Phonon dispersion curves were calculated for the 3C (cubic zinc blende), 2H (wurtzite), and 4H hexagonal structures (Karch *et al.*, 1994). For the 3C structure, elastic and Grüneisen constants were calculated as well (Karch *et al.*, 1994). The behavior under pressure of phonon dispersions, effective charges, and dielectric tensor was studied by several authors (Wang *et al.*, 1996a; Wellenhofer *et al.*, 1996; Karch, Bechstedt *et al.*, 1996). Interest in the dynamical properties of SiC under pressure was prompted by a report (Liu and Vohra, 1994) that the splitting between longitudinal-optic (LO) and transverse-optic (TO) modes of 6H SiC increases with increasing pressure until $P=60$ GPa, then decreases. This was attributed to a decrease in the effective charges. This interpretation was not confirmed by any of the above theoretical studies, which pointed out instead that an incorrect volume dependency for the dielectric tensor was assumed in the analysis of experimental data.

*e. Nitrides*

The group-III nitrides are very interesting materials for optoelectronic applications at short wavelengths, as well as in high-frequency and high-temperature electronic devices. Several groups have performed calculations of lattice-dynamical properties for zinc-blende and wurtzite GaN (Karch *et al.*, 1998), BN and AlN (Karch and Bechstedt, 1997), wurtzite AlN, GaN, and InN (Bungaro *et al.*, 2000), wurtzite GaN (Ruf *et al.*, 2000), and AlN (Schwoerer-Böhning *et al.*, 1999). All calculations yield good agreement with available experiments, not only for mode frequencies but also for displacement patterns. In particular, the calculated eigenvector for the Raman-active $E_2$ mode in wurtzite GaN compares well with the eigenvector obtained from the study of the isotope effect (Zhang *et al.*, 1997). The comparison with recent high-resolution inelastic x-ray scattering measurement in wurtzite GaN (Ruf *et al.*, 2000) and AlN (Schwoerer-Böhning *et al.*, 1999) shows good agreement with scattering intensities, thus validating the correctness of computed eigenvectors.

The phonon dispersions in BN and AlN are quite different from those of III-V semiconductors not containing first-row elements: phonon dispersions for BN are similar to those of diamond, while AlN dispersions are close to those of SiC. Furthermore, the difference between BN and AlN phonon dispersions cannot be explained by a simple mass approximation, but derives from the quite different degree of ionicity and covalent strength of the two materials. The marked ionicity of AlN bonding yields a pronounced structural and dielectric anisotropy in the wurtzite structure, larger than that of wurtzite BN and SiC (Karch and Bechstedt, 1997). The three-phonon decay of the LO phonon into two acoustic phonons is not allowed in GaN and InN, since the LO frequency is much larger than the acoustic frequencies over the entire frequency spectrum (Bungaro *et al.*, 2000).

The pressure dependence of the dielectric and lattice-dynamical properties of both zinc-blende and wurtzite GaN and AlN has been recently calculated by Wagner and Bechstedt (2000).

*f. Other semiconductors*

Phonon dispersions of the zinc blende semiconductor CuCl were calculated using the LAPW method (Wang *et al.*, 1994). CuCl exhibits large anharmonic effects. In particular, many peaks in neutron-scattering measurements disappear at temperatures as low as room temperature. The calculated phonon dispersions, however, agree well with low-temperature experimental results.

Phonon dispersion in the bulk layered semiconductor $\epsilon$-GaSe was calculated by Adler *et al.* (1998). The bulk dispersion agrees well both with neutron-scattering results and with surface phonon measurements done using inelastic helium-atom scattering. The calculation of (0001) surface phonons at the $\bar{K}$ point yields small differences with respect to the corresponding bulk phonons, as expected for a layered material. This rules out previous assumptions of anomalous surface phonon dispersions. In a subsequent study (Panella *et al.*, 1999), phonon dispersion in the similar material InSe was calculated. The bulk dispersions for both GaSe and InSe compare favorably with experiments on (001) thin films epitaxially grown on hydrogen-terminated Si(111) $(1\times1)$ surfaces.

The face-centered orthorhombic intermetallic semiconductor $Al_2Ru$ exhibits strong far-IR absorption by optical phonons. Zone-center phonon frequencies, effective charges, and the dielectric tensor were calculated by

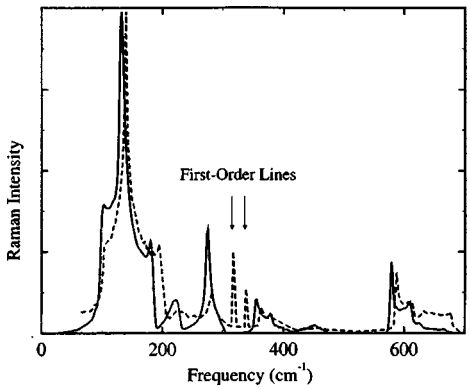


FIG. 2. Second-order Raman spectrum of AlSb in the $\Gamma_1$ representation at room temperature: solid line, the theoretical calculation; dashed line, the experimental spectrum. From Windl *et al.*, 1996.

Öğüt and Rabe (1996), showing anomalously large Born effective charges, in agreement with experiments. An analysis of the valence charge density shows, however, that the static ionic charges of Al and Ru are negligible. Hybridization is proposed as the origin of both of the semiconducting gap and the anomalous Born effective charges.

#### *g. Second-order Raman spectra in simple semiconductors*

Neglecting matrix element effects, second-order Raman spectra are approximately given by the overtone density of states: $I(\omega)=g(\omega/2)$, where $g(\omega)$ is the vibrational DOS. A more accurate description is obtained by combining the *ab initio* phonon spectra with phenomenological polarizability coefficients. This technique was applied in an effort to settle the long-standing controversy over the sharp peak in the spectrum of diamond near the two-phonon cutoff (Windl *et al.*, 1993). As already observed by Pavone *et al.* (1993), the sharp peak is due to a maximum in the vibrational density of states, originating from the overbending of the uppermost phonon branch. Such overbending, and the maximum in the vibrational density of states, are absent in the other elemental semiconductors Si and Ge. Neither two-phonon bound states nor polarizability matrix element effects are needed to explain the peak.

A similar technique was applied to the calculation of second-order Raman spectrum of AlSb in the $\Gamma_1$ symmetry (Windl *et al.*, 1996). The calculated spectrum, shown in Fig. 2, agrees well with recent experimental data. Both theory and experiment give clear evidence for the existence of overbending in the highest-frequency branch of the phonon dispersion, with a saddle point at the $\Gamma$ point as predicted by Giannozzi *et al.* (1991). This evidence is derived from a general discussion of the critical-point behavior. Furthermore, the overbending in AlSb is explained as an effect of the very different masses of the Al and Sb atoms in contrast to the overbending in diamond, whose origin lies in a peculiarity of the force constants.

In the above cases, a one-to-one correspondence between the overtone density of states and the second-order Raman spectrum is quite visible. This is not the case for SiC (Windl *et al.*, 1994). The $\Gamma_1$ spectrum of SiC exhibits three distinct peaks at 1302, 1400, and 1619 $\mathrm{cm}^{-1}$ which occur in the gaps of the overtone density of states. This shows the importance of taking into account the coupling matrix elements.

#### *h. Piezoelectricity in binary semiconductors*

DFPT is used to evaluate the linear response of wave functions to a macroscopic electric field, from which—using the stress theorem of Nielsen and Martin (1985a, 1985b)—one finds the induced stress. Due to large cancellations between contributions of opposite sign, the results are very sensitive to the overall accuracy of the calculation. Well-converged calculations yield results in good agreement with available experimental data in III-V (de Gironcoli *et al.*, 1989) and in II-VI compounds, with the exception of ZnTe (de Gironcoli *et al.*, 1990). Nonlinear piezoelectricity in CdTe was studied as well (Dal Corso, Resta, and Baroni, 1993). It was found that piezoelectricity is linear over a wide range of volume-conserving strains, while it displays strong nonlinearity whenever the strain is not volume conserving. This implies that the observed nonlinear effects can be accurately accounted for by the linear piezoelectric response of the cubic system at the strained volume.

### 2. Simple metals and superconductors

An early calculation of phonon dispersion in Nb and Mo metals was performed by Zein (1992), using a mixed basis set. The aim of the calculation was to explain the presence of a dip in the $(\zeta 00)$ branch of Nb and its absence in Mo.

The accuracy of DFPT for metals (described in Sec. II.C.4) was demonstrated by de Gironcoli (1995) for three test cases: fcc Al, fcc Pb, and bcc Nb (see Fig. 3). In all cases the calculated dispersion curves are in good agreement with experiments if an appropriate smearing technique is used. Phonons in fcc Cu, Ag, Au were calculated as a test case for the use of ultrasoft pseudopotentials (Dal Corso *et al.*, 1997). The alternative linear response technique of Quong and Klein (1992) was applied to the phonon dispersions and interatomic force constants of fcc Al. Phonons of magnetic bcc Fe and fcc Ni have been recently calculated by Dal Corso and de Gironcoli (2000). For these metals, good agreement with experiment is obtained using a spin-polarized generalized-gradient-approximation functional for the exchange and correlation energy (see Fig. 4). Phonons in hcp Ru were calculated and measured with inelastic neutron scattering (Heid, Pintschovius, *et al.*, 2000). Many phonon anomalies were found. Phonons in fcc Ag and in hcp Y were calculated as a test of the mixed-basis-set technique (Heid and Bohnen, 1999).

The main interest of phonon calculations in metals stems from their transport properties, especially superconductivity. The availability of accurate phonon disper-

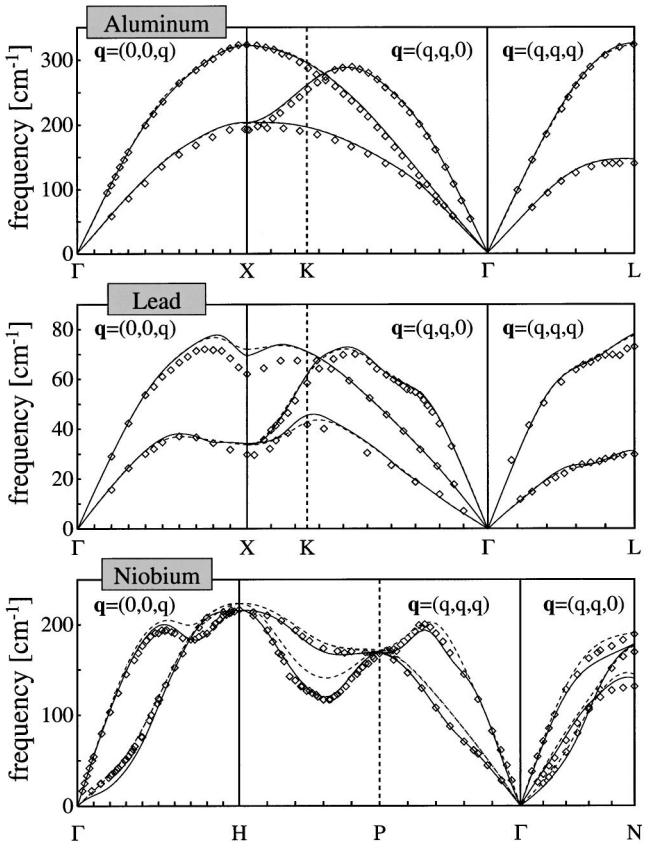


FIG. 3. Calculated phonon dispersions for fcc simple metal Al and Pb and for the bcc transition metal Nb: solid lines, 0.3 eV smearing width; dashed line 0.7 eV, smearing width; ◇, experimental data. From de Gironcoli, 1995.

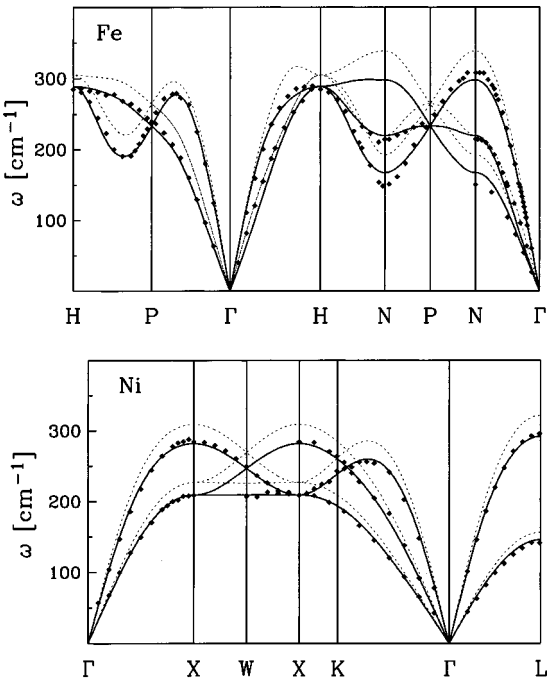


FIG. 4. Calculated phonon dispersions in magnetic transition metals. Upper panel, bcc Fe. Solid lines, calculated GGA phonon dispersions; ◆, inelastic neutron scattering data; dotted lines, dispersions calculated within local spin- density approximation (LSDA). Lower panel, Ni. Solid lines, calculated GGA phonon dispersions; ◆, inelastic neutron scattering data; dotted lines, calculated LSDA dispersions. From Dal Corso and de Gironcoli, 2000.

sions over the entire Brillouin zone allows the calculation of the electron-phonon (Eliashberg) spectral function $\alpha^2F(\omega)$ and of the mass enhancement parameter λ that enters the MacMillan equation for the transition temperature $T_c$ to superconductivity. Other important quantities that can be calculated are the transport spectral function $\alpha^2_{tr}F(\omega)$ and the $\lambda_{tr}$ coefficients, which determine the electrical and thermal resistivity in the normal state. In simple metals, calculations of λ and $\alpha^2F(\omega)$ have been performed for Al, Pb, and Li (Liu and Quong, 1996); for Al, Cu, Mo, Nb, Pb, Pd, Ta, and V (Savrasov and Savrasov, 1996); and for Al, Au, Na, and Nb (Bauer *et al.*, 1998). Transport spectral functions and coefficients (Savrasov and Savrasov, 1996; Bauer *et al.*, 1998) and phonon linewidths due to electron-phonon coupling (Bauer *et al.*, 1998) have also been calculated. Figure 5 shows the results of Savrasov and Savrasov, 1996 for $\alpha^2F(\omega)$.

The calculation of electron-phonon coefficients found a remarkable application, beyond simple metals, in the study of the behavior of molecular solids S, Se, and Te under pressure. With increasing pressure, these transform first to a base-centered orthorhombic superconducting structure, followed by a rhombohedral β-Po phase, and finally for Se and Te by a bcc phase.

At the phase transition between the β-Po and the bcc phase, a jump is observed in $T_c$ in Te. The origin of this jump was clarified (Mauri *et al.*, 1996) through the study of phonon dispersions and of the electron-phonon interactions. The phonon contribution to the free energy was shown to be responsible for the difference in the structural transition pressure observed in low- and room-temperature experiments.

In S, the β-Po phase is predicted to be followed by a simple cubic phase that is stable over a wide range of pressures (280 to 540 GPa), in contrast to what is observed in Se and Te. The calculated phonon spectrum and electron-phonon coupling strength (Rudin and Liu, 1999) for the lower-pressure β-Po phase is consistent with the measured superconducting transition temperature of 17 K at 160 GPa. The transition temperature is calculated to drop below 10 K upon transformation to the predicted simple cubic phase.

### 3. Oxides

Oxides present a special interest and a special challenge for anyone interested in phonon physics. On the one hand, many very interesting materials, such as ferroelectrics and high-$T_c$ superconductors, are oxides. On the other hand, good-quality calculations on oxides are usually nontrivial, both for technical and for more fundamental reasons. In a straightforward PW-PP framework, the hard pseudopotential of oxygen makes calculations expensive: the use of ultrasoft pseudopotentials is generally advantageous. The LDA is known to be insufficiently accurate in many cases (and sometimes the

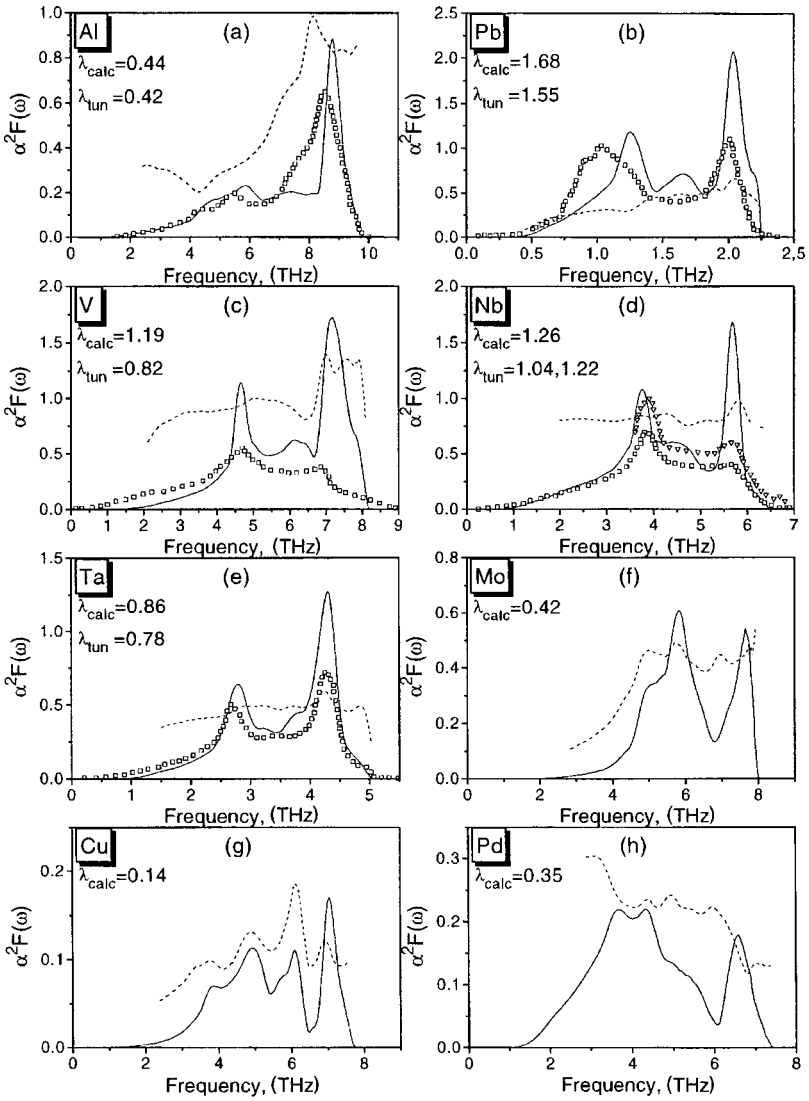


FIG. 5. Electron-phonon interaction for the eight elemental metals considered in Savrasov and Savrasov (1996). Solid lines, calculated spectral functions $\alpha^2F(\omega)$; dashed lines, behavior of the electron-phonon prefactor $\alpha^2(\omega)$ [defined simply as the ratio $\alpha^2F(\omega)/F(\omega)$]; symbol plots, results of available tunneling experiments. From Savrasov and Savrasov, 1996.

entire band-structure approach is questionable in oxides). Many oxides have complex structural arrangements. In spite of all these problems, there have been several calculations of phonon-related properties in oxides from first principles. These calculations are described in the remainder of this section, with the exception of work on phase transitions, which is deferred to Sec. V.D.

### *a. Insulators*

In the alkaline-earth oxides MgO, CaO, and SrO in the rocksalt structure, the LDA yields good agreement with available experimental data for lattice vibrations (Schütt *et al.*, 1994). The investigation of phonon-induced charge-density fluctuations in MgO and CaO at the L point of the Brillouin zone partially supports the breathing-shell model of lattice dynamics and rules out the charge-transfer model for this class of materials. Moreover, the calculations show that the breathinglike charge-density response is more pronounced for oxygen than for the cations in these compounds.

Silicon dioxide ($SiO_2$) is a much-studied prototypical tetrahedrally coordinated compound, existing in a large

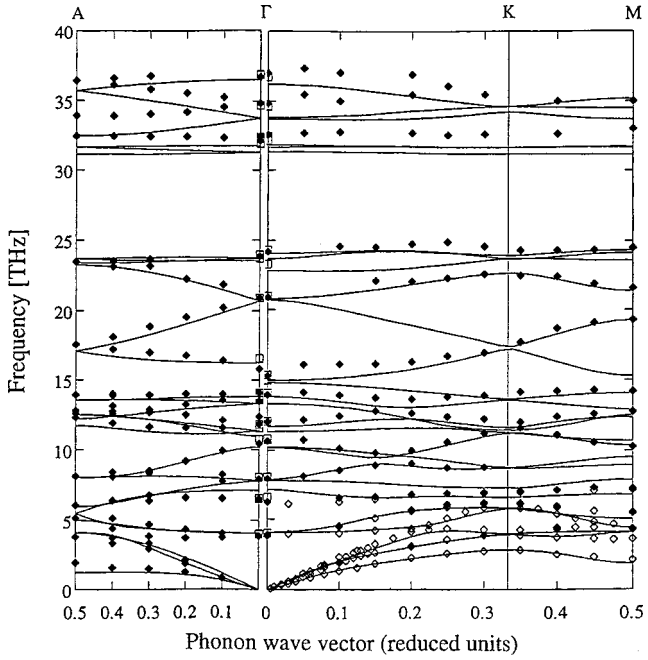


FIG. 6. Phonon band structure of $\alpha$-quartz along selected directions. Symbols, experimental data; lines, theoretical results. From Gonze *et al.*, 1994.

variety of different structures. At ambient conditions the ground-state structure of $SiO_2$ is $\alpha$-quartz, whose phonon dispersions, dielectric tensor, and effective charges were studied by Gonze *et al.* (1992). Effective charges in $\alpha$-quartz are anisotropic (here calculated for the first time in DFPT) and those for O exhibit some anomalous character (see following section). Figure 6 shows the calculated phonon dispersions for $\alpha$-quartz. Interatomic force constants in $\alpha$-quartz were calculated in a subsequent paper (Gonze *et al.*, 1994). The availability of force constants is important because it permits extensives testing of semiempirical interatomic potentials, which are used in molecular-dynamics simulations of silica. The phonons, dielectric tensor, and effective charges of the high-pressure, sixfold-coordinated phase stishovite were studied by Lee and Gonze (1994a).

The phonon dispersions of $\alpha$-$Al_2O_3$ (sapphire) have been recently calculated by Heid, Strauch, and Bohnen (2000), using the LDA and a mixed basis set. Sapphire has a rhombohedral unit cell containing two formula units (ten atoms). A weak anisotropy in the dielectric tensor and in the effective charges was found.

### b. Ferroelectrics

The phonon frequencies at $\Gamma$, the dielectric tensor, and the effective charges of titanium dioxide ($TiO_2$) in the rutile structure were calculated by Lee and Gonze (1994b). Rutile $TiO_2$ is an *incipient ferroelectric*: the frequency of the TO mode $A_{2u}$ decreases with temperature but never goes to zero. It was found that the Born effective charges of $TiO_2$ rutile are much larger than the nominal ionic charges of Ti $(4+)$ and O $(2-)$ ions (and much larger than those of stishovite in spite of the similar structure). This may sound rather counterintuitive but it is typical of all $ABO_3$ ferroelectrics in the perovskite structure (Ghosez *et al.*, 1998b), whose prototypical material is barium titanate ($BaTiO_3$). The effective charges of $BaTiO_3$ and similar compounds exhibit anomalous values that are definitely larger than the ionic charge, as well as a strong anisotropy. For the oxygen atoms in the cubic structure, the effective charge is anomalous only for displacements parallel to the Ti-O bond and is close to the normal ionic value in the orthogonal direction. By performing an appropriate band-by-band decomposition (Ghosez and Gonze, 2000) of contributions, one can track this effect to the dynamical change of hybridization, mainly between O $2p$ and Ti $3d$ orbitals (Ghosez *et al.*, 1995). Born effective charges for cubic $WO_3$ in the defect-perovskite structure (Detraux *et al.*, 1997) and for $KNbO_3$ (Wang *et al.*, 1996b) follow the same pattern. The important role of covalence in determining the anomalous polarization was also demonstrated by Posternak *et al.* (1994), by computing the effective charges of a fake material, similar to $KNbO_3$, in which covalence was artificially removed by an additional potential.

Phonons at $\Gamma$ for the cubic (ideal perovskite) and rhombohedral phases of $BaTiO_3$ were calculated by Ghosez *et al.* (1996). The complete phonon dispersions for the cubic structure, together with an analysis of the interatomic force constants, can be found in Ghosez *et al.* (1998a).

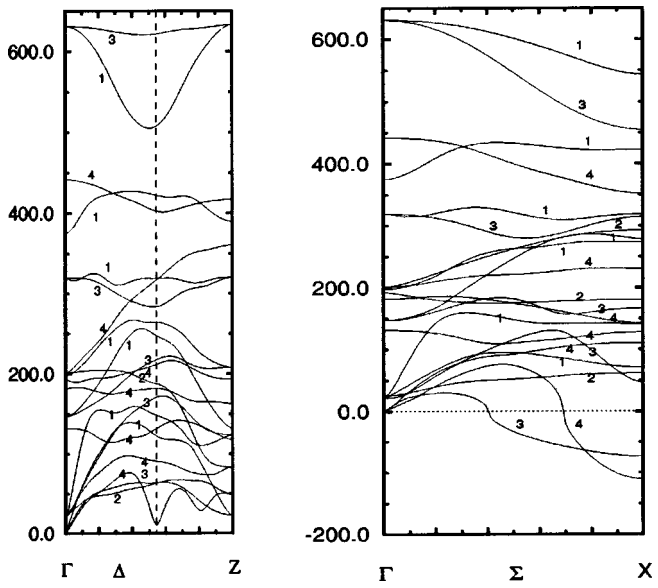


FIG. 7. Calculated phonon dispersion of tetragonal $La_2CuO_4$ along the $(\xi,\xi,0)$ ($\Sigma$) and $(\xi,0,0)$ ($\Delta$) directions. The frequencies are in $cm^{-1}$ and the imaginary frequencies are represented as negative numbers. The vertical dashed line corresponds to the boundary of the first Brillouin zone. From Wang *et al.*, 1999.

### c. High-$T_c$ superconductors

Although the microscopic mechanism that gives rise to superconductivity in high-$T_c$ oxides is still under active debate, accurate phonon dispersions and electron-phonon coefficients constitute important pieces of information for understanding the properties of these materials. Calculations have been performed—at the LDA level—for $CaCuO_2$ (Savrasov and Andersen, 1996), $Ba_{0.6}K_{0.4}BiO_3$ (Meregalli and Savrasov, 1998), and $La_2CuO_4$ (Wang *et al.*, 1999).

In hole-doped ($n=0.24$) $CaCuO_2$, the phonon dispersions and electron-phonon coupling, for both $s$- and $d$-wave pairing, were calculated using LMTO linear-response techniques. The resulting values of $\lambda \simeq 0.3$ for $d_{x^2-y^2}$ symmetry and $\lambda \simeq 0.4$ for $s$ symmetry suggest that the electron-phonon mechanism alone is insufficient to explain the high $T_c$ but could enhance another $d$- wave pairing mechanism (Savrasov and Andersen, 1996).

Similar calculations (Meregalli and Savrasov, 1998) were performed for $Ba_{0.6}K_{0.4}BiO_3$, using the virtual crystal and mass approximations. The $\lambda$ parameter, including anharmonic contributions, is found to be $\lambda=0.34$, a value too small to explain high-$T_c$ superconductivity in this system within the standard mechanism.

In tetragonal $La_2CuO_4$, the phonon frequencies and eigenvectors were calculated using LAPW linear response techniques (Wang *et al.*, 1999). The results (see Fig. 7) are generally in good agreement with experiments, with the exception of the lowest-lying branches

TABLE I. $K_6C_{60}$: Theoretical and experimental frequencies $\omega$ of the optically $C_{60}$-like active modes and shifts $\Delta\omega$ with respect to $C_{60}$. We use the labeling of the $I_h$ group. The $H_g$ modes split into a triplet $T_g$ (left) and a doublet $E_g$ (right). The experimental values are ascribed according to the calculated ordering. Their shifts refer to the centers of gravity. Units are in $cm^{-1}$ (Giannozzi and Andreoni, 1996).

| | $\omega$ | | | $\Delta\omega$ | |
|---|---|---|---|---|---|
| Mode | Theory | Expt.[a] | Expt.[b] | Theory | Expt.[a,b] |
| $A_g(1)$ | 507 | 502 | 501 | 12 | 9, 6 |
| $A_g(2)$ | 1469 | 1432 | 1431 | −35 | −36,−36 |
| $H_g(1)$ | 274, 266 | 281, 269 | 280, 268 | 11 | 6, 5 |
| $H_g(2)$ | 412, 419 | 419, 427 | 419, 427 | −12 | −8,−9 |
| $H_g(3)$ | 660, 660 | 656, 676 | 656, 676 | −51 | −44,−47 |
| $H_g(4)$ | 770, 769 | 761 | 760, 728 | −13 | −11,−25 |
| $H_g(5)$ | 1107,1109 | 1094,1120 | 1093,1122 | −12 | 5, 6 |
| $H_g(6)$ | 1264,1268 | 1237 | 1232,1237 | −15 | −11,−14 |
| $H_g(7)$ | 1423,1414 | 1383 | 1384 | −31 | −43,−38 |
| $H_g(8)$ | 1508,1498 | 1476 | 1481,1474 | −74 | −97,−95 |
| | | Expt.[c] | Expt.[d] | | Expt.[c,d] |
| $T_{1u}(1)$ | 466 | 467 | 467 | −61 | −61,−60 |
| $T_{1u}(2)$ | 571 | 565 | 564 | −15 | −12,−12 |
| $T_{1u}(3)$ | 1215 | 1182 | 1183 | −3 | 0, 0 |
| $T_{1u}(4)$ | 1395 | 1340 | 1341 | −67 | −86,−88 |

[a]Data from Eklund *et al.* (1992).
[b]Data from Kuzmany *et al.* (1994).
[c]Data from Martin *et al.* (1993).
[d]Data from Pichler *et al.* (1994).

involving anharmonic motion of the apical oxygen atoms parallel to the $CuO_2$ planes. The octahedral tilt mode at the $X$ point is found to be the most unstable mode throughout the Brillouin zone, consistent with the observed phase transition to the orthorhombic structure at low temperature. The calculated dispersion of the highest-frequency $\Sigma_3$ branch is in good agreement with experiment, showing that a proposed large renormalization of the phonon spectrum by a Jahn-Teller electron-phonon interaction is unlikely.

#### 4. Other materials

Fullerene $C_{60}$ forms a molecular solid that can be doped with up to six alkali atoms (K, Rb, Cs) per $C_{60}$. The alkalis lose their electrons, which fill the conduction band of $C_{60}$, originated by molecular $t_{1g}$ states. Sizable frequency shifts and a large enhancement in the intensity of the four IR-active modes of molecular $C_{60}$ are observed when K (or Rb, or Cs) is added to solid $C_{60}$. The ten Raman-active modes of molecular $C_{60}$ also exhibit large shifts. In insulating bcc $K_6C_{60}$, the phonons at $\Gamma$ and the effective charges were calculated (Giannozzi and Andreoni, 1996). The frequencies of Raman- and IR-active modes are reported in Table I. It is found that the structural relaxation of the $C_{60}$ molecule is primarily responsible for the frequency changes, while the change in IR relative intensities is a consequence of electron transfer. The potassium vibrations are found to lie within the range 68–125 $cm^{-1}$ and are well decoupled from the $C_{60}$ intramolecular modes. The DFPT results do not support the so-called *charged-phonon* model.

Elemental boron and boron-rich solids tend to form complex structures formed by assembly of icosahedral $B_{12}$ units. The exact structure and vibrational properties of such materials are not well known. A comparison of accurate phonon calculations with IR and Raman measurements is of great help in determining the atomic structure.

Icosahedral boron presents a very sharp peak at 525 $cm^{-1}$ whose vibrational character has long been denied. Recently, new Raman scattering experiments under pressure were compared with *ab initio* lattice dynamics calculations (Vast *et al.*, 1997). The very good agreement of the mode frequencies and their pressure coefficients yields unambiguous assignments of all observed features, including the 525-$cm^{-1}$ line, which is a highly harmonic librational mode of the icosahedron and mainly involves bond bending. This mode is also identified in the Raman spectrum of other icosahedral boron-rich solids (Vast *et al.*, 1997).

Boron carbide, $B_4C$, is the third hardest material after diamond and cubic BN. The building blocks of the crystal are distorted icosahedral $B_{11}C$ units, but their precise arrangement is still experimentally unknown. The structure of icosahedral $B_4C$ boron carbide was theoretically determined by comparing existing IR and Raman spectra with accurate *ab initio* lattice-dynamical calculations, performed for different structural models (Lazzari *et al.*,

1999). An examination of the inter- and intraicosahedral contributions to the stiffness showed that intraicosahedral bonds are harder than intericosahedral ones, contrary to previous conjectures (Lazzari *et al.*, 1999).

Phonons in solid Cl—a typical molecular solid—were calculated by Bauer *et al.* (1995). The calculated intramolecular distance was too large by 8%, possibly due to the pseudopotentials used, and as a consequence the internal phonon frequencies were too low. Intermolecular distances were in good agreement with experiment,[6] as were most of the calculated external phonons (calculated at $\Gamma$ and $Y$; Bauer *et al.*, 1995).

The phonon dispersions of transition-metal carbide NbC were studied as a sample application in a technical paper (Savrasov, 1996). NbC presents several peculiar phonon anomalies, which are well reproduced by the LMTO calculations.

Zone-center phonons and dielectric properties ($\epsilon_\infty$, $Z^*$) of cubic rocksalt alkali hydrides LiH and NaH were calculated by Blat *et al.* (1991). More complete phonon dispersions for LiH and LiD appeared in Roma *et al.* (1996).

### B. Phonons in semiconductor alloys and superlattices

The calculation of phonon dispersions in systems described by large unit cells or lacking periodicity altogether presents a special challenge. Disordered systems (such as amorphous materials or substitutionally disordered alloys) can be described in a PW-PP framework by periodically repeated fictitious *supercells*. However, the needed computational effort quickly grows with the size of the unit cell or supercell (as $\propto N^\alpha$, where $N$ is the number of atoms, $\alpha \sim 3-4$ in practical calculations), so that even with the best algorithms and the best computers available one is limited to systems having at most $\sim 100$ atoms. Such size may or may not be adequate for the physical system under investigation. If it is not, the brute-force approach must be supplemented by a more targeted approach. Typically, accurate first-principles calculations in suitably chosen small systems are used to set up a computationally manageable model for the large system.

#### 1. GaAs/AlAs superlattices

GaAs/AlAs superlattices and alloys are a very successful example of how first-principles calculations supplemented by an appropriate model can lead to an accurate description of the dynamical properties of real systems. As already mentioned in Sec. V.A.1.a, mass approximation is the key for obtaining accurate dynamical matrices for large systems at a modest computational cost, once the interatomic force constants in real space for GaAs (or for the $Ga_xAl_{1-x}As$ virtual crystal) are obtained.

The current interest in phonons in GaAs/AlAs superlattices is a consequence of progress in epitaxial techniques allowing the growth of ultrathin superlattices (with a period of $<10$ atomic layers), in particular along the (100) direction. Owing to the large difference between cationic masses, GaAs and AlAs optic modes occur in different frequency ranges. In a superlattice, optical vibrations are confined in one or the other of the materials. In perfectly ordered superlattices, the relation between confined modes and bulk dispersions of the component materials is given by the *unfolding model* (Jusserand and Cardona, 1989).

It was not at first clear how valid the unfolding model was for ultrathin superlattices, how much disorder at the interfaces (cation intermixing) was present, and what the effect of disorder would be. Simulations of the dynamical properties of ordered and partially disordered superlattices, using the mass approximation and large supercells (Baroni, Giannozzi, and Molinari 1990; Molinari *et al.*, 1992) were able to clarify the problem. It was found that the unfolding model is well verified in ultrathin superlattices, but that a sizable amount of cation intermixing is needed in order to explain the details of the Raman spectra. These findings later received independent confirmation (Gammon *et al.*, 1991; Kechrakos *et al.*, 1991).

It should be remarked that the ability to obtain such results depends critically on the quality of the modeling used. Empirical models, even good ones like the bond-charge model, are too crude and do not adequately describe the dispersions of AlAs and, as a consequence, the details of the spectrum.

Calculation of the phonon spectra in more exotic GaAs/AlAs systems proceeds in the same way. For instance, the vibrational properties of an array of GaAs thin wires embedded in AlAs were calculated by Rossi *et al.* (1993).

#### 2. GaAs/AlAs alloys

The same approach used for GaAs/AlAs superlattices was also used to clarify the results of Raman measurements in GaAs/AlAs homogeneous alloys. The Raman spectrum has two distinct peaks, corresponding to the vibrations of each cationic species separately. This is called *two-mode behavior* and is typical of all $A_xB_{1-x}C$ III-V alloys, with the exception of $Ga_xIn_{1-x}P$. The peaks are shifted and asymmetrically broadened with respect to the pure materials. This asymmetry was interpreted assuming that Raman-active phonon modes are localized on a scale of $\sim 100$ Å, but this assumption was challenged by other experimental results indicating that phonons have well-defined momentum and are coherent over distances $>700$ Å. The results of simulations using a 512-atom supercell (Fig. 8) clearly indicate that the latter picture is the correct one (Baroni, de Gironcoli, and Giannozzi *et al.*, 1990).

[6]The agreement is possibly fortuitous, since LDA does not correctly treat van der Waals interactions and materials held together by them.

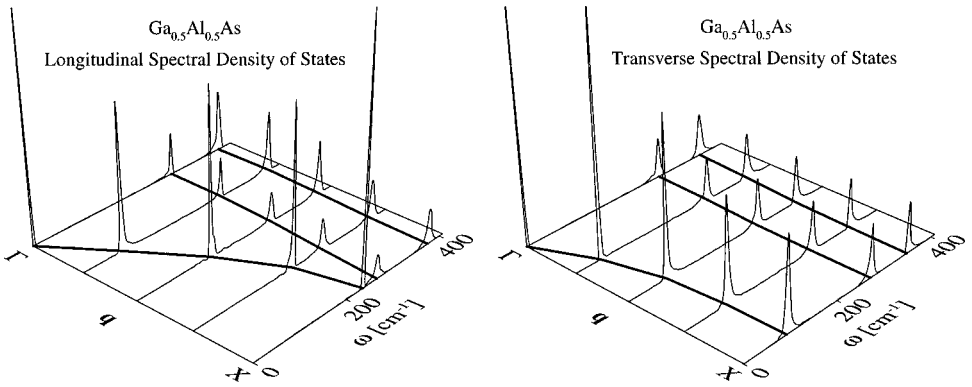


FIG. 8. Spectral densities of states of $Ga_{0.5}Al_{0.5}As$ along the $\Gamma$-$X$ direction: solid lines, positions of the peaks in the $\omega$-$\mathbf{q}$ plane. From Baroni, Gironcoli *et al.*, 1990.

### 3. Si/Ge superlattices and alloys

Si/Ge superlattices and alloys are not only more difficult to grow, but also more problematic as a subject of theoretical study than GaAs/AlAs systems. The mass approximation in Si/Ge systems is quite poor, yielding errors of as much as 20 $cm^{-1}$ for optic phonons. Moreover in Si/Ge systems the lattice parameters of the two components differ by as much as 4%, thus giving rise to sizable strain and atomic relaxations which must be taken into account. GaAs/AlAs systems, in contrast, are almost perfectly matched (their lattice mismatch is a modest 0.2%).

In order to achieve the same level of accuracy for Si/Ge systems as for GaAs/AlAs systems, one has to supplement the mass approximation with a correction that takes into account the effects of strain and atomic relaxation. This goal is achieved by introducing higher-order interatomic force constants that are fitted to first-principles results for a few selected configurations (de Gironcoli, 1992). More complex systems can then be simulated by suitable supercells as for GaAs/AlAs. In this way the vibrational properties of $Si_xGe_{1-x}$ have been studied (de Gironcoli, 1992). In particular this approach was to reproduce the Raman spectra for $Si_{0.5}Ge_{0.5}$, including details due to the local arrangement of atoms, while the mean-field approach (coherent potential approximation, or CPA) badly failed in reproducing the three-mode character of the spectra (de Gironcoli and Baroni, 1992). Higher-order interatomic force constants were also used to study the vibrational properties of ideal and realistically intermixed Si/Ge superlattices (de Gironcoli *et al.*, 1993; Schorer *et al.*, 1994; de Gironcoli and Molinari, 1994).

### 4. AlGaN alloys

The zone-center vibrational properties of wurtzite $Al_xGa_{1-x}N$ alloys, over the entire range of composition from pure GaN to pure AlN, were studied by Bungaro and de Gironcoli (2000) using mass approximation and the arithmetic average of the interatomic force constants of the two pure materials, as previously calculated by Bungaro *et al.* (2000). While some of the alloy modes displayed two-mode-like behavior, they did not preserve well-defined symmetry and had large broadening. The LO modes, in contrast, displayed one-mode behavior and had well-defined symmetry, small broadening, and a pronounced dependence of the frequency upon alloy composition. Therefore these modes were proposed as the best candidates for the compositional characterization of the alloy (Bungaro and de Gironcoli, 2000).

### 5. GaP/InP alloys

A different approach to the study of phonons in semiconductor alloys uses suitably chosen small supercells, or *special quasi random structures* (Zunger *et al.*, 1990) to simulate a disordered system. The evolution of the vibrational properties in GaP/InP systems with long-range order was studied using this approach (with a 16-atom cell) to calculate the phonon spectra of random $Ga_{0.5}In_{0.5}P$ (Ozoliņš and Zunger, 1998). The phonon spectra of pure GaP, InP, and of CuPt-type ordered $GaInP_2$ were calculated for comparison. It was found that ordered $GaInP_2$ and $Ga_{0.5}In_{0.5}P$ had qualitatively different phonon spectra: ordered $GaInP_2$ exhibited two-mode behavior, with two GaP-like and two InP-like phonon modes, while disordered $Ga_{0.5}In_{0.5}P$ exhibited *pseudo-one-mode behavior*: two LO modes, one of GaP and another of mixed GaP/InP character, appeared, while the TO modes of GaP and InP merged into a single alloy mode. This is in remarkable agreement with experiments (Ozoliņš and Zunger, 1998).

### 6. Localized vibrations at defects

Localized vibrational modes of impurities contain a wealth of information on the local structure of the defect. Their analysis requires an accurate knowledge of the phonon spectra of the host crystal. The isotopic fine structure of substitutional impurities in III-V semiconductors was studied using DFPT for the bulk crystal and a Green's-function technique, with results far superior to those obtained using model calculations (Robbie *et al.*, 1995). With these techniques, the host isotope fine structure of $^{12}$C:As and $^{11}$B:As local modes in GaAs (Robbie *et al.*, 1995), of the As:P gap mode (Grosche *et al.*, 1995), and of B:Ga gap and local modes in GaP (Robbie *et al.*, 1996) were successfully analyzed.

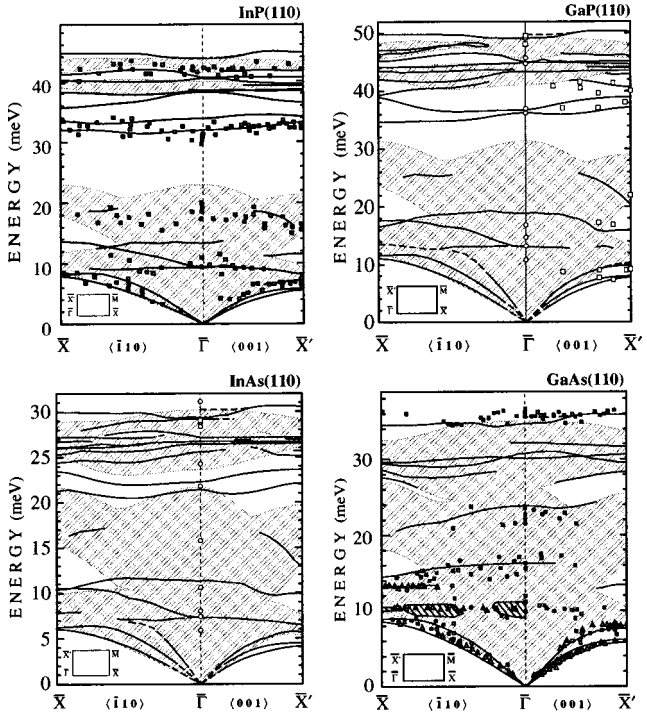


FIG. 9. Phonon dispersion of InP, GaP, InAs, and GaAs(110). The large shaded areas represent the surface projected bulk states. Surface-localized and resonant modes are indicated by *solid* and *dashed* lines. The squares and triangles represent data from HREELS and HAS, respectively. Earlier local density approximation results are indicated by circles. From Eckl, Honke *et al.*, 1997.

### C. Lattice vibrations at surfaces

Most DFPT calculations on surface phonons have focused on semiconductor surfaces (Fritsch and Schröder, 1999; Eckl, Honke, *et al.*, 1997; Stigler *et al.*, 1998).[7] The work on semiconductor surface phonons has been described in a recent extensive review article (Fritsch and Schröder, 1999). In Fig. 9 we show an example of the accuracy that can be reached by these calculations in III-V surfaces.

Other DFPT calculations have been performed for H-covered and clean W(110) surfaces (Bungaro *et al.*, 1996), for Be(0001) (Lazzeri and de Gironcoli, 1998), and for Ag(111) (Xie *et al.*, 1999b) surfaces. Description of the two latter studies is deferred to Sec. V.E.3.

[7]Calculations have been performed for GaAs(110) (Fritsch *et al.*, 1993), InP(110) (Fritsch, Pavone, and Schröder 1995), GaP(110) and InAs(110) (Eckl, Fritsch *et al.*, 1997), InSb(110) (Buongiorno Nardelli, Cvetko *et al.*, 1995); for Si(111) (Ancilotto *et al.* 1991) for Si(001) (Fritsch and Pavone, 1995) and Ge (001) (Stigler *et al.*, 1997); for H-covered (110) surfaces of GaAs, InP (Fritsch, Eckert *et al.*, 1995), and of GaP, InAs (Eckl, Honke *et al.*, 1997), for H- and As-covered Si(111) (1 $\times$1) surfaces (Eckl, Honke *et al.*, 1997; Honke, Pavone, and Schröder, 1996), for Ga- and B-covered Si(111) ($\sqrt{3}\times\sqrt{3}$) R30 (Eckl, Honke *et al.*, 1997); for Ge on GaAs(110) (Honke, Fritsch *et al.*, 1996); and for As-covered (110) surfaces of GaAs, GaP, InAs, InP (Fritsch *et al.*, 2000).

The hydrogen-covered (110) surface of W exhibits phonon anomalies, clearly caused by H adsorption, whose nature is still unclear. An anomaly in the upper Rayleigh phonon branch along the (001) direction has been observed both in helium-atom scattering and in electron energy-loss spectra (EELS). In the lower branch, a similar anomaly is observed by EELS, whereas a much deeper one is only detected by helium-atom scattering. DFPT calculations (Bungaro *et al.*, 1996) yield excellent agreement with both helium-atom scattering and EELS for the upper anomalous branch, and with EELS for the lower branch, provided that a careful sampling of the surface Brillouin zone is performed. Such anomalies are interpreted as due to Fermi-surface nesting (Kohn anomaly). However, the calculations do not predict the deep anomaly observed by helium-atom scattering in the lower branch, whose nature is still not clear. As a byproduct of these calculations, the phonon dispersions for bulk bcc W and for a clean (110) surface have been calculated, and both were found to be in excellent agreement with experiment (Bungaro *et al.*, 1996).

### D. Soft phonons and pressure-induced lattice transformations

Many phase transitions, both those induced by pressure and those induced by temperature, are driven by a lattice instability. This may be an elastic instability (leading to a change of shape of the unit cell) or a phonon instability (a *soft phonon*, whose energy goes to zero). When soft phonons have a nonzero **k** vector (usually at the border of the Brillouin zone) the distortion that sets up causes an increase in the dimensions of the unit cell. The identification of the soft phonon responsible for the phase transition is only the first step in understanding the phase transition. The next step is usually the construction of a realistic model that takes into account all the relevant anharmonic interactions responsible for stabilization of the low-symmetry structure (these may include coupling with the strain, multiple soft modes, and so on).

The earliest calculation using DFPT of a phonon instability was performed on the narrow-gap semiconductors GeTe, SnTe, and PbTe (Zein *et al.*, 1992). The first two exhibit a transition from a high-temperature cubic rocksalt phase to a low-temperature rhombohedral phase, at $T\sim700$ K and $T\sim140$ K, respectively. A calculation of the dielectric and zone-center phonons in the cubic phase yields negative values for $\omega_{TO}$ in GeTe and SnTe and an anomalously low value in PbTe, consistent with experimental observations.

#### 1. Ferroelectrics

The ferroelectric transition in perovskite materials, of which the most famous example is $BaTiO_3$, is closely related to a lattice instability. In ferroelectrics (and in general in temperature-induced phase transitions) anharmonicity plays a fundamental role: harmonic calculations generally yield a negative frequency for the soft

mode at zero temperature. At higher temperature, anharmonicity stabilizes the soft mode. Accurate phonon calculations are in any case the starting point for constructing an effective Hamiltonian for the ferroelectric transition through the use of a localized, symmetrized basis set of *lattice Wannier functions* (Rabe and Waghmare, 1995). These are the phonon analogs of electronic Wannier functions for electrons. Furthermore, the mapping of the phonon instabilities in the full Brillouin zone gives a real-space picture of ferroelectric instability, even when it involves coordinated atomic displacements in several unit cells.

Ferroelectric phase transitions have been studied using DFPT in barium titanate, $BaTiO_3$ (Ghosez *et al.*, 1997), potassium niobate, $KNbO_3$ (Yu and Krakauer, 1995; Wang *et al.*, 1996b), strontium titanate, $SrTiO_3$ (LaSota *et al.*, 1997), lead titanate, $PbTiO_3$ (Waghmare and Rabe, 1997), and lead zirconate, $PbZrO_3$ (Ghosez *et al.*, 1999).

In $KNbO_3$ phonons at the $\Gamma$ point, effective charges, and the dielectric tensor were calculated for the cubic, tetragonal, and rhombohedral perovskite structure. In the hypothetical cubic structure, soft modes are present: one of these modes is stabilized in the experimentally observed tetragonal structure, and all of them are stable in the rhombohedral structure, which turns out to be the most stable one. An effective Hamiltonian has been constructed using lattice Wannier functions by Waghmare *et al.* (1998). For the cubic structure a complete mapping of the phonon dispersion in the Brillouin zone has been computed. The results show a soft-mode dispersion that exhibits an instability of a pronounced two-dimensional nature in reciprocal space and suggests a one-dimensional chain-type instability oriented along the (100) direction of displaced Nb atoms (Yu and Krakauer, 1995). Similar phonon dispersions and chain-type instability were also found in $BaTiO_3$ (Ghosez *et al.*, 1998a).

$SrTiO_3$ exhibits both ferroelectric and antiferrodistortive instabilities. In the cubic structure, phase space of the ferroelectric instability is greatly reduced compared to $KNbO_3$. Antiferrodistortive instabilities exist in one-dimensional cylindrical tubes extending along the entire R-M-R line in the Brillouin zone. The one-dimensional character of these tubes corresponds to real-space planar instabilities characterized by rotations of oxygen octahedra (LaSota *et al.*, 1997).

In $PbTiO_3$, phonons at $\Gamma$, $R$, $X$, $M$ for the cubic structure were used to construct lattice Wannier functions for an effective Hamiltonian. In contrast with the results for $BaTiO_3$ and $KNbO_3$, a significant involvement of the Pb atom in the lattice instability was found. Monte Carlo simulations for this Hamiltonian showed a first-order cubic-tetragonal transition at 660 K. The resulting temperature dependence of spontaneous polarization, $c/a$ ratio, and unit-cell volume near the transition were in good agreement with experiment. Both coupling with strain and fluctuations are necessary to produce the first-order character of this transition (Waghmare and Rabe, 1997).

The full phonon dispersion relations of $PbTiO_3$ and of $PbZrO_3$ in the cubic perovskite structure were computed and compared with previous results for barium titanate by Ghosez *et al.* (1999). The comparison (see Fig. 10) shows that the change of a single constituent has a deep effect on the character and dispersion of unstable modes, with significant implications for the nature of the phase transitions and the dielectric and piezoelectric responses of the compounds. The unstable localized ferroelectric mode of $PbTiO_3$ has a much weaker dispersion with respect to $BaTiO_3$. As a consequence ferroelectric distortion is almost isotropic in real space. Furthermore, there is an antiferrodistortive instability at the $R$ point, not present in $BaTiO_3$ or $KNbO_3$. In $PbZrO_3$ the ground state is antiferroelectric and is obtained by freezing mainly modes at $R$ and $\Sigma$. The phonon dispersions therefore show even more pronounced instabilities. The unstable branches are dominated by Pb and O displacements. Examination of the interatomic force constants in real space for the three structures $PbTiO_3$, $PbZrO_3$, and $BaTiO_3$ shows that while most are very similar, it is the difference in a few key interactions which produces the observed changes in the phonon dispersions. This suggests the possibility of using the transferability of force constants to predict the lattice dynamics of perovskite solid solutions.

### 2. Pressure-induced phase transitions

The subject of pressure-induced phase transitions has become increasingly important since the invention of the diamond anvil cell. Beyond a fundamental interest, the behavior of matter at very high pressures (such as those found in the interior of the earth and of other planets) is relevant in geology and astronomy.

Contrary to what happens in temperature-induced phase transitions, anharmonicity does not necessarily play an important role in pressure-induced phase transitions. One or more harmonic frequencies may become soft as a consequence of the changes in volume and atomic positions caused by applied pressure. It is therefore important to determine whether phonon instabilities occur and whether they occur at lower or higher pressure with respect to other possible instabilities.

#### *a. Cesium halides*

Cesium halides—CsI, CsBr, CsCl—crystallize in the cubic B2 structure at low pressure. Under high pressure, CsI makes a continuous transition to a lower-symmetry phase, whose onset is as low as $P \simeq 15$ GPa. The lower-symmetry phase was originally thought to be tetragonal, but it was later identified as an orthorhombic phase, approaching a hexagonal close-packed structure with increasing pressure (Mao *et al.*, 1989, 1990). CsBr also has a phase transition around $P = 53$ GPa, while it is not clear if such a transition is present in CsCl.

A detailed study of the phonon spectra and of the elastic stability of CsI (see Fig. 11) reveals that an elastic instability leading to a cubic-to-tetragonal transition is in competition with a phonon instability of zone-boundary

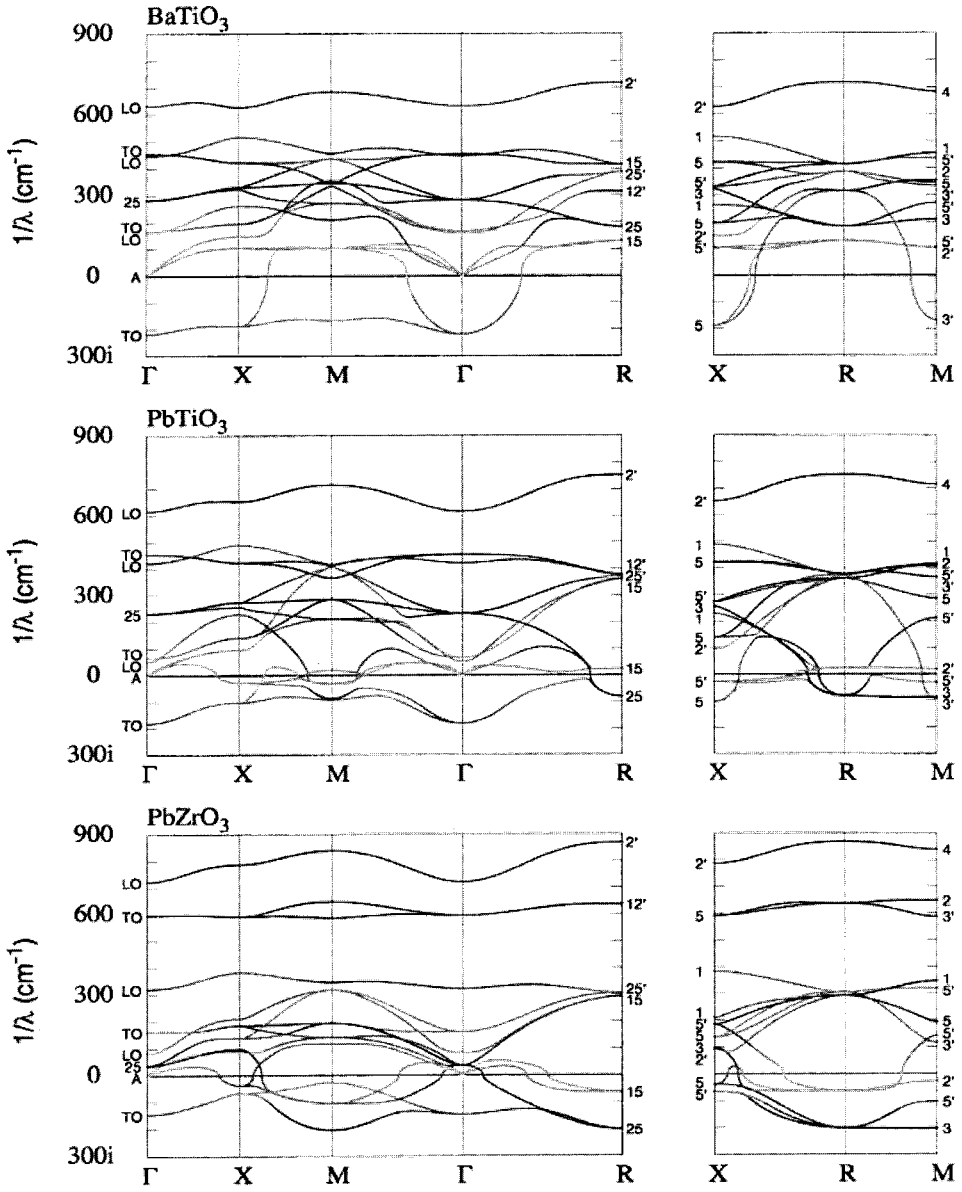


FIG. 10. Calculated phonon dispersion relations of $BaTiO_3$, $PbTiO_3$, and $PbZrO_3$ along various high-symmetry lines in the simple cubic Brillouin zone. From Ghosez *et al.*, 1999.

$M_5^-$ modes (Buongiorno Nardelli, Baroni, and Glannozzi, 1995). In the framework of Landau theory, a phenomenological model for the free energy around the transition can be set up using the results from first-principles calculations. Group theory allows one to restrict the search for minimum-energy structures to those whose symmetry group is a subgroup of the group of the undistorted structure. The resulting model is still quite complex: the order parameter (the amplitude of the soft phonons) is six dimensional. In CsI, the coupling between phonons and strain plays a crucial role in favoring the transition, driven by a soft phonon, to an orthorhombic structure from the tetragonal one. In CsBr, by contrast, the elastic instability leading to the cubic-to-tetragonal transition may instead occur before the phonon instability. Finally, in CsCl, no softness of the zone-boundary phonons and a very weak tendency towards elastic instability are observed (Buongiorno Nardelli, Baroni, and Giannozzi, 1995).

### b. Cesium hydride

Like most alkali hydrides, CsH crystallizes in the rocksalt (cubic $B1$) structure and undergoes a transition to the CsCl (cubic $B2$) structure under moderate pressure. A second transition from the $B2$ structure to a new orthorhombic phase (assigned to a CrB structure, space group $D_{2h}^{17}$) has been observed in CsH at $P \sim 17$ GPa (Ghandehari *et al.*, 1995). Saitta *et al.* (1997) have shown that this first-order transition is intimately related to a displacive second-order transition (driven by a soft phonon at the $M$ point of the BZ, $M_2^-$) which would occur upon application of a shear strain to the (110) planes.

### c. Silicon dioxide

Silicon dioxide exists in a large number of different phases, both crystalline and amorphous. A surprising and still not fully understood phenomenon (observed in many other materials as well) is pressure-induced amorphization, taking place for $SiO_2$ at room temperature

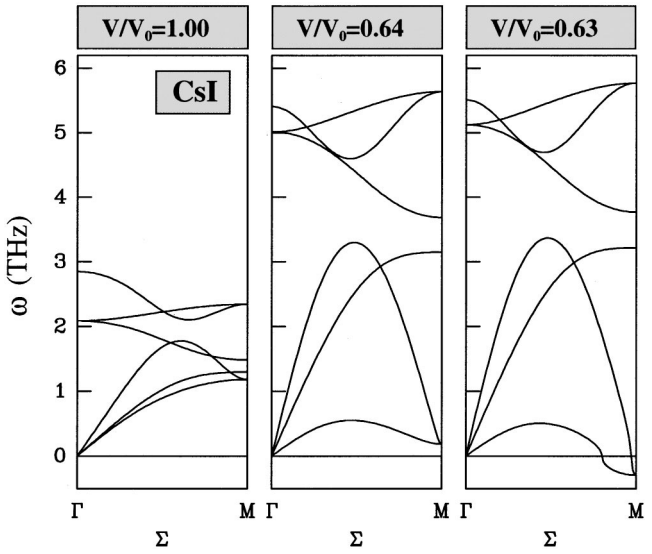


FIG. 11. Phonon dispersion relation along the Σ (110) for CsI at equilibrium volume and just above and below the softening pressure of the $M_5^-$ acoustic mode. Negative frequencies actually mean imaginary (i.e., negative squared frequencies). From Buongiorno, Nardelli, Baroni *et al.*, 1999.

with an onset around 15–25 GPa (Kingma, Meade *et al.*, 1993; Kingma, Hemley *et al.*, 1993). DFPT calculations (Fig. 12) show that a zone-boundary phonon, at the $K$ point of the Brillouin zone, becomes soft at $P \sim 30$ GPa. Baroni and Giannozzi (1998) suggested that the extreme flatness of an acoustic phonon band whose edge goes soft may be related to the strange behavior of amorphization. As a matter of fact, a transition to a disordered state is observed in a simple model for (strongly) anharmonic vibrations in one dimension when the strength of the harmonic coupling is smaller than some critical value. The isostructural compound $AlPO_4$ berlinite, which undergoes a similar pressure-induced amorphization, also has a soft phonon at the $K$ point of the Brillouin zone (Baroni and Giannozzi, 1999), and displays a similar—although less pronounced—flattening of the acoustic band just before amorphization.

The stability of stishovite (tetragonal rutile structure) under high pressure was studied by Lee and Gonze

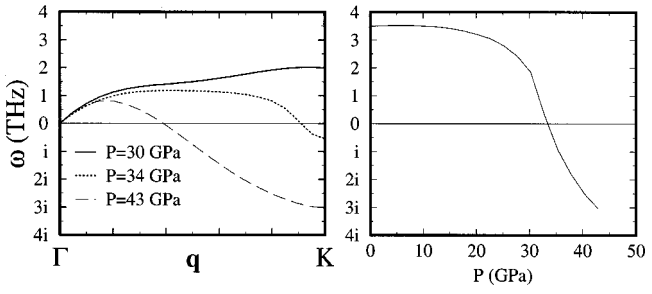


FIG. 12. Soft mode in $\alpha$-quartz. Left panel, $\alpha$-quartz phonon spectra along the $\Gamma$-$L$ line for the soft mode: solid line, at $P = 30$ GPa; dotted line, $P = 34$ GPa; dashed line, $P = 43$ GPa. Right panel: dependence of the soft-mode frequency at the $K$-point upon pressure. From Baroni and Giannozzi, 1998.

(1997). Both a ferroelastic instability to the orthorhombic $CaCl_2$ phase and a softening of the $B_{1g}$ phonon mode at Γ were found. The former preceded the latter, at $P = 64$ GPa, thus leading to a second-order transition to the $CaCl_2$ structure.

### d. Semiconductors

In $A^N B^{8-N}$ octet semiconductors, one would expect a sequence of transitions with increasing pressure into the structures of more ionic binary compounds: zinc blende→NaCl→$\beta$-tin. Earlier experimental and theoretical data supported this picture. However, newer and more accurate angle-dispersive x-ray measurements have revealed that the high-pressure structures of most III-V semiconductors are more complex than expected on the basis of this simple picture. The reason is that the NaCl and $\beta$-tin structures may become unstable with respect to lattice instabilities (soft phonons). Ozoliņš and Zunger (1999) explain the systematic absence of the NaCl phase for all covalent compounds below a critical ionicity value in terms of the instability of a zone-boundary transverse-acoustic (TA) phonon at the $X$ point, leading to a $Cmcm$ phase. The $\beta$-tin structure turns out to be unstable for all but the most covalent compound, due to the presence of a phonon anomaly along the $c$-axis direction in the LO branch (Ozoliņš and Zunger, 1999). A similar approach (Kim *et al.* 1999) shows that in most III-V semiconductors the CsCl structure, which was believed to follow the $\beta$-tin structure at very high pressure, is actually unstable for GaP, GaAs, InP, and InAs, due to the softening of TA phonons at the $M$ point. A Landau analysis of the phase transition leads to two candidate high-pressure structures, the InBi and the AuCd structures, respectively.

The softening of zone-boundary TA modes in germanium was studied both experimentally with inelastic neutron scattering and theoretically with DFPT calculations by Klotz *et al.* (1997). Softening is prevented by an unrelated first-order transition to the $\beta$-tin structure occurring at $P = 9.7$ GPa.

### e. Solid hydrogen

The nature of the high-pressure phases of solid hydrogen is a fascinating subject. In the gas and diluted solid phases, quantum effects are very important and the homopolar $H_2$ molecules, interacting via electric quadrupole-quadrupole interactions, rotate freely even at low temperature. Upon compression, solid hydrogen undergoes a first transition to a broken-symmetry phase (phase II) where the molecule rotation is frozen. At $P \sim 150$ GPa hydrogen undergoes a second transition from phase II to a phase III, not clearly identified, and characterized experimentally by a strong increase in IR activity in the vibronic range. A theoretical study combining constant-pressure *ab initio* molecular dynamics and density-functional perturbation calculations (Kohanoff *et al.*, 1999) addressed this transition and found that phase II (identified as a quadrupolar $Pca2_1$ hcp phase) becomes unstable due to a zone-boundary soft phonon. The resulting candidate structures for phase III have larger unit cells, accounting for the many libronic peaks

experimentally observed, and much larger effective charges, leading to strongly increased IR activity, as observed experimentally.

#### f. Metals

The lattice dynamics of the bcc and fcc phases of W under pressure were studied by Einarsdotter *et al.* (1997). The bcc phase is stable at zero pressure. Under applied pressure, the bcc phase develops phonon softening anomalies for $P \sim 1200$ GPa. At this pressure, however, the fcc and hcp phases have a lower enthalpy than the bcc phase. The fcc phase of W has elastic instabilities at zero pressure that stabilize with increasing pressure before its enthalpy becomes lower than that of the bcc phase.

Phonon instabilities in bcc Sc, Ti, La, and Hf were studied by Persson *et al.* (2000). These metals exhibit hexagonal (Sc, Ti, Hf) or double hexagonal (La) close-packed structure at low temperature, while at high temperature they become bcc.

### 3. Other phase transitions

In the substitutionally disordered narrow-gap semiconductor $Pb_{1-x}Ge_xTe$, a finite-temperature cubic-to-rhombohedral transition appears above a critical concentration $x \sim 0.005$. A hypothetical ordered cubic $Pb_3GeTe_4$ supercell has been studied as a model for such alloys (Cockayne and Rabe, 1997). Unstable lattice modes were found, dominated by off-centering of the Ge ions coupled with displacements of their neighboring Te ions. A model Hamiltonian for this system (using the lattice Wannier function formalism) was constructed and studied via Monte Carlo simulations. A transition temperature of $\sim 620$ K was found for the cubic model, compared to the experimental value of $\sim 350$ K for the alloy.

## E. Thermal properties of crystals and surfaces

The knowledge of the entire phonon spectrum granted by DFPT makes possible the calculation of several important thermodynamic quantities and of the relative stability of different phases as functions of temperature. The first calculation of a thermal property (expansion coefficients in Si) using DFPT dates back to 1989 (Fleszar and Gonze, 1989).

The thermodynamic properties of a system are determined by the appropriate thermodynamic potential relevant to the given ensemble. In an ensemble where the sample volume and temperature are independent variables, the relevant potential is the Helmholtz free energy, $F = E - TS$. For a solid in the adiabatic approximation, the free energy can be written as the sum of an electronic and a vibrational term. The electronic entropy contribution is easily evaluated in metals, although usually neglected, whereas it is totally negligible for insulators: $F_{el} \simeq E_{el}$. The key quantity to calculate in order to have access to the thermal properties and to the phase stability is the vibrational free energy $F_{ph}$.

Far from the melting point, the vibrational free energy $F_{ph}$ can be conveniently calculated within the *quasiharmonic approximation*. This consists in calculating $F_{ph}$ in the harmonic approximation, retaining only the implicit volume dependence through the frequencies:

$$F_{ph}(T,V) = -k_B T \log(\mathrm{Tr} e^{-\mathcal{H}_{ph}(V)/k_B T}), \tag{173}$$

where $\mathcal{H}_{ph}(V)$ is the phonon Hamiltonian at a given volume. In terms of the phonon spectra, $F_{ph}$ can be written as

$$F_{ph}(T,V) = -k_B T \sum_{i,\mathbf{k}} \log\left( \sum_n e^{-(n+1/2)\hbar\omega_{i\mathbf{k}}(V)/k_B T} \right). \tag{174}$$

Once the sum over occupation numbers $n$ is performed, one gets the final formula:

$$F_{ph}(T,V) = k_B T \sum_{i,\mathbf{k}} \log\{2 \sinh[\hbar\omega_{i\mathbf{k}}(V)/2k_B T]\}. \tag{175}$$

In practical calculations, the force constants are calculated at a few volumes and interpolated in between to get the volume dependence. Once the phonon spectrum over the entire Brillouin zone is available, the calculation of $F_{ph}$ reduces to a straightforward integration over the Brillouin zone.

The quasiharmonic approximation accounts only partially for the effects of anharmonicity, through the volume dependence of the phonon spectra (this is clearly an anharmonic effect: the perfect harmonic crystal would have no volume expansion with temperature) but it turns out to be a very good approximation at temperatures not too close to the melting point.

The quantities that can be calculated in the quasiharmonic approximation include equilibrium lattice parameters and elastic constants, specific heat, and thermal expansion coefficients, as a function of the temperature. Corrections due to quantum fluctuations (*zero-point motion*) at zero temperature can be estimated as well. A comparison of the free energies of different phases (not related by symmetry relations, unlike those considered in Sec. V.D) yields the relative stability as a function of pressure and temperature. Most calculations in this field have been performed on simple systems, but there are a few examples of applications to surfaces, notably to anomalous thermal expansion.

### 1. Metals

The equilibrium lattice parameter and thermal expansion coefficients for bcc Li and fcc Al and Na were computed by Quong and Liu (1997). The relative stability of the various polymorphs of Li (bcc, fcc, hcp, $9R$) was examined by Liu *et al.* (1999). It was found that the transformation from the $9R$ structure at low temperatures to the bcc phase upon heating is driven by the large vibrational entropy associated with low-energy phonon modes in bcc Li. The strength of the electron-phonon interaction in Li was calculated and found to be significantly reduced in the low-temperature $9R$ phases

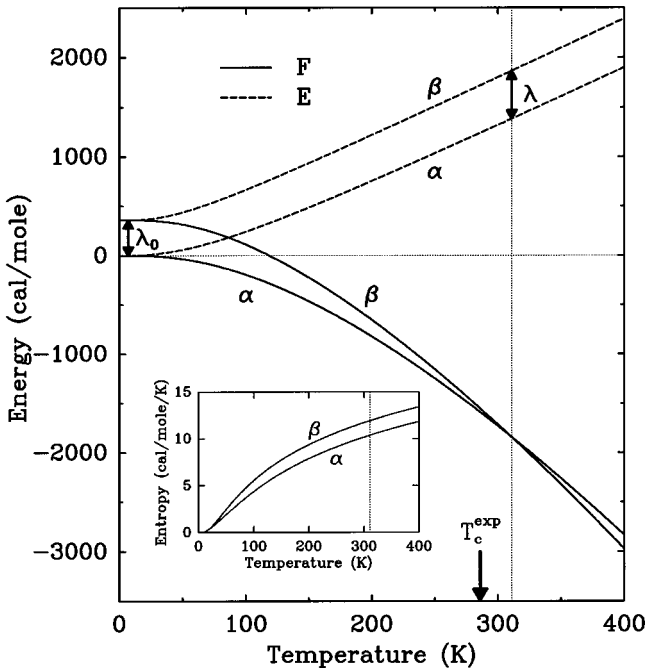


FIG. 13. Zero-pressure energy curves for the $\alpha$ and $\beta$ phases of tin as functions of temperature: solid lines, free energy; dashed lines, internal energy. The thin vertical dotted line indicates the theoretical transition temperature, while the experimental value for $T_c$ is shown by the arrow. $\lambda_0 = 359$ cal/mole is the $T=0$ K free-energy difference—including the zero-point contribution—while $\lambda = 482$ cal/mole indicates and the latent heat adsorbed in the $\alpha \leftrightarrow \beta$ transition. Finally, the inset displays the temperature dependence of the vibrational entropies of the two phases. From Pavone *et al.*, 1998.

as compared to the bcc phase, consistent with the observed lack of a superconducting transition in Li (Liu *et al.*, 1999).

The thermal properties of fcc Ag, plus the Grüneisen parameters, were calculated by Xie *et al.* (1999a).

The $\alpha$-$\beta$ phase transition in tin was studied by Pavone *et al.* (1998). At $T=0$ K, the free energy of the $\beta$ phase lies $\sim 359$ cal/mole above that of the $\alpha$ structure. The narrower frequency range spanned by the vibrational band in the $\beta$ phase makes its entropy larger at high temperature. As a consequence, the free energies of the two phases, shown in Fig. 13, equal each other at a temperature of $\sim 38$ C, in close agreement with the observed transition temperature $T_c = 13$ C (Pavone *et al.*, 1998).

### 2. Semiconductors and insulators

Calculations have been reported of the thermal properties and Grüneisen parameters of Si (Rignanese *et al.*, 1996), of the thermal-expansion coefficients of diamond (Pavone *et al.*, 1993) and of the thermal-expansion coefficient and specific heat of cubic SiC in the $3C$ structure (Karch *et al.*, 1994).

In diamond, thermal properties were calculated at high pressures, up to 1000 GPa (Xie, Chen *et al.*, 1999). The $P$-$V$-$T$ equation of states was calculated from the Helmholtz free energy. The thermal-expansion coefficient was found to decrease with the increase of pressure, and at ultrahigh pressure (700 GPa), diamond exhibited a negative thermal-expansion coefficient at low temperatures.

The temperature dependence of the diamond-$\beta$-tin phase transition in Si and Ge, which occurs under pressure at $\sim 10$ GPa, was calculated by Gaál-Nagy *et al.* (1999) using the quasiharmonic approximation.

Thermal properties (specific heat, entropy, phonon contribution to the free energy, and atomic temperature factors) for $SiO_2$ in the $\alpha$-quartz phase and in the high-pressure stishovite phase were calculated by Lee and Gonze (1995).

The ability of the quasiharmonic approximation to yield thermodynamic properties of materials over a considerable pressure-temperature regime has been asserted in recent papers by Karki *et al.* (1999, 2000). In these works the thermoelastic properties of MgO were calculated over a wide range of pressures and temperatures. Thermodynamic potentials and several derived quantities (such as the temperature dependence of elastic constants at high pressures) were computed and successfully compared with experimental data (Karki *et al.*, 1999, 2000).

### 3. Surfaces

The thermal expansion of surfaces has been calculated for Ag(111) (Xie *et al.*, 199b) and for Be(0001) (Lazzeri and de Gironcoli, 1998).

In Ag(111), the top-layer relaxation changes from an inward contraction ($-0.8\%$) to an outward expansion ($+6.3\%$) as the temperature increases from $T = 0-1150$ K, in agreement with experimental findings. The calculated surface phonon dispersion curves at room temperature are in good agreement with helium-scattering measurements (Xie *et al.*, 1999b).

At the Be(0001) surface, an anomalously large thermal expansion was recently observed in low-energy electron diffraction experiments. The calculations were tested in bulk Be, where they described the thermal expansion very well, and checked against first-principles molecular-dynamics simulations for the surface. A large thermal expansion was not found. This discrepancy could be explained assuming that the actual surface were less ideal than assumed (Lazzeri and de Gironcoli, 1998).

### 4. Alloys

The vibrational contribution to the free energy is known to affect the phase stability of alloys. The importance of this effect has been examined in two metallic alloys, the Cu-Au (Ozoliņš *et al.*, 1998) and Re-W systems (Persson *et al.*, 1999).

Cu-Au systems were studied using a combination of DFPT and cluster expansion methods. The vibrational free energy of the alloy was calculated by a cluster expansion over a small set of representative ordered structures having small supercells, in much the same way as the configurational free energy is calculated. Anhar-

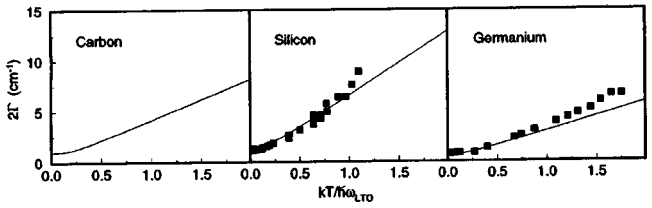


FIG. 14. Temperature dependence of the full width at half maximum, $2\Gamma$, of the zone-center optical phonon in diamond, Si, and Ge: solid lines, the result of DFPT calculation; ■, experimental data. From Debernardi *et al.*, 1995.

monic effects were taken into account through the quasiharmonic approximation. The results indicated that the vibrational free energy contributes significantly to the phase stabilities and thermodynamic functions of the CuAu system. In particular it tends to stabilize the compounds and alloys with respect to the phase-separated state and lowers the order-disorder transition temperatures. It was found that the vibrational free energy, not the vibrational entropy, is the relevant quantity, due to the larger thermal-expansion coefficients of the alloy with respect to the ordered ground states (Ozoliņš *et al.*, 1998).

A somewhat similar approach was applied to the study of the dynamical and thermodynamical stability of the bcc and fcc disordered $Re_xW_{1-x}$ system. As a byproduct, the phonon dispersion curves for fcc and bcc Re were calculated. Fcc Re is dynamically stable but has pronounced phonon anomalies; bcc Re exhibits phonon instabilities in large parts of the Brillouin zone, similar to those found in fcc W. Due to the instabilities in bcc Re and fcc W, the vibrational entropy, and therefore the free energy, is undefined. This problem was circumvented by using the virtual-crystal approximation to calculate the phonon dispersions of disordered $Re_xW_{1-x}$ and by applying a concentration-dependent nonlinear interpolation to the force constants. A region was found where the bcc phase would become thermodynamically unstable towards a phase decomposition into disordered bcc and fcc phases (Persson *et al.*, 1999).

### F. Anharmonic effects

Third-order energy derivatives can be calculated directly from the linear response using the $2n+1$ theorem (See Sec. II.F). The first calculation of anharmonic force constants using DFPT and the $2n+1$ theorem was performed for the lifetimes of zone-center optical phonons in diamond, Si, and Ge (Debernardi *et al.*, 1995) due to their anharmonic decay into two phonons of lower frequency. Anharmonic decay is the main contribution to the linewidth of such Raman-active modes, once isotopic and other inhomogeneous broadening contributions are subtracted. The temperature and pressure dependences of anharmonic lifetimes were calculated as well (see Fig. 14 for the former). The results are in good agreement with experimental data. The microscopic mechanisms responsible for the decay are found to be different for different materials and to depend sensitively on the applied pressure (Debernardi *et al.*, 1995).

Subsequent work was performed in the zinc-blende semiconductors GaAs, AlAs, GaP, InP (Debernardi, 1998) and in SiC (Debernardi *et al.*, 1999). In III-V semiconductors, the linewidth of Raman-active modes, both transverse and longitudinal, and their temperature dependence were computed. For longitudinal phonons a simple approximation consisting of neglecting the effect of the macroscopic electric field in the anharmonic terms yielded good results (Debernardi, 1998). In 3C (cubic zinc blende) SiC the pressure dependence, up to 35 GPa, of the linewidths of the LO and TO modes at the Brillouin zone center was calculated. An anomalous behavior was found: the linewidth of the transverse mode changed very little with pressure, while the longitudinal mode showed a monotonic increase up to 26 GPa, decreasing abruptly above this pressure. The results are in good agreement with new experimental data, up to 15 GPa (Debernardi *et al.*, 1999).

A different approach to anharmonicity combines DFPT to calculate harmonic force constants and frozen phonons to calculate higher-order force constants through numerical differentiation. This approach is less elegant and more sensitive to numerical accuracy than the use of the $2n+1$ theorem. However it allows one to calculate quartic anharmonic terms and those third-order energy derivatives whose calculation with the $2n+1$ theorem is hindered by technical difficulties, such as Raman cross sections in the nonresonant limit (Giannozzi and Baroni, 1994). This approach was first used to calculate the contribution of quantum fluctuations (zero-point motion) to the bulk modulus of diamond and to the dielectric constant of diamond, Si, and Ge. It was also used to calculate the temperature dependence of these quantities (Karch, Dietrich *et al.*, 1996). More recently, the anharmonic shift of the Raman frequency of diamond and Si, in which both cubic and quartic anharmonic terms are equally important, has been calculated (Debernardi, 1999). The temperature dependence of the Raman frequency and the contribution of zero-point motion were calculated as well as the Raman linewidth. The same quantities were calculated in Ge using the $2n+1$ theorem for the cubic terms and assuming that the quartic anharmonic force constants could be approximated by those of silicon (Lang *et al.*, 1999).

### G. Isotopic broadening of Raman lines

In the harmonic approximation, the effect of isotopic disorder or of isotopic substitution is only reflected in the change of masses in the dynamical matrix. The frequency shift caused by isotopic substitution depends on phonon displacement patterns and may be used as a probe of the latter. DFPT results have been applied to the interpretation of Raman experiments in isotopically substituted $C_{60}$ (Guha *et al.*, 1994), in GaN (Zhang *et al.*, 1997), and in SiC (Widulle, Ruf *et al.*, 1999).

Isotopic disorder is also responsible for a broadening and further shift of the Raman lines beyond the virtual-

crystal approximation which replaces the masses of each individual atom with their composition-averaged value. Disorder effects are usually treated within some kind of mean-field approximation (such as the coherent potential approximation). Steininger *et al.* (1999) used both the coherent potential approximation and a supercell approach to calculate the broadening of Raman peaks in Si, Ge, and $\alpha$-tin, employing interatomic force constants calculated from first principles.

Recently Vast and Baroni (2000) presented a new method for studing the effects of isotopic composition on the Raman spectra of crystals beyond the mean-field approximation. The Raman cross section is expressed as a diagonal element of the vibrational Green's function, which is accurately and efficiently calculated using the recursion technique. This method was applied to diamond—where isotopic effects dominate over the anharmonic ones—as well as to Ge, where anharmonic effects are larger. In both cases the results were in very good agreement with experiment (Vast and Baroni, 2000).

Other effects of isotopic substitution appear beyond the harmonic approximation. The molecular volume of crystals depends on isotopic masses through the zero-point motion. This is a tiny but measurable effect, which can be calculated using the quasiharmonic approximation (Sec. V.E). The dependence of the crystal lattice constant on isotopic composition has been calculated for the elemental semiconductors diamond, Si, and Ge (Pavone and Baroni, 1994) and for the compound zinc-blende semiconductors GaAs and ZnSe (Debernardi and Cardona, 1996). In the latter case, the temperature dependence of the derivatives of the lattice constant with respect to both the anion and the cation mass was computed, together with the linear thermal-expansion coefficients and mode Grüneisen parameters.

The dependence of the Raman linewidth in 3C-SiC on both isotopic composition and temperature for longitudinal and transverse modes was calculated by Debernardi and Cardona (1998). The linewidths exhibited a marked and nontrivial dependence on isotopic composition.

### H. Vibrational broadening of electronic core levels

Phonons cause a temperature-dependent broadening of core-level spectra. The calculation of such broadening requires an accurate description of both phonon spectra and of core-excited electronic states. A theoretical framework within which to deal with this problem has been provided by Mäder and Baroni (1997), together with an application to the 1*s* core exciton of diamond, for which a strong vibronic coupling is present. The *sudden approximation* (optical absorption and emission taking place in much shorter times than typical phonon response times) is assumed, leading to a Franck-Condon picture. The electronic and vibrational degrees of freedom are consistently treated using density functional theory. A suitable pseudopotential, generated on the excited atomic configuration, allows one to simulate the excited electronic states. Due to the large lattice distorsion, anharmonicity cannot be neglected. In the limit of infinite core-hole lifetime, anharmonic effects are included within a self-consistent phonon approach. Mäder and Baroni (1997) found the Stokes shift for the 1*s* exciton level to be about 3 eV (the harmonic approximation would overestimate it by about 1.4 eV) and the phonon broadening to be about 2 eV.

## VI. CONCLUSIONS AND PERSPECTIVES

The results reviewed in this paper witness the blossoming of *ab initio* lattice-dynamical calculations in solids, based on density-functional (perturbation) theory. Our ability to predict from first principles the phonon-related properties of materials depends both on the accuracy of the *ab initio* calculation of lattice vibrations and on the quality of the approximations needed to relate these calculations to the specific property one is interested in (e.g., the electric conductivity or the temperature dependence of the crystal volume). The accuracy of the calculations can be appraised by comparing the calculated frequencies with infrared, Raman, or neutron-diffraction experiments. It is fair to state that lattice dynamics is the one field of solid-state physics in which the accuracy of *ab initio* calculations can compete with that of absorption or diffraction spectroscopies. Of course, it would be vain to put much effort into the calculation of quantities that can be measured with comparable or better accuracy. The real value of first-principles calculations is their ability to provide unbiased predictions for those materials and in those cases which are not easily accessible to experiment.

Even though necessarily oversimplified, the physical conditions of the sample being studied numerically are under our total control and can therefore be varied at will. This allows us to assess the quality and validity of models that relate the atomic and electronic structure of materials, which is usually unknown, to their macroscopic and experimentally accessible properties. Once the accuracy of the calculated phonon frequencies has been assessed, the agreement of the predictions for derived quantities gives an indication of the validity of the approximations used to derive them. When inter-atomic distances depend upon temperature, for instance, comparing calculated values with experiment gives an indication of the validity of the quasiharmonic approximation used to calculate them. Rather surprisingly, it turns out that in a variety of cases, this approximation gives precise results almost up to the melting temperature.

In conclusion, the field of lattice-dynamical calculations based on density-functional perturbation theory is developed enough to allow systematic application of DFPT to systems and materials of increasing complexity. The availability to a larger scientific community of the software necessary to perform such calculations will make them a routine ingredient of current research, in much the same way as has occurred for standard density functional theory calculations over the past five years or

so.[8] Among the most promising fields of application, we mention the characterization of materials through the prediction of the relationship between their atomic structure and experimentally detectable spectroscopic properties; the study of the structural (in)stability of materials at extreme pressure conditions; and the prediction of the thermal dependence of different materials' properties using the quasiharmonic approximation.

## ACKNOWLEDGMENTS

Finally, we would like to thank all those collaborators and friends, mainly but not exclusively former SISSA students, who have greatly contributed to the development of this field and without whom this review would be much shorter or would never have been conceived at all. Among them, we are pleased to mention Marco Buongiorno Nardelli, Claudia Bungaro, Alberto Debernardi, Michele Lazzeri, Kurt Mäder, Pasquale Pavone, Andrea Testa, Raffaele Resta, and Nathalie Vast. We wish to thank X. Gonze for providing a hardcopy of Fig. 6. This work has been partially funded by Italian MURST through a COFIN99 project (*Progetti di ricerca di rilevante interesse nazionale*), and by INFM through *Iniziativa Trasversale Calcolo Parallelo*.

## APPENDIX A: PLANE-WAVE PSEUDOPOTENTIAL IMPLEMENTATION

### 1. Pseudopotentials

Norm-conserving pseudopotentials are relatively smooth functions, whose long-range tail looks like $-Z_v e^2/r$ where $Z_v$ is the number of valence electrons. There is a different pseudopotential for each atomic angular momentum $l$:

$$\hat{V} = V_{loc}(r) + \sum_l V_l(r)\hat{P}_l, \tag{A1}$$

where $\hat{P}_l = \Sigma_{m=-l}^{l} |lm\rangle\langle lm|$ is the projection operator on states of angular momentum $l$, and where $|lm\rangle$ is the angular state with $(l,m)$ angular quantum numbers. Usually $V_{loc}(r) \simeq -Z_v e^2/r$ for large $r$, so that the $V_l(r)$ are short-ranged. Pseudopotentials in this form are called *semilocal*:

$$V(\mathbf{r},\mathbf{r}') = V_{loc}(r)\,\delta(\mathbf{r}-\mathbf{r}') + \sum_{lm} Y_{lm}(\mathbf{r}) V_l(r) \times \delta(r-r') Y_{lm}^*(\mathbf{r}'), \tag{A2}$$

where the $Y_{lm}(\mathbf{r}) = \langle \mathbf{r}|lm\rangle$ are the usual spherical harmonics.

[8] An open source computer code for performing DFT-DFPT pseudopotential calculation has been made available by the present authors on the net, at URL http://www.pwscf.org

Pseudopotentials are usually recast into the Kleinman and Bylander (1982) *separable form*. Each pseudopotential is projected onto the atomic reference pseudo wave functions $\phi_l^{ps}$:

$$\hat{V} = V_{loc} + V_L + \sum_l \frac{|V_l' \phi_l^{ps}\rangle\langle V_l' \phi_l^{ps}|}{\langle \phi_l^{ps}|V_l'|\phi_l^{ps}\rangle}, \tag{A3}$$

where $V_L(r)$ is an arbitrary function, $V_l'(r) = V_l(r) - V_L(r)$. By construction, the original pseudopotential and the projected pseudopotentials $\hat{V}$ have the same eigenvalues and eigenvectors on the reference states $\phi_l^{ps}$. The separable form may fail badly in some cases due to the appearance of spurious *ghost states*. Solutions have been devised to avoid such a problem (Gonze *et al.*, 1990, 1991).

### 2. Matrix elements

A plane-wave basis set is defined as

$$\langle \mathbf{r}|\mathbf{k}+\mathbf{G}\rangle = \frac{1}{V} e^{i(\mathbf{k}+\mathbf{G})\cdot\mathbf{r}}, \quad \frac{\hbar^2}{2m}|\mathbf{k}+\mathbf{G}|^2 \leqslant E_{cut}, \tag{A4}$$

where the $\mathbf{G}$'s are reciprocal-lattice vectors, $\mathbf{k}$ is the wave vector in the Brillouin zone, $V$ is the crystal volume, and $E_{cut}$ is the cutoff on the kinetic energy of the plane wave.

In the PW-PP implementation, Sec. III.A, we assume that the electron-ion potential $V_{ion}(\mathbf{r},\mathbf{r}')$ is written as

$$V_{ion}(\mathbf{r},\mathbf{r}') = \sum_{ls} v_s(\mathbf{r}-\mathbf{R}_l-\boldsymbol{\tau}_s, \mathbf{r}'-\mathbf{R}_l-\boldsymbol{\tau}_s) \tag{A5}$$

where $v_s$ is the pseudopotential for the $s$th atomic species, whose general form is

$$v_s(\mathbf{r},\mathbf{r}') = v_{s,loc}(r)\,\delta(\mathbf{r}-\mathbf{r}') + \sum_l v_{s,l}(\mathbf{r},\mathbf{r}'). \tag{A6}$$

The plane-wave matrix elements of the above operator are given by

$$\langle \mathbf{k}+\mathbf{G}|v_s|\mathbf{k}+\mathbf{G}'\rangle = \tilde{v}_{s,loc}(\mathbf{G}-\mathbf{G}') + \sum_l \tilde{v}_{s,l}(\mathbf{k}+\mathbf{G},\mathbf{k}+\mathbf{G}'), \tag{A7}$$

where

$$\tilde{v}_{s,loc}(\mathbf{G}) = \frac{1}{\Omega}\int v_{s,loc}(r) e^{-i\mathbf{G}\cdot\mathbf{r}} d\mathbf{r} \tag{A8}$$

and

$$\tilde{v}_{s,l}(\mathbf{k}_1,\mathbf{k}_2) = \frac{1}{\Omega}\int e^{-i\mathbf{k}_1\cdot\mathbf{r}} v_{s,l}(\mathbf{r},\mathbf{r}') e^{i\mathbf{k}_2\cdot\mathbf{r}'} d\mathbf{r} d\mathbf{r}'. \tag{A9}$$

For pseudopotentials in the semilocal form, Eq. (A2),

$$v_{s,l}(\mathbf{r},\mathbf{r}') = \hat{P}_l f_{s,l}(r), \tag{A10}$$

and

$$\tilde{v}_{s,l}(\mathbf{k}_1,\mathbf{k}_2)=\frac{4\pi}{\Omega}(2l+1)P_l(\hat{\mathbf{k}}_1\cdot\hat{\mathbf{k}}_2)\times\int_0^\infty r^2 j_l(k_1 r)j_l(k_2 r)f_{s,l}(r)dr, \quad \text{(A11)}$$

where the $j_l$'s are spherical Bessel functions, and the $P_l$'s are Legendre polynomials of degree $l$.

For pseudopotentials in the separable form, Eq. (A3),

$$v_{s,l}(\mathbf{r},\mathbf{r}')=c_{s,l}\beta^*_{s,l}(\mathbf{r})\beta_{s,l}(\mathbf{r}'), \quad \text{(A12)}$$

and

$$\tilde{v}_{s,l}(\mathbf{k}_1,\mathbf{k}_2)=c_{s,l}\tilde{\beta}^*_{s,l}(\mathbf{k}_1)\tilde{\beta}_{s,l}(\mathbf{k}_2), \quad \text{(A13)}$$

where the $\tilde{\beta}(\mathbf{k})$'s are the Fourier transform of $\beta(\mathbf{r})$, as in Eq. (A8).

The matrix elements between plane waves of the derivatives of the ionic potential, Eq. (88), are

$$\left\langle \mathbf{k}+\mathbf{q}+\mathbf{G}\left|\frac{\partial V_{ion}}{\partial u_s^\alpha(\mathbf{q})}\right|\mathbf{k}+\mathbf{G}'\right\rangle = -i(q_\alpha+G_\alpha-G'_\alpha)e^{-i(\mathbf{q}+\mathbf{G}-\mathbf{G}')\cdot\boldsymbol{\tau}_s}\times\left(\tilde{v}_{s,loc}(\mathbf{q}+\mathbf{G}-\mathbf{G}')+\sum_l \tilde{v}_{s,l}(\mathbf{k}+\mathbf{q}+\mathbf{G},\mathbf{k}+\mathbf{G}')\right). \quad \text{(A14)}$$

The screening contribution to $\partial V_{SCF}/\partial u_s^\alpha(\mathbf{q})$, which is a local potential in density functional theory, can be advantageously evaluated in real space and transformed back to reciprocal space by the FFT technique.

The matrix elements of the commutator $[H_{SCF},\mathbf{r}]$ between plane waves are

$$\langle\mathbf{k}_1|[H_{SCF},\mathbf{r}]|\mathbf{k}_2\rangle=\frac{\hbar^2}{m}\mathbf{k}_1\delta_{\mathbf{k}_1\mathbf{k}_2}-i\sum_{s,l} e^{-i(\mathbf{k}_1-\mathbf{k}_2)\cdot\boldsymbol{\tau}_s}\times\left(\frac{\partial}{\partial\mathbf{k}_1}+\frac{\partial}{\partial\mathbf{k}_2}\right)\tilde{v}_{s,l}(\mathbf{k}_1,\mathbf{k}_2), \quad \text{(A15)}$$

where $\delta_{\mathbf{k}_1\mathbf{k}_2}=1$ if $\mathbf{k}_1=\mathbf{k}_2$, and $\delta_{\mathbf{k}_1\mathbf{k}_2}=0$ otherwise.

The matrix elements of the second derivative of the electron-ion interaction potential appearing in the second term of Eq. (86) are given by

$$\left\langle \mathbf{k}+\mathbf{G}\left|\frac{\partial^2 V_{ion}}{\partial u_s^\alpha(\mathbf{q}=0)\partial u_s^\beta(\mathbf{q}=0)}\right|\mathbf{k}+\mathbf{G}'\right\rangle = -(G_\alpha-G'_\alpha)(G_\beta-G'_\beta)e^{-i(\mathbf{G}-\mathbf{G}')\cdot\boldsymbol{\tau}_s}\times\left(\tilde{v}_s(\mathbf{G}-\mathbf{G}')+\sum_l \tilde{v}_{s,l}(\mathbf{k}+\mathbf{G},\mathbf{k}+\mathbf{G}')\right). \quad \text{(A16)}$$

## APPENDIX B: FORCE CONSTANTS, IONIC TERM

The total energy of a crystal contains a divergent ion-ion energy term, Eq. (3), that combines with the divergent $\mathbf{G}=0$ terms in the electron-ion energy [the second term in Eq. (18)] to yield the *Ewald* term $E_{Ew}$:

$$E_{Ew}=\frac{4\pi N_c}{\Omega}\frac{e^2}{2}\sum_{\mathbf{G}\neq 0}\frac{e^{-G^2/4\eta}}{G^2}\left|\sum_s Z_s e^{i\mathbf{G}\cdot\boldsymbol{\tau}_s}\right|^2 + \frac{N_c e^2}{2}\sum_{s,t}\sum_{\mathbf{R}}\frac{Z_s Z_t\,\mathrm{erfc}(\sqrt{\eta}|\boldsymbol{\tau}_s-\boldsymbol{\tau}_t-\mathbf{R}|)}{|\boldsymbol{\tau}_s-\boldsymbol{\tau}_t-\mathbf{R}|} - \frac{\pi N_c e^2}{\Omega\eta}\left(\sum_s Z_s\right)^2 - N_c e^2\sqrt{\frac{\eta}{\pi}}\sum_s Z_s^2, \quad \text{(B1)}$$

where $\mathrm{erfc}(x)=1-\mathrm{erf}(x)$ (erf is the error function); the sum over $\mathbf{R}$ space excludes $\boldsymbol{\tau}_s-\boldsymbol{\tau}_t-\mathbf{R}=0$; $N_c$ is the number of unit cells in the crystal; $Z_s$ indicates the bare ionic charges for the $s$th atom (pseudocharges in a PP-PW framework); and $\eta$ is an arbitrary parameter, whose value ensures good convergence of both sums over $\mathbf{G}$ and $\mathbf{R}$ space.

The second derivative of the Ewald term yields the ionic contribution to the force constants:

$$\begin{aligned}{}^{ion}\tilde{C}^{\alpha\beta}_{st}(\mathbf{q})=&\frac{4\pi e^2}{\Omega}\sum_{\mathbf{G}}\frac{e^{-(\mathbf{q}+\mathbf{G})^2/4\eta}}{(\mathbf{q}+\mathbf{G})^2}Z_s Z_t\times e^{i(\mathbf{q}+\mathbf{G})\cdot(\boldsymbol{\tau}_s-\boldsymbol{\tau}_t)}(q_\alpha+G_\alpha)(q_\beta+G_\beta)\\ &-\frac{2\pi e^2}{\Omega}\sum_{\mathbf{G}\neq 0}\frac{e^{-G^2/4\eta}}{G^2}\times\left[Z_s\sum_l Z_l e^{i\mathbf{G}\cdot(\boldsymbol{\tau}_s-\boldsymbol{\tau}_l)}G_\alpha G_\beta+\text{c.c.}\right]\delta_{st}\\ &+e^2\sum_{\mathbf{R}} Z_s Z_t e^{i\mathbf{q}\cdot\mathbf{R}}\times[\delta_{\alpha\beta}f_2(x)+f_1(x)x_\alpha x_\beta]_{\mathbf{x}=\boldsymbol{\tau}_s-\boldsymbol{\tau}_t-\mathbf{R}}\\ &-e^2\delta_{st}\sum_{\mathbf{R}}\sum_l Z_s Z_l\times[\delta_{\alpha\beta}f_2(x)+f_1(x)x_\alpha x_\beta]_{\mathbf{x}=\boldsymbol{\tau}_s-\boldsymbol{\tau}_l-\mathbf{R}} \quad \text{(B2)}\end{aligned}$$

where the sum over $\mathbf{G}$ space excludes $\mathbf{q}+\mathbf{G}=0$, the sums over $\mathbf{R}$ space exclude $\boldsymbol{\tau}_s-\boldsymbol{\tau}_t-\mathbf{R}=0$, and the functions $f_1$ and $f_2$ are defined as

$$f_1(r)=\frac{3\,\mathrm{erfc}(\sqrt{\eta}r)+2\sqrt{\frac{\eta}{\pi}}r(3+2\eta r^2)e^{-\eta r^2}}{r^5}, \quad \text{(B3)}$$

$$f_2(r)=\frac{-\mathrm{erfc}(\sqrt{\eta}r)-2\sqrt{\frac{\eta}{\pi}}re^{-\eta r^2}}{r^3}. \quad \text{(B4)}$$

## REFERENCES

Ackland, G. J., M. C. Warren, and S. J. Clark, 1997, J. Phys.: Condens. Matter **9**, 7861.

Adler, C., R. Honke, P. Pavone, and U. Schröder, 1998, Phys. Rev. B **57**, 3726.

Amos, R. D., 1987, in *Ab Initio Methods in Quantum Chemistry–I*, edited by K. P. Lawley (Wiley, New York), p. 99.
Ancilotto, F., A. Selloni, W. Andreoni, S. Baroni, R. Car, and M. Parrinello, 1991, Phys. Rev. B **43**, 8930.
Baroni, S., and P. Giannozzi, 1998, in *High Pressure Materials Research*, edited by R. M. Wentzcovitch *et al.*, Mater. Res. Soc. Symp. Proc. No. 499 (Materials Research Society, Pittsburgh), p. 233.
Baroni, S., and P. Giannozzi, 1999, unpublished.
Baroni, S., P. Giannozzi, and E. Molinari, 1990, Phys. Rev. B **41**, 3870.
Baroni, S., P. Giannozzi, and A. Testa, 1987a, Phys. Rev. Lett. **58**, 1861.
Baroni, S., P. Giannozzi, and A. Testa, 1987b, Phys. Rev. Lett. **59**, 2662.
Baroni, S., S. de Gironcoli, and P. Giannozzi, 1990, Phys. Rev. Lett. **65**, 84.
Baroni, S., and R. Resta, 1986a, Phys. Rev. B **33**, 5969.
Baroni, S., and R. Resta, 1986b, Phys. Rev. B **33**, 7017.
Bauer, R., A. Schütt, P. Pavone, W. Windl, and D. Strauch, 1995, Phys. Rev. B **51**, 210.
Bauer, R., A. Schmid, P. Pavone, and D. Strauch, 1998, Phys. Rev. B **57**, 11276.
Becke, A. D., 1988, Phys. Rev. A **38**, 3098.
Bertoni, C. M., V. Bortolani, C. Calandra, and E. Tosatti, 1972, Phys. Rev. Lett. **28**, 1578.
Blat, D. Kh., N. E. Zein, and V. I. Zinenko, 1991, J. Phys. C **3**, 5515.
Born, M., and J. R. Oppenheimer, 1927, Ann. Phys. (Leipzig) **84**, 457.
Born, M., and K. Huang, 1954, *Dynamical Theory of Crystal Lattices* (Oxford University Press, Oxford).
Böttger, H., 1983, *Principles of the Theory of Lattice Dynamics* (Physik-Verlag, Weinheim).
Bungaro, C., S. de Gironcoli, and S. Baroni, 1996, Phys. Rev. Lett. **77**, 2491.
Bungaro, C., and S. de Gironcoli, 2000, Appl. Phys. Lett. **76**, 2101.
Bungaro, C., K. Rapcewicz, and J. Bernholc, 2000, Phys. Rev. B **61**, 6720.
Buongiorn Nardelli, M., S. Baroni, and P. Giannozzi, 1995, Phys. Rev. B **51**, 8060.
Buongiorno Nardelli, M., D. Cvetko, V. de Renzi, L. Floreano, A. Morgante, M. Peloi, and F. Tommasini, 1995, Phys. Rev. B **52**, 16720.
Car, R., and M. Parrinello, 1985, Phys. Rev. Lett. **55**, 2471.
Ceperley, D. M., and B. J. Alder, 1980, Phys. Rev. Lett. **45**, 566.
Cochran, W., and R. A. Cowley, 1962, J. Phys. Chem. Solids **23**, 447.
Cockayne, E., and K. M. Rabe, 1997, Phys. Rev. B **56**, 7974.
Colombo, L., and P. Giannozzi, 1995, Solid State Commun. **96**, 49.
Dal Corso, A., 2001, submitted to Phys. Rev. B.
Dal Corso, A., S. Baroni, R. Resta, and S. de Gironcoli, 1993, Phys. Rev. B **47**, 3588.
Dal Corso, A., and S. de Gironcoli, 2000, Phys. Rev. B **62**, 273.
Dal Corso, A., and F. Mauri, 1994, Phys. Rev. B **50**, 5756.
Dal Corso, A., F. Mauri, and A. Rubio, 1996, Phys. Rev. B **53**, 15638.
Dal Corso, A., A. Pasquarello, and A. Baldereschi, 1997, Phys. Rev. B **56**, R11369.
Dal Corso, A., R. Resta, and S. Baroni, 1993, Phys. Rev. B **47**, 16252.
Debernardi, A., 1998, Phys. Rev. B **57**, 12847.
Debernardi, A., 1999, Solid State Commun. **113**, 1.
Debernardi, A., and S. Baroni, 1994, Solid State Commun. **91**, 813.
Debernardi, A., S. Baroni, and E. Molinari, 1995, Phys. Rev. Lett. **75**, 1819.
Debernardi, A., and M. Cardona, 1996, Phys. Rev. B **54**, 11305.
Debernardi, A., and M. Cardona, 1998, Nuovo Cimento D **20**, 923.
Debernardi, A., and M. Cardona, 1999, Physica B **263–264**, 687.
Debernardi, A., N. M. Pyka, A. Göbel, T. Ruf, R. Lauck, S. Kramp, and M. Cardona, 1997, Solid State Commun. **103**, 297.
Debernardi, A., C. Ulrich, K. Syassen, and M. Cardona, 1999, Phys. Rev. B **59**, 6774.
De Cicco, P. D., and F. A. Johnson, 1969, Proc. R. Soc. London, Ser. A **310**, 111.
de Gironcoli, S., 1992, Phys. Rev. B **46**, 2412.
de Gironcoli, S., 1995, Phys. Rev. B **51**, 6773.
de Gironcoli, S., and S. Baroni, 1992, Phys. Rev. Lett. **69**, 1959.
de Gironcoli, S., S. Baroni, and R. Resta, 1989, Phys. Rev. Lett. **62**, 2853.
de Gironcoli, S., S. Baroni, and R. Resta, 1990, Ferroelectrics **111**, 19.
de Gironcoli, S., and E. Molinari, 1994, Solid-State Electron. **37**, 621.
de Gironcoli, S., E. Molinari, R. Schorer, and G. Abstreiter, 1993, Phys. Rev. B **48**, 8959.
Detraux, F., Ph. Ghosez, and X. Gonze, 1997, Phys. Rev. B **56**, 983
Detraux, F., Ph. Ghosez, and X. Gonze, 1998, Phys. Rev. Lett. **81**, 3297.
De Vita, A., 1992, Ph.D. thesis (University of Keele).
Dreizler, R. M., and E. K. U. Gross, 1990, *Density Functional Theory* (Springer, Berlin).
Eckl, C., J. Fritsch, P. Pavone, and U. Schröder, 1997, Surf. Sci. **394**, 47.
Eckl, C., R. Honke, J. Fritsch, P. Pavone, and U. Schröder, 1997, Z. Phys. B: Condens. Matter **104**, 715.
Einarsdotter, K., B. Sadigh, G. Grimvall, and V. Ozoliņš, 1997, Phys. Rev. Lett. **79**, 2073; **79**, 5188(E).
Eklund, P. C., P. Zhou, K. A. Wang, G. Dresselhaus, and M. S. Dresselhaus, 1992, J. Phys. Chem. Solids **53**, 1391.
Epstein, S., 1974, *The Variation Method in Quantum Chemistry* (Academic, New York).
Favot, F., and A. Dal Corso, 1999, Phys. Rev. B **60**, 11427.
Feynman, R. P., 1939, Phys. Rev. **56**, 340.
Feynman, R. P., 1972, *Statistical Mechanics* (Benjamin, Reading), p. 249.
Fleszar, A., and X. Gonze, 1990, Phys. Rev. Lett. **64**, 2961.
Fleszar, A., and R. Resta, 1986, Phys. Rev. B **34**, 7140.
Frank, W., C. Elsässer, and M. Fähnle, 1995, Phys. Rev. Lett. **74**, 1791.
Fritsch, J., M. Arnold, and U. Schröder, 2000, Phys. Rev. B **61**, 16682.
Fritsch, J., A. Eckert, P. Pavone, and U. Schröder, 1995, J. Phys.: Condens. Matter **7**, 7717.
Fritsch, J., and P. Pavone, 1995, Surf. Sci. **344**, 159.
Fritsch, J., P. Pavone, and U. Schröder, 1993, Phys. Rev. Lett. **71**, 4194.

Fritsch, J., P. Pavone, and U. Schröder, 1995, Phys. Rev. B **52**, 11326.
Fritsch, J., and U. Schröder, 1999, Phys. Rep. **309**, 209.
Fu, C.-L., and K.-M. Ho, 1983, Phys. Rev. B **28**, 5480.
Gaál-Nagy, K., A. Bauer, M. Schmitt, K. Karch, P. Pavone, and D. Strauch, 1999, Phys. Status Solidi B **211**, 275.
Gammon, D., B. V. Shanabrook, and D. S. Katzer, 1991, Phys. Rev. Lett. **67**, 1547.
Gerratt, J., and I. M. Mills, 1968, J. Chem. Phys. **49**, 1719.
Ghandehari, K., H. Huo, A. L. Ruoff, S. S. Trail, and F. J. Di Salvo, 1995, Phys. Rev. Lett. **74**, 2264.
Ghosez, Ph., E. Cockayne, U. V. Waghmare, and K. M. Rabe, 1999, Phys. Rev. B **60**, 836.
Ghosez, Ph., and X. Gonze, 2000, J. Phys.: Condens. Matter **12**, 9179.
Ghosez, Ph., X. Gonze, Ph. Lambin, and J.-P. Michenaud, 1995, Phys. Rev. B **51**, 6765.
Ghosez, Ph., X. Gonze, and J.-P. Michenaud, 1996, Europhys. Lett. **33**, 713.
Ghosez, Ph., X. Gonze, and J.-P. Michenaud, 1997, Ferroelectrics **194**, 39.
Ghosez, Ph., X. Gonze, and J.-P. Michenaud, 1998a, Ferroelectrics **206–207**, 205.
Ghosez, Ph., J.-P. Michenaud, and X. Gonze, 1998b, Phys. Rev. B **58**, 6224.
Giannozzi, P., 1995, in *Computational Approaches to Novel Condensed Matter Systems: Applications to Classical and Quantum Systems*, edited by D. Neilson and M. P. Das (Plenum, New York), p. 67.
Giannozzi, P., and W. Andreoni, 1996, Phys. Rev. Lett. **76**, 4915.
Giannozzi, P., and S. Baroni, 1994, J. Chem. Phys. **100**, 8537.
Giannozzi, P., S. de Gironcoli, P. Pavone, and S. Baroni, 1991, Phys. Rev. B **43**, 7231.
Gonze, X., 1995a, Phys. Rev. A **52**, 1086.
Gonze, X., 1995b, Phys. Rev. A **52**, 1096; **54**, 4591(E).
Gonze, X., 1997, Phys. Rev. B **55**, 10337.
Gonze, X., D. C. Allan, and M. P. Teter, 1992, Phys. Rev. Lett. **68**, 3603.
Gonze, X., J.-C. Charlier, D. C. Allan, and M. P. Teter, 1994, Phys. Rev. B **50**, 13035.
Gonze, X., P. Kaeckell, and M. Scheffler, 1990, Phys. Rev. B **41**, 12264.
Gonze, X., and C. Lee, 1997, Phys. Rev. B **55**, 10355.
Gonze, X., R. Stumpf, and M. Scheffler, 1991, Phys. Rev. B **44**, 8503.
Gonze, X., and J. P. Vigneron, 1989, Phys. Rev. B **39**, 13120; **44**, 3494(E).
Grosche, E. G., M. J. Ashwin, R. C. Newman, D. A. Robbie, M. J. L. Sangster, T. Pletl, P. Pavone, and D. Strauch, 1995, Phys. Rev. B **51**, 14758.
Guha, S., J. Menéndez, J. B. Page, G. B. Adams, G. S. Spencer, J. P. Lehman, P. Giannozzi, and S. Baroni, 1994, Phys. Rev. Lett. **72**, 3359.
Hamann, D. R., M. Schlüter, and C. Chiang, 1979, Phys. Rev. Lett. **43**, 1494.
Hedin, L., 1999, J. Phys.: Condens. Matter **11**, R489.
Heid, R., and K.-P. Bohnen, 1999, Phys. Rev. B **60**, R3709.
Heid, R., L. Pintschovius, W. Reichardt, and K.-P. Bohnen, 2000, Phys. Rev. B **61**, 12059.
Heid, R., D. Strauch, and K.-P. Bohnen, 2000, Phys. Rev. B **61**, 8625.
Hellmann, H., 1937, *Einführung in die Quantenchemie* (Deuticke, Leipzig).
Herman, F., 1959, J. Phys. Chem. Solids **8**, 405.
Hohenberg, P., and W. Kohn, 1964, Phys. Rev. **136**, B864.
Honke, R., J. Fritsch, P. Pavone, and U. Schröder, 1996, Phys. Rev. B **53**, 9923.
Honke, R., P. Pavone, U. Schröder, 1996, Surf. Sci. **367**, 75.
Hybertsen, M. S., and S. G. Louie, 1987, Phys. Rev. B **35**, 5585.
Jones, R. O., and O. Gunnarson, 1989, Rev. Mod. Phys. **61**, 689.
Jusserand, B., and M. Cardona, 1989, in *Light Scattering in Solids V*, edited by M. Cardona and G. Güntherodt (Springer, Berlin), p. 49.
Kane, E. O., 1985, Phys. Rev. B **31**, 7865.
Karch, K., and F. Bechstedt, 1997, Phys. Rev. B **56**, 7404.
Karch, K., F. Bechstedt, P. Pavone, and D. Strauch, 1996, Phys. Rev. B **53**, 13400.
Karch, K., T. Dietrich, W. Windl, P. Pavone, A. P. Mayer, and D. Strauch, 1996, Phys. Rev. B **53**, 7259.
Karch, K., P. Pavone, W. Windl, O. Schütt, and D. Strauch, 1994, Phys. Rev. B **50**, 17054.
Karch, K., J.-M. Wagner, and F. Bechstedt, 1998, Phys. Rev. B **57**, 7043.
Karki, B. B., R. M. Wentzcovitch, S. de Gironcoli, and S. Baroni, 1999, Science **286**, 1705.
Karki, B. B., R. M. Wentzcovitch, S. de Gironcoli, and S. Baroni, 2000, Phys. Rev. B **61**, 8793.
Kechrakos, D., P. R. Briddon, and J. C. Inkson, 1991, Phys. Rev. B **44**, 9114.
Kern, G., G. Kresse, and J. Hafner, 1999, Phys. Rev. B **59**, 8551.
Kim, K., V. Ozoliņš, and A. Zunger, 1999, Phys. Rev. B **60**, R8449.
King-Smith, R. D., and R. J. Needs, 1990, J. Phys.: Condens. Matter **2**, 3431.
King-Smith, R. D., and D. Vanderbilt, 1993, Phys. Rev. B **47**, 1651.
Kingma, K. J., R. J. Hemley, H. K. Mao, and D. R. Veblen, 1993, Phys. Rev. Lett. **70**, 3927.
Kingma, K. J., C. Meade, R. J. Hemley, H. K. Mao, and D. R. Veblen, 1993, Science **259**, 666.
Kleinman, L., and D. M. Bylander, 1982, Phys. Rev. Lett. **48**, 1425.
Klotz, S., J. M. Besson, M. Braden, K. Karch, P. Pavone, D. Strauch, and W. G. Marshall, 1997, Phys. Rev. Lett. **79**, 1313.
Kohanoff, J., 1994, Comput. Mater. Sci. **2**, 221.
Kohanoff, J., W. Andreoni, and M. Parrinello, 1992, Phys. Rev. B **46**, 4371.
Kohanoff, J., S. Scandolo, S. de Gironcoli, and E. Tosatti, 1999, Phys. Rev. Lett. **83**, 4097.
Kohn, W., and L. J. Sham, 1965, Phys. Rev. **140**, A1133.
Kulda, J., D. Strauch, P. Pavone, and Y. Ishii, 1994, Phys. Rev. B **50**, 13347.
Kunc, K., and R. M. Martin, 1983, in *Ab Initio Calculation of Phonon Spectra*, edited by J. T. Devreese, V. E. van Doren, and P. E. van Camp (Plenum, New York), p. 65.
Kuzmany, H., M. Matus, B. Burger, and J. Winter, 1994, Adv. Mater. **6**, 731.
Laasonen, K., A. Pasquarello, R. Car, C. Lee, and D. Vanderbilt, 1993, Phys. Rev. B **47**, 10142.
Lang, G., K. Karch, M. Schmitt, P. Pavone, A. P. Mayer, R. K. Wehner, and D. Strauch, 1999, Phys. Rev. B **59**, 6182.

LaSota, C., C-Z. Wang, R. Yu, and H. Krakauer, 1997, Ferroelectrics **194**, 109.
LaSota, C., C.-Z. Wang, R. Yu, and H. Krakauer, 1998, in *First-Principles Calculations for Ferroelectrics*, Willamsburg, VA, 1998, edited by R. E. Cohen, AIP Conf. Proc. No. 436, (AIP, Melville, N.Y.), p. 139.
Lawrence Marple, S., Jr., 1987, *Digital Spectral Analysis with Applications* (Prentice-Hall, Englewood Cliffs, NJ).
Lazzari, R., N. Vast, J. M. Besson, S. Baroni, and A. Dal Corso, 1999, Phys. Rev. Lett. **83**, 3230.
Lazzeri, M., 1999, *A first principles study of the thermal expansion in some metallic surfaces*, Ph.D. thesis (SISSA-ISAS, Trieste), URL http//www.sissa.it/cm/thesis/1999/lazzeri.ps.gz
Lazzeri, M., and S. de Gironcoli, 1998, Phys. Rev. Lett. **81**, 2096.
Lazzeri, M., and S. de Gironcoli, 2000, Surf. Sci. **454–456**, 442.
Lee, C., and X. Gonze, 1994a, Phys. Rev. Lett. **72**, 1686.
Lee, C., and X. Gonze, 1994b, Phys. Rev. B **50**, 13379.
Lee, C., and X. Gonze, 1995, Phys. Rev. B **51**, 8610.
Lee, C., and X. Gonze, 1997, Phys. Rev. B **56**, 7321.
Littlewood, P. B., 1980, J. Phys. C **13**, 4893.
Liu, A. Y., and A. A. Quong, 1996, Phys. Rev. B **53**, R7575.
Liu, A. Y., A. A. Quong, J. K. Freericks, E. J. Nicol, and E. C. Jones, 1999, Phys. Rev. B **59**, 4028.
Liu, J., and Y. K. Vohra, 1994, Phys. Rev. Lett. **72**, 4105.
Louie, S. G., S. Froyen, and M. L. Cohen, 1982, Phys. Rev. B **26**, 1738.
Mäder, K. A., and S. Baroni, 1997, Phys. Rev. B **55**, 9649.
Mahan, G. D., 1980, Phys. Rev. A **22**, 1780.
Mao, H. K., Y. Wu, R. J. Hemley, L. C. Chen, J. F. Shu, and L. W. Finger, 1989, Science **246**, 649.
Mao, H. K., Y. Wu, R. J. Hemley, L. C. Chen, J. F. Shu, L. W. Finger, and D. E. Cox, 1990, Phys. Rev. Lett. **64**, 1749.
Martin, R. M., 1972, Phys. Rev. B **5**, 1607.
Martin, M. C., D. Koller, and L. Mihaly, 1993, Phys. Rev. B **47**, 14607.
Martyna, G. J., M. L. Klein, and M. Tuckerman, 1992, J. Chem. Phys. **97**, 2635.
Marzari, N., D. Vanderbilt, A. De Vita, and M. C. Payne, 1999, Phys. Rev. Lett. **82**, 3296.
Mauri, F., G. Galli, and R. Car, 1993, Phys. Rev. B **47**, 9973.
Mauri, F., O. Zakharov, S. de Gironcoli, S. G. Louie, and M. L. Cohen, 1996, Phys. Rev. Lett. **77**, 1151.
Meregalli, V., and S. Y. Savrasov, 1998, Phys. Rev. B **57**, 14453.
Mermin, N. D., 1965, Phys. Rev. **137**, A1441.
Meskini, N., and K. Kunc, 1978, Technical Report No. 5, Université P. et M. Curie, unpublished.
Messiah, A., 1962, *Quantum Mechanics* (North-Holland, Amsterdam), p. 686 ff.
Methfessel, M., and A. Paxton, 1989, Phys. Rev. B **40**, 3616.
Molinari, E., S. Baroni, P. Giannozzi, and S. de Gironcoli, 1992, Phys. Rev. B **45**, 4280.
Nielsen, O. H., and R. M. Martin, 1985a, Phys. Rev. B **32**, 3780.
Nielsen, O. H., and R. M. Martin, 1985b, Phys. Rev. B **32**, 3792.
Nunes, R. W., and D. Vanderbilt, 1994, Phys. Rev. Lett. **73**, 712.
Öğüt, S., and K. M. Rabe, 1996, Phys. Rev. B **54**, R8297.
Ortiz, G., and P. Ballone, 1994, Phys. Rev. B **50**, 1391; **56**, 9970(E).
Ozoliņš, V., C. Wolverton, and A. Zunger, 1998, Phys. Rev. B **58**, R5897.
Ozoliņš, V., and A. Zunger, 1998, Phys. Rev. B **57**, R9404.
Ozoliņš, V., and A. Zunger, 1999, Phys. Rev. Lett. **82**, 767.
Panella, V., A. L. Glebov, J. P. Toennies, C. Sébenne, C. Eckl, C. Adler, P. Pavone, and U. Schröder, 1999, Phys. Rev. B **59**, 15772.
Parlinski, K., Z. Q. Li, and Y. Kawazoe, 1997, Phys. Rev. Lett. **78**, 4063.
Parlinski, K., Z. Q. Li, and Y. Kawazoe, 1998, Phys. Rev. Lett. **81**, 3298.
Parlinski, K., Z. Q. Li, and Y. Kawazoe, 2000, Phys. Rev. B **61**, 272.
Parr, R. G., and W. Yang, 1989, *Density Functional Theory of Atoms and Molecules* (Oxford University Press, New York).
Pavone, P., and S. Baroni, 1994, Solid State Commun. **90**, 295.
Pavone, P., S. Baroni, and S. de Gironcoli, 1998, Phys. Rev. B **57**, 10421.
Pavone, P., R. Bauer, K. Karch, O. Schütt, S. Vent, W. Windl, D. Strauch, S. Baroni, and S. de Gironcoli, 1996, Physica B **219–220**, 439.
Pavone, P., K. Karch, O. Schütt, D. Strauch, W. Windl, P. Giannozzi, and S. Baroni, 1993, Phys. Rev. B **48**, 3156.
Payne, M. C., M. P. Teter, D. C. Allen, T. A. Arias, and J. D. Joannopoulos, 1992, Rev. Mod. Phys. **64**, 1045.
Perdew, J. P., K. Burke, and M. Ernzerhof, 1996, Phys. Rev. Lett. **77**, 3865.
Perdew, J. P., S. Kurth, A. Zupan, and P. Blaha, 1999, Phys. Rev. Lett. **82**, 2544.
Perdew, J. P., and A. Zunger, 1981, Phys. Rev. B **23**, 5048.
Persson, K., M. Ekman, and G. Grimvall, 1999, Phys. Rev. B **60**, 9999.
Persson, K., M. Ekman, and V. Ozoliņš, 2000, Phys. Rev. B **61**, 11221.
Pichler, T., R. Winkler, and H. Kuzmany, 1994, Phys. Rev. B **49**, 18879.
Pick, R., M. H. Cohen, and R. M. Martin, 1970, Phys. Rev. B **1**, 910.
Pickett, W. E., 1989, Comput. Phys. Rep. **9**, 115.
Posternak, M., R. Resta, and A. Baldereschi, 1994, Phys. Rev. B **50**, 8911.
Press, W. H., S. A. Teukolsky, W. T. Vetterling, and B. P. Flannery, 1989, *Numerical Recipes: The Art of Scientific Computing* (Cambridge University Press, Cambridge, U.K.).
Pulay, P., 1969, Mol. Phys. **17**, 197.
Quong, A. A., 1994, Phys. Rev. B **49**, 3226.
Quong, A. A., and B. M. Klein, 1992, Phys. Rev. B **46**, 10734.
Quong, A. A., and A. Y. Liu, 1997, Phys. Rev. B **56**, 7767.
Rabe, K. M., and U. V. Waghmare, 1995, Phys. Rev. B **52**, 13236.
Rahman, A., 1964, Phys. Rev. **136**, A405.
Rappe, A. M., K. Rabe, E. Kaxiras, and J. D. Joannopoulos, 1990, Phys. Rev. B **41**, 1227.
Resta, R., 1983, Phys. Rev. B **27**, 3620.
Resta, R., 1994, Rev. Mod. Phys. **66**, 899.
Resta, R., and A. Baldereschi, 1981, Phys. Rev. B **24**, 4839.
Rignanese, G. M., J.-P. Michenaud, and X. Gonze, 1996, Phys. Rev. B **53**, 4488.
Robbie, D. A., M. J. L. Sangster, E. G. Grosche, R. C. Newman, T. Pletl, P. Pavone, and D. Strauch, 1996, Phys. Rev. B **53**, 9863.
Robbie, D. A., M. J. L. Sangster, and P. Pavone, 1995, Phys. Rev. B **51**, 10489.
Roma, G., C. M. Bertoni, and S. Baroni, 1996, Solid State Commun. **98**, 203.

Rossi, F., L. Rota, C. Bungaro, P. Lugli, and E. Molinari, 1993, Phys. Rev. B **47**, 1695.
Rudin, S. P., and A. Y. Liu, 1999, Phys. Rev. Lett. **83**, 3049.
Ruf, T., J. Serrano, M. Cardona, P. Pavone, M. Pabst, M. Krisch, M. D'Astuto, T. Suski, I. Grzegory, and M. Leszczynski, 2000, in *Proceedings of the 17th International Conference on Raman Spectroscopy*, Beijing, 2000, edited by S.-L. Zhang and B. Zhu (Wiley, New York), p. 428.
Saad, Y., and M. H. Schultz, 1986, SIAM (Soc. Ind. Appl. Math.) J. Sci. Stat. Comput. **7**, 856.
Sághi-Szabó, G., R. E. Cohen, and H. Krakauer, 1998, Phys. Rev. Lett. **80**, 4321.
Saitta, A. M., D. Alfè, S. de Gironcoli, and S. Baroni, 1997, Phys. Rev. Lett. **78**, 4958.
Savrasov, S. Y., 1992, Phys. Rev. Lett. **69**, 2819.
Savrasov, S. Y., 1996, Phys. Rev. B **54**, 16470.
Savrasov, S. Y., 1998, Phys. Rev. Lett. **81**, 2570.
Savrasov, S. Y., and O. K. Andersen, 1996, Phys. Rev. Lett. **77**, 4430.
Savrasov, S. Y., and D. Y. Savrasov, 1996, Phys. Rev. B **54**, 16487.
Savrasov, S. Y., D. Y. Savrasov, and O. K. Andersen, 1994, Phys. Rev. Lett. **72**, 372.
Schorer, R., G. Abstreiter, S. de Gironcoli, E. Molinari, H. Kibbel, and H. Presting, 1994, Phys. Rev. B **49**, 5406.
Schütt, O., P. Pavone, W. Windl, K. Karch, and D. Strauch, 1994, Phys. Rev. B **50**, 3746.
Schwoerer-Böhning, M., A. T. Macrander, M. Pabst, and P. Pavone, 1999, Phys. Status Solidi B **215**, 177.
Steininger, B., P. Pavone, and D. Strauch, 1999, Phys. Status Solidi B **215**, 127.
Sternheimer, R. M., 1954, Phys. Rev. **96**, 951.
Štich, I., R. Car, M. Parrinello, and S. Baroni, 1989, Phys. Rev. B **39**, 4997.
Stigler, W., P. Pavone, and J. Fritsch, 1998, Phys. Rev. B **58**, 13686.
Stigler, W., P. Pavone, U. Schröder, J. Fritsch, G. Brusdeylins, T. Wach, and J. P. Toennies, 1997, Phys. Rev. Lett. **79**, 1090.
Troullier, N., and J. L. Martins, 1991, Phys. Rev. B **43**, 1993.
Vanderbilt, D., 1985, Phys. Rev. B **32**, 8412.
Vanderbilt, D., 1990, Phys. Rev. B **41**, 7892.
Vanderbilt, D., 2000, J. Phys. Chem. **61**, 147.
Vast, N., and S. Baroni, 2000, Phys. Rev. B **61**, 9387.
Vast, N., S. Baroni, G. Zerah, J. M. Besson, A. Polian, M. Grimsditch, and J. C. Chervin, 1997, Phys. Rev. Lett. **78**, 693.
Waghmare, U. V., and K. M. Rabe, 1997, Phys. Rev. B **56**, 6161.
Waghmare, U. V., K. M. Rabe, H. Krakauer, R. Yu, and C.-Z. Wang, 1998, in *First-Principles Calculations for Ferroelectrics*, Willamsburg, VA, 1998, edited by R. E. Cohen, AIP Conf. Proc. No. 436 (AIP, Melville, NY), p. 32.
Wagner, J.-M., and F. Bechstedt, 2000, Phys. Rev. B **62**, 4526.
Wang, C.-Z., R. Yu, and H. Krakauer, 1994, Phys. Rev. Lett. **72**, 368.
Wang, C.-Z., R. Yu, and H. Krakauer, 1996a, Phys. Rev. B **53**, 5430.
Wang, C.-Z., R. Yu, and H. Krakauer, 1996b, Phys. Rev. B **54**, 11161.
Wang, C.-Z., R. Yu, and H. Krakauer, 1999, Phys. Rev. B **59**, 9278.
Wei, S., and M. Y. Chou, 1992, Phys. Rev. Lett. **69**, 2799.
Wei, S., and M. Y. Chou, 1994, Phys. Rev. B **50**, 2221.
Wei, S., C. Li, and M. Y Chou, 1994, Phys. Rev. B **50**, 14587.
Wellenhofer, G., K. Karch, P. Pavone, U. Rössler, and D. Strauch, 1996, Phys. Rev. B **53**, 6071.
Widulle, F., S. Kramp, N. M. Pyka, A. Göbel, T. Ruf, A. Debernardi, R. Lauck, and M. Cardona, 1999, in *Proceedings of the 9th International Conference on Phonon Scattering in Condensed Matter*, Lancaster, 1998, edited by M. Giltrow, A. Kozorezov, and K. Wigmore, Physica B **263/264**, p. 448.
Widulle, F., T. Ruf, O. Buresch, A. Debernardi, and M. Cardona, 1999, Phys. Rev. Lett. **82**, 3089.
Windl, W., K. Karch, P. Pavone, O. Schütt, D. Strauch, D. Strauch, W. H. Weber, K. C. Hass, and L. Rimai, 1994, Phys. Rev. B **49**, 8764.
Windl, W., P. Pavone, K. Karch, O. Schütt, D. Strauch, P. Giannozzi, and S. Baroni, 1993, Phys. Rev. B **48**, 3164.
Windl, W., P. Pavone, and D. Strauch, 1996, Phys. Rev. B **54**, 8580.
Xie, J., S. P. Chen, J. S. Tse, S. de Gironcoli, and S. Baroni, 1999, Phys. Rev. B **60**, 9444.
Xie, J., S. de Gironcoli, S. Baroni, and M. Scheffler, 1999a, Phys. Rev. B **59**, 965.
Xie, J., S. de Gironcoli, S. Baroni, and M. Scheffler, 1999b, Phys. Rev. B **59**, 970
Yin, T. M, and M. L. Cohen, 1982, Phys. Rev. B **26**, 3259.
Yu, R., and H. Krakauer, 1994, Phys. Rev. B **49**, 4467.
Yu, R., and H. Krakauer, 1995, Phys. Rev. B **74**, 4067.
Zein, E. N., 1984, Fiz. Tverd. Tela (Leningrad) **26** 3024 [Sov. Phys. Solid State **26**, 1825 (1984)].
Zein, E. N., 1992, Phys. Lett. A **161**, 526.
Zein, E. N., V. I. Zinenko, and A. S. Fedorov, 1992, Phys. Lett. A **164**, 115.
Zhang, J. M., T. Ruf, M. Cardona, O. Ambacher, M. Stutzmann, J.-M. Wagner, and F. Bechstedt, 1997, Phys. Rev. B **56**, 14399.
Zhang, J. M., T. Ruf, A. Göbel, A. Debernardi, R. Lauck, and M. Cardona, 1996, in *Proceedings of the 23rd International Conference on the Physics of Semiconductors*, Berlin, 1996, edited by M. Scheffler and R. Zimmermann (World Scientific, Singapore), p. 201.
Zunger, A., S.-H. Wei, L. G. Ferreira, and J. E. Bernard, 1990, Phys. Rev. Lett. **65**, 353.